

**ON THE POTENTIAL OF CARBON MATERIALS FOR
SOLID STATE HYDROGEN STORAGE**

A THESIS

submitted by

M. SANKARAN

for the award of the degree

of

DOCTOR OF PHILOSOPHY



**NATIONAL CENTRE FOR CATALYSIS RESEARCH
DEPARTMENT OF CHEMISTRY
INDIAN INSTITUTE OF TECHNOLOGY MADRAS
CHENNAI - 600 036**

APRIL 2007

*Dedicated
To
My Parents*

THESIS CERTIFICATE

This is to certify that the thesis entitled “**ON THE POTENTIAL OF CARBON MATERIALS FOR SOLID STATE HYDROGEN STORAGE**” submitted by **M. Sankaran** to the Indian Institute of Technology Madras for the award of degree of **Doctor of Philosophy** is a bonafide record of research work carried out by him under our supervision. The contents of this thesis, in full or in parts, have not been submitted to any other Institute or University for the award of any degree or diploma.

Research Guides

Prof. S. Srinivasa Murthy
Department of Mechanical Engg.
IIT Madras, Chennai – 36.

Prof. B. Viswanathan
Department of Chemistry
IIT Madras, Chennai – 36.

Date

Place:

ACKNOWLEDGEMENTS

I express my sincere thanks and deep sense of gratitude to **Prof. B. Viswanathan**, my research guide for his constant encouragement, thought providing discussions, unfailing guidance and creating scientific temperament at every stage of the research programme. I am beholden to him for introducing the quintessence of science and orienting me into a logical line of thinking and rationalizing the problems. He is a venerable guide, philosopher and excellent scientist and I owe him a great intellectual and inspirational debt. I feel privileged to have been associated with him.

I am indebted to **Prof. S. Srinivasa Murthy** for his constant encouragement and support to carry out my research work.

I express my thanks to all my doctoral committee members **Prof. T. K. Varadarajan**, **Prof. T. Pradeep**, **Prof. S. Ramaprabhu** and **Prof. M. P. Mayia** for their interesting feedback and valuable suggestions.

I thank **Prof. R. P. Viswanath** for his encouragement through out my research.

I sincerely thank **Prof. S. Vancheesan**, **Prof. M. N. Sudheendra Rao**, **Prof. G. Sundrarajan** the former Heads and **Prof. S. Sankararaman**, the present Head of the Department of Chemistry, IIT Madras for providing the necessary infrastructural facilities during my research tenure.

I gratefully acknowledge **MNES** and **CSIR**, New Delhi, for the financial assistance. **DST**, Government of India is gratefully acknowledged for creating the National Centre for Catalysis Research, where most of this work was carried out.

I wish to thank the **IIT Madras** for providing all the facilities to carry out the research work.

My sincere thanks are due to all the staff members of chemistry department in my research work. I thank the Head and staff members of **CGBS**, **SAIF** and Department

of Metallurgy IIT Madras for providing the necessary instrumentation facilities. I am thankful to **Mr. RamKumar, Mr. A. Narayanan, Mr. Mohan, Mr. Balgunan Mr. Jayaraman, Mr. Gopinath, Mr. Sankaran, Mr. Janarthanan, Mr. Sugumar, Mr. Thirumalai, Mr. Prabhakar, Mr. P. Amulraj, K.S. Narashima rao** for their untiring and spontaneous help.

I thank **Dr. A. Kalaiselvan** and **Mr. K. Muthu Kumar** helping me in learning the theoretical calculations.

I would like to thank the authorities at **Computer Centre, IIT Madras** for providing necessary facilities to carry out theoretical calculations.

I express my heartfelt gratitude to my seniors **Dr. Rajesh, Dr. Raghuv eer, Dr. Ganesan, Dr. Aulice Scibioh, Dr. Subramanian, Dr. Shanmugham, Dr. Mishra**, for their timely help, friendship and encouragement, which they have extended to me at IIT Madras.

Words are inadequate to express my heartfelt gratitude to **Dr. V. Chidambaram, Dr. M. Sathish, Mr. P. Suresh, Mr. G Raguraman, Mr. A. Vivek, Ms A. Suvitha Ms S. Deepa, Mr. V. Ramesh, Dr. S. Srimurugan, Mr. S. Mahalingam and Mr. A. Aravind** with whom I have spent many memorable occasions and who have been helpful and supportive both in personal and academic activities.

I thank my colleagues **Mr. T. Maiyalagan, Ms. S. Chandravathanam, Mr. Ch. Venkateswara Rao, Mr. L. Hima Kumar, Mr. P. Indra Neel, Mr. S. Navaladian, Mr. P. Satyananda Kishore, Ms. J. Rajeswari, Ms. C.M. Janet, Ms. M. Helen, Mr. G. Magesh and Mr. B. Kuppan** for their help in all aspects.

I am thankful to **Dr. P. Muthu Kumar, Mr. D. Ebenezer, Mr. E. Anil Kumar, Mr. M. Ajay, Mr. M. Siva Shankar, Mr. G. Mohan and Mr. Gurudutt**, for their help to carry out experiments at Refrigeration and Air conditioning Laboratory.

My thanks are due to **Mr. Raja, Mr. Kumar, Mr. Anbu, Mr. Umapathi,** of **M/s. Raja Xerox & Prints** for their printing and Xeroxing throughout the programme. I also thank **Mr. Surya Prakash and Mr. Karuppia** for his help in the drawing work.

I thank my friends **Mr. P. Selvamani, Mr. Muruganatham, Mr. M. Ganavel, Mr. K. Mohan, Mr. S. Asaithambi and Mr. R. Magesh** for their support in all stages of research program.

I am ever indebted to my parents for their untiring efforts in providing me, love and affection and the highest quality of education. I sincerely acknowledge my brothers for their affection and encouragement.

M. SANKARAN

ABSTRACT

KEYWORDS: Hydrogen storage, carbon nanomaterials, heteroatoms, Density Functional Theory, volumetric method

All the three components of the hydrogen economy, namely, production, storage and application of hydrogen have been posing challenges to the scientific community for the past several decades. At present, storage of hydrogen in solid matrices appears to be the appropriate option. The scientific community in their anxiety and enthusiasm has come up with remarkable but not reproducible results for hydrogen storage in solid state. The desirable storage capacity for viable commercial exploitation of hydrogen as energy source is at least 6.5 weight % as originally postulated by US-DOE. However, any figure up to 67 weight % has been claimed as possible storage capacity in solids especially in carbon based materials. This has led to a variety of investigations dealing with modification of carbon materials like metal loading, preparing carbon materials in various geometrical forms, and phase purity and addition of metal oxides. However, none of these studies have unambiguously established that carbon nanomaterials can store hydrogen to the extent required by the original DOE standards at ambient conditions. This situation is critical, demanding definite and exploratory solutions from practicing scientists. The essential questions that require immediate attention are:

- (i) Are the carbon materials appropriate for solid state hydrogen storage?
- (ii) If this was to be true, what types of materials or treatments for the existing carbon materials are suitable to achieve the desirable levels of hydrogen storage?
- (iii) What are the stumbling blocks in achieving the desirable storage of hydrogen in solid state?

- (iv) Where does the lacuna lie? Is it in the theoretical foundation of the postulate or is it in our inability to experimentally realize the desired levels of storage?

Against this background, the need for an activator for hydrogenation in carbon materials is realized, which should be easily hydridable compared to carbon and facilitate migration of the dissociated hydrogen to equipotential carbon surface. While considering these aspects, heteroatoms like N, P, S and B seem to be promising as activators due to their properties like higher redox potential than that of carbon. This can result in the tuning of the electronic property of the carbon materials.

In the light of the above, the present study is aimed at establishing the role of heteroatom for hydrogen storage in the carbon materials, both by theoretical and experimental methodologies. The appropriateness of carbon nanomaterials as storage materials and the necessity for a suitable activator for hydrogen have been theoretically examined within the frame work of DFT calculations. In correlation to theoretical results, experiments were carried out to show the role of heteroatoms for hydrogen activation. In this context experiments were done with modified activated carbon and heteroatom (nitrogen and boron) substituted carbon nanomaterials prepared by template assisted method. The synthesized carbon nanomaterials were characterized and the hydrogen absorption activity was studied volumetrically.

TABLE OF CONTENTS

	Title	Page
	ACKNOWLEDGEMENT	i
	ABSTRACT	iv
	LIST OF TABLES	xi
	LIST OF FIGURES	xiii
	LIST OF SCHEMES	xvii
	ABBREVIATIONS	xviii
	NOTATIONS	xix
	 CHAPTER 1 INTRODUCTION	
1	Hydrogen economy.....	1
1.1	Why is there a need for alternative energy source?.....	1
1.2	Why Hydrogen?.....	3
1.3	Production of hydrogen	5
1.3.1	Electrolysis	5
1.3.2	Direct thermal decomposition of water	6
1.3.3	Photocatalytic decomposition of water.....	6
1.3.4	Biological methods for decomposition of water.....	7
1.4	Hydrogen storage.....	8
1.4.1	Why should there be a target of hydrogen storage?	8
1.5	Gaseous hydrogen storage	11
1.6	Liquid hydrogen storage.....	12
1.7	Solid hydrogen storage	12
1.7.1	Metal hydrides	12
1.7.2	Complex metal hydrides.....	20
1.7.3	Zeolites	23
1.7.4	Glass Spheres.....	24
1.7.5	Metal organic frameworks (MOFs).....	25
1.7.6	Chemical Storage.....	26

Table of Contents (Contd.)		Page
1.8	Carbon materials.....	27
1.8.1	Why carbon materials for hydrogen storage?.....	27
1.8.2	Activated carbon.....	31
1.8.3	Fullerene	32
1.8.4	Carbon nanofibres.....	36
1.8.5	Carbon nanotubes	36
1.8.5.1	Synthesis of carbon nanotubes	39
1.8.5.2	Hydrogen storage in carbon nanotubes	40
1.9	What alternatives?	46
1.10	Objectives and scope of the present investigation	48
 CHAPTER 2 MATERIALS AND METHODS		
2.1	Chemicals and materials used.....	50
2.2	Purification of hydrogen.....	50
2.3	Preparation of the catalyst	51
2.3.1	Preparation of nickel supported on activated carbon.....	51
2.3.2	Chemical treatment of activated carbon	51
2.3.3	Preparation of Polymer Derived Carbon (PDC) having the nitrogen content	52
2.3.4	Preparation of microemulsion mediated synthesis of nitrogen containing carbon (MEC).....	52
2.3.5	Preparation of nitrogen containing carbon nanotubes using polyprrole as carbon source.....	53
2.3.6	Preparation of carbon nanotubes without nitrogen content.....	53
2.3.7	Preparation of pillared clays	54
2.3.8	Preparation of carbon nanotubes by chemical vapor deposition (CVD) method	55
2.4	Characterization.....	56
2.4.1	UV-Visible absorption studies.....	56
2.4.2	Powder X-ray Diffraction (XRD).....	56
2.4.3	Transmission Electron Microscopic studies (TEM).....	56
2.4.4	Scanning Electron Microscopic studies (SEM).....	56

Table of Contents (Contd.)		Page
2.4.5	X-ray Photoelectron Spectroscopy (XPS)	56
2.4.6	Thermogravimetric Analysis (TGA)	57
2.4.7	Infrared (IR) Absorption studies	57
2.4.8	Raman Spectral Studies	57
2.4.9	Elemental Analysis	57
2.4.10	Cyclic Voltammetric measurements.....	58
2.4.11	Evolved Gas Analysis (EGA).....	58
2.4.12	Hydrogen storage apparatus	59
2.4.12.1	Low pressure absorption apparatus	59
2.4.12.2	High pressure apparatus.....	60
 CHAPTER 3 THEORETICAL STUDIES ON CARBON NANOTUBES AND FULLERENES 		
3.1	Theoretical studies on carbon nanotubes.....	62
3.1.1	Introduction	62
3.1.2	Computational models	65
3.1.2.1	An overview of computational chemistry	65
3.1.2.2	Methods for Electronic structure	66
3.1.2.3	Density Functional Theory (DFT).....	68
3.1.2.4	KOHN and SHAM method	69
3.1.2.5	Basis set	74
3.1.2.6	Effective core potential basis sets.....	77
3.1.2.7	Molecular mechanics	78
3.1.3	Heteroatom containing CNTs - their relevance.....	80
3.1.4	Model design and methodology	80
3.1.5	Results and discussion	83
3.2	Theoretical studies on fullerenes	90
3.2.1	Introduction	90
3.2.2	Theoretical methods and model.....	94
3.2.3	Results and discussion	96

CHAPTER 4 HYDROGEN STORAGE IN ACTIVATED CARBON

4.1	Introduction	101
4.2	Experimental methods for hydrogen storage determination in carbon materials.....	103
4.2.1	Volumetric method.....	103
4.2.2	Gravimetric method.....	103
4.2.3	Temperature programmed desorption (TPD)	104
4.3	Results and discussion.....	104
4.3.1	Metal loading in Calgon carbon	104
4.3.2	CDX-975 and its chemical modification.....	110
4.4	Conclusions	114

CHAPTER 5 NITROGEN CONTAINING CARBON NANOTUBES – SYNTHESIS, CHARACTERIZATION AND HYDROGEN ABSORPTION ACTIVITY

5.1	Introduction	115
5.2	Results and discussion.....	118
5.2.1	Nitrogen containing carbon nanomaterials.....	118
5.2.2	Template assisted synthesis of carbon nanotubes and nitrogen containing carbon nanotubes	120
5.2.2.1	Alumina membrane as the template	120
5.2.2.2	Zeolite as template.....	123
5.2.2.3	Clay as template.....	124
5.2.3	Elemental analysis	126
5.2.4	Hydrogen activation studies	127
5.2.6	Hydrogen storage capacity	130
5.3	Conclusions	134

CHAPTER 6 BORON SUBSTITUTED CARBON NANOTUBES – SYNTHESIS, CHARACTERIZATION AND HYDROGEN ABSORPTION ACTIVITY

6.1	Introduction	135
-----	--------------------	-----

Table of Contents (Contd.)		Page
6.2	Experimental section	138
6.2.1	Synthesis of boron containing carbon from hydroborane polymers.....	138
6.2.2	Synthesis of boron containing carbon from boron containing resin.....	142
6.2.3	Template based synthesis of carbon nanotubes	142
6.2.3.1	Alumina membrane	142
6.2.3.2	Zeolite and clay as template	143
6.3	Results and discussion	144
6.3.1	XRD studies.....	144
6.3.2	FT-IR spectroscopy	146
6.3.3	Raman studies.....	146
6.3.4	Electron microscopy study	147
6.3.5	Solid state ¹³ C and ¹¹ B MAS NMR measurements	150
6.3.6	Hydrogen absorption activity	154
6.4	Conclusions	156
CHAPTER 7	SUMMARY AND CONCLUSIONS	157
	REFERENCES	163
	LIST OF PUBLICATIONS	180

LIST OF TABLES

Table	Title	Page
1.1	Properties of hydrogen compared to other fuel system.....	4
1.2	DOE targets for on-board hydrogen storage	10
1.3	Hydrogen storage capacity of metallic and intermetallic systems	19
1.4	Common complex hydrides for hydrogen storage applications.....	21
1.5	Classification scheme for carbon allotropes, molecular crystals and derived forms	29
1.6	Hydrogen storage capacity of fullerene determined by various methods	35
1.7	Summary of reported hydrogen storage capacities in carbon nanostructures.....	43
3.1	Geometric parameters of the CNT cluster optimized by employing Universal Force Field (UFF 1.02) method.....	82
3.2	Bond length and dissociation energy of hydrogen on the CNTs calculated using B3LYP with 6-31g (p, d) basis set on the UFF optimized structure	84
3.3	Percentage orbital contribution of the HOMO level of the pure CNT and heteroatom substituted CNT before and after hydrogen interaction	86
3.4	Transition state optimized parameters of the cluster and the value of the activation energy calculated by B3LYP with 6-31g (p, d) basis set	89
3.5	Bond length and dissociation energy of hydrogen molecule on interaction with fullerene molecule is calculated using B3LYP with 6-31g (p, d) basis set on the UFF optimized structure.....	96
3.6	Geometrical parameters of the simple cluster considered for the mechanistic pathway employing hybrid density functional B3LYP method with 6-31g (d) basis set	99
3.7	Transition state optimized parameters of the cluster and the value of the activation energy calculated by B3LYP with 6-31g (p, d) basis set	99
4.1	Comparison of amount of nickel loaded and the nickel determined from the SEM / EDAX analysis.....	106
4.2	Hydrogen absorption activity at 1 atm and at various temperatures for the Calgon carbon and its modification by various percentage of nickel loading.....	109
4.3	Comparison of SSA and hydrogen absorption activity of CDX and chemically modified CDX samples	112

List of Tables (Contd.)	Page
5.1 Total nitrogen content in the prepared nitrogen containing carbon nanomaterials	126
5.2 Hydrogen absorption activity of carbon nanomaterials at 1 atm and at different temperatures (corresponding specific surface area (SSA) evaluated by BET method are indicated)	131
6.1 Specific surface area by BET method of various boron containing samples and their hydrogen absorption activity at 1 atm in different temperatures	155

LIST OF FIGURES

Figure	Title	Page
1.1	Global energy systems transition, 1850 – 2150	2
1.2	A comparison of volumetric and gravimetric density of hydrogen with various storage media.....	10
1.3	Schematic of hydrogen chemisorption on metal	13
1.4	Schematic of phase transition in the metal hydride	14
1.5	Rate of hydrogen adsorption by LaNi ₅ . a) Polycrystalline, b) Nanocrystalline, c) Nanocrystalline with catalyst.....	15
1.6	Pressure composition isotherms for hydrogen absorption in a typical metal hydride.....	17
1.7	Van't Hoff plot of some selected hydrides. The stabilization of the hydrides of LaNi ₅ by the partial substitution of Ni with Al in LaNi ₅ is shown, as well as the substitution of La with misch metal (example, 51% La, 33% Ce, 12% Nd, 4% Pr)	19
1.8	Framework structures of zeolites: (a) zeolite A, (b) zeolites X and Y. The corners on each framework represent Si or Al and these are linked by oxygen bridges represented by the lines on the frameworks ...	23
1.9	FCC unit cell of the Buckminster fullerene crystal. Each lattice point has a C ₆₀ molecule.....	33
1.10	The activation energy profile of fullerene to form hydrides	34
1.11	The graphitic nanofibres (GNFs) (a) platelet (b) ribbon (c) herringbone structures	36
1.12	The graphene sheet rolled to form cylindrical single walled nanotube (SWNT).....	37
1.13	(a) Basic structure of a sheet of graphene. Consider the carbon atoms to be placed on each point on the edge of the hexagon. (b). Three different classification of nanotubes, (a) shows a (9,0) zigzag tube, (b) shows a (5,5) armchair tube and (c) shows a (6,4) chiral tube.....	38
1.14	Standard redox potential (V) values of some selected species	47
1.15	Ellingham diagram of the various heteroatoms (hydriding property)	48
2.1	Low pressure volumetric hydrogen absorption apparatus (glass).....	59
2.2	High pressure hydrogen absorption apparatus.....	60

List of Figures (Contd.)	Page
3.1 (a) The side view of the UFF optimized CNT (4, 4) cluster taken for the study, where the terminal positions are saturated with hydrogen (b) Top view of the heteroatom (arrow indicated ball) containing CNT cluster with the hydrogen molecule interaction	81
3.2 The transition state energy profile of the heteroatom substituted CNTs cluster calculated by DFT method (B3LYP) with 6-31g (p, d) basis set	88
3.3 The transition state energy profile of boron substituted CNTs cluster calculated by DFT method (B3LYP) with 6-31g (p, d) basis set	88
3.4 Cluster model chosen for hydrogen activation study in substituted and un substituted fullerene (C ₆₀): (a) heteroatom (X = N, P, S and B) substituted fullerene with hydrogen interaction (b) boron atoms substituted in adjacent positions (c) boron atoms substituted in alternate positions	95
4.1 XRD patterns of various percentages of nickel supported on Calgon carbon.....	105
4.2 SEM images of various weight percentage of nickel loaded on Calgon carbon (a) 2 wt%, (b) 5 wt%, (c) 20 wt% and (d) SEM EDAX of 20 wt% loaded Ni/C	106
4.3 Hydrogen absorption activity of Calgon carbon at various temperatures (a) Hydrogen absorption isotherms at different temperatures (b) Van't Hoff plot of Calgon carbon.....	107
4.4 (a) Hydrogen absorption activity of 20 wt% Ni/C at various temperatures (b) hydrogen absorption activity at 1 atm and at various temperatures (c) Van't Hoff plot for 20 wt % Ni supported on Calgon carbon	108
4.5 Hydrogen absorption activity of 2 wt% Ni/C at various temperatures....	109
4.6 XRD patterns of CDX carbon and its modification by the chemical treatment	110
4.7 FT-IR spectra of CDX-975 and treated CDX-975 samples.....	111
4.8 Hydrogen absorption isotherms of CDX-975 at various temperatures....	112
4.9 Hydrogen storage capacity of CDX-975, Calgon carbon and 20 wt % Nickel loaded on Calgon carbon.....	113
5.1 (a-b) X-ray diffraction pattern of PDC and Raman spectrum of PDC and MEC carbon respectively.....	118

List of Figures (Contd.)	Page
5.2 (a-b) SEM pictures of nitrogen containing carbon nanomaterials prepared by using silica source PDC and MEC respectively. (c - d) the TEM images of PDC and MEC	120
5.3 (a-b) SEM images of carbon nanotubes CNT1 and NCNT1 (c-d) TEM images of CNT1 and NCNT1 respectively	121
5.4 (a-b) XRD pattern and Raman spectra of CNT1 and nitrogen containing CNT (NCNT1) respectively	122
5.5 XRD pattern and Raman spectra of CNT2 and NCNT2 prepared from zeolite as template by using chemical vapor deposition method	123
5.6 (a-b) SEM images of CNT2 and NCNT2. (c-d) TEM images of CNT2 and NCNT2 respectively	124
5.7 XRD pattern and Raman spectra of CNT3 and NCNT3	125
5.8 SEM and TEM images of carbon nanotubes prepared by chemical vapor deposition (CVD) method using clay as template. (a-b) SEM images of CNT3 and NCNT3 and (c-d) TEM images of CNT3 and NCNT3 respectively	125
5.9 (a) EGA profile of Nitrogen containing CNT (b) The EGA profile of Nitrogen containing CNT after recycling (c) EGA profile of pure CNT prepared from polyphenyl acetylene	128
5.10 Cyclic voltammograms of CNT1 and NCNT1	129
5.11 Hydrogen storage capacity of PDC and MEC as a function of hydrogen pressure	132
5.12 High pressure hydrogen absorption activity of carbon nanotubes prepared from alumina membrane and zeolite templates	133
5.13 High pressure hydrogen absorption activity of carbon nanotubes prepared from clay template (CNT3 and NCNT3)	133
6.1 ¹¹ B NMR spectrum of hydroborane polymer in CDCl ₃ solution locked with D ₂ O and BF ₃ .etherate as the standard reference	139
6.2 ¹ H NMR spectrum of hydroborane polymer taken in CDCl ₃ solvent	140
6.3 ¹³ C NMR spectrum of hydroborane polymer	140
6.4 (a-b) TGA and DSC of hydroborane polymer respectively	141
6.5 Pictorial representation of chemical vapor deposition carried out for the production of boron containing carbon nanotubes	144
6.6 X-ray diffraction pattern of boron containing carbon (BC) prepared by polymer carbonization and the inset diagram shows the selected area electron diffraction (SAED) of the sample from TEM analysis	145

List of Figures (Contd.)		Page
6.7	X-ray diffraction patterns of boron containing carbon nanotubes (BCNTs).....	145
6.8	FT-IR spectra of the boron containing carbon nanotubes (BCNTs).....	146
6.9	Raman spectra of boron containing carbon nanotubes prepared by various methods	147
6.10	(a-b) SEM and TEM images of boron containing carbon (BC) sample respectively	148
6.11	SEM images of the boron containing carbon nanotube: (a) side view of the vertically aligned nanotubes of BCNT (b-c) top view of the carbon nanotubes (BCNT 2 and 3) prepared by using zeolite and clay as template respectively	149
6.12	(a) TEM picture of boron containing carbon nanotube (BCNT1) prepared from polymer precursor (b-c) TEM images of boron containing carbon nanotubes (BCNTs 2 and 3) prepared by chemical vapor deposition (CVD) method.....	150
6.13	(a) ^{13}C CP MAS NMR of BCNT and (b) ^{11}B MAS NMR spectrum of boron containing carbon nanotubes	152
6.14	(a) X-ray photoelectron spectrum of boron substituted carbon nanotube (b) The deconvoluted XPS spectrum of B 1s.....	153
6.15	Hydrogen absorption isotherms of boron containing carbon nanotube (BCNT 1) at various temperatures (77 K, 373 K and 423 K).....	155
6.16	High pressure hydrogen absorption activity of boron containing carbon nanotubes	156
7.1	Comparison of hydrogen storage capacity and their morphology variation due to templates used in preparation of carbon nanotubes.....	161

LIST OF SCHEMES

Scheme	Title	Page
3.1	(a) The proposed mechanistic path way for hydrogenation of heteroatom substituted CNTs. (b) Mechanistic pathway for the hydrogenation of boron substituted CNTs in adjacent and alternate positions.....	87
3.2	Proposed transition state pathways for hydrogen storage in fullerene and heteroatom (N, P, S & B) containing fullerene	98
6.1	The preparation of hydroborane polymer.....	138

ABBREVIATIONS

AR	-	Analytical Reagent
atm	-	atmosphere
BE	-	Binding Energy
BET	-	Brunauer, Emmett and Teller
CNT	-	Carbon nanotube
CP MAS NMR-	-	Coupled Plasma Magic Angle Spinning Nuclear Magnetic Resonance
deg	-	degrees
DFT	-	Density Functional Theory
DSC	-	Differential Scanning Calorimetry
E _a	-	Activation energy
HOMO	-	Highest Occupied Molecular Orbital
Hz	-	Hertz
IR	-	Infrared Spectroscopy
LUMO	-	Lowest Occupied Molecular Orbital
ml	-	milliliter
mmol	-	millimoles
MPa	-	Mega Pascal
ppm	-	parts per million
SEM	-	Scanning electron microscopy
SSA	-	Specific Surface Area
TEM	-	Transmission Electron Microscopic
TGA	-	Thermogravimetry Analysis
THF	-	Tetrahydrofuran
UV-Vis	-	Ultraviolet-Visible
XPS	-	X-ray Photoelectron Spectroscopy
XRD	-	X-ray Diffraction

NOTATIONS

eV	-	electron volt
m ² /g	-	Square meter per gram
K	-	Kelvin
G	-	gram
Å	-	Angstrom
d	-	Interplanar spacing planar
nm	-	Nanometer
V	-	Volts
wt	-	Weight
kJ	-	Kilo Joule
h	-	hour
θ	-	Bragg angle
v	-	Frequency
cc	-	Cubic centimeter
%	-	Percentage
°C	-	Degree Celsius
kCal	-	Kilo Calories
μmol	-	Micro mole
μl	-	Micro liter
kCal	-	Kilo Calories
P _o	-	Saturated vapour pressure

CHAPTER 1

INTRODUCTION

1. HYDROGEN ECONOMY

1.1 Why is there a need for alternative energy source?

Fossil fuels in the form of coal, oil, and natural gas have powered human society for few centuries. But, the continuation of fossil fuel based powering of the world threatens our energy supply and puts enormous strain on the environment. Unfortunately, forecasts for energy demands are not so encouraging, due to both the rate of population growth and the increasing energy consumption. The rate of population growth is high and the subsequent compensation of energy demand by the use of fossil fuels is simply unmanageable. Moreover, the global oil and gas reserves were concentrated in a very few regions of the world while the demand is growing everywhere day by day. As a result, a secure supply is becoming increasingly difficult to achieve. The economy of the energy source is truly determined by the countries that possess the petroleum reserve. But, the cost of processing the crude petroleum to the desired user end product is highly expensive.

During the combustion of fossil fuels, the gases released are carbon dioxide and other greenhouse gas emissions. These are associated with global warming that threatens the stability of earth's climate. Hence, new renewable energy systems must be developed. These include solar energy, wind energy, tidal energy and nuclear energy. A major problem with several of the renewable energy sources is that they are intermittent and their energy density is low. Thus, there is a need for an energy carrier

that can act both as a storage and transportation medium to connect the energy source to the energy consumer.

A variety of alternative fuels have been proposed to address these problems including methanol, ethanol, methane, synthetic liquids from natural gas or coal, and hydrogen. Of these, hydrogen offers the largest potential benefits in terms of reduced emissions of pollutants and greenhouse gases and diversified primary energy supply. Hydrogen is an energy carrier which can be used with high efficiency and zero or near zero emissions at the point of use. It has been technically demonstrated that hydrogen can be used for transportation, heating and power generation, and could replace current fuels in all their present uses. The transition towards hydrogen economy is seen from the history of development and it is more evident from the atomic view of energy.

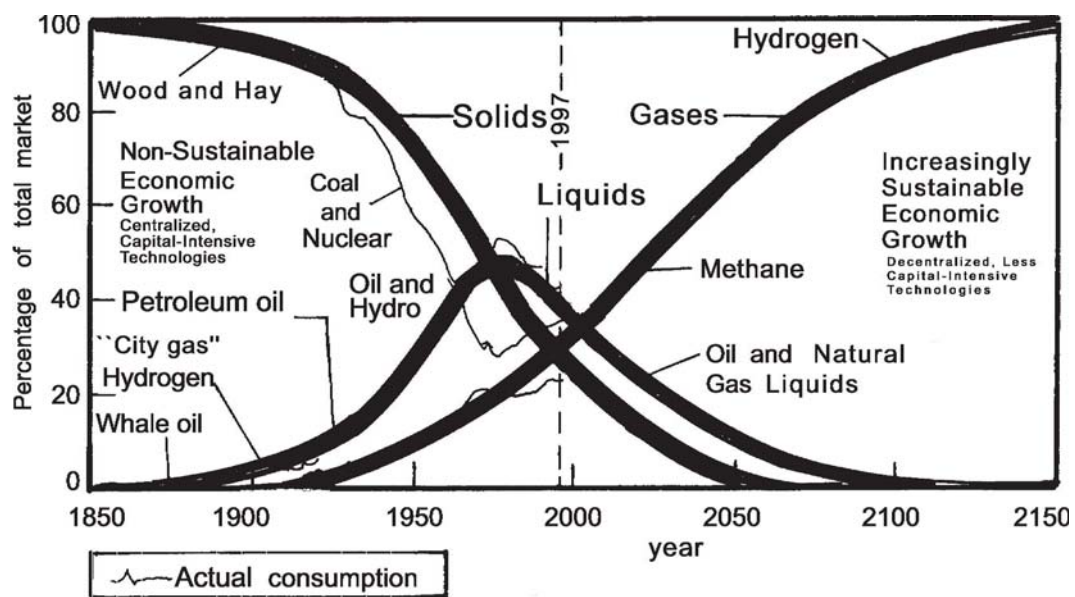


Fig. 1.1 Global energy systems transition, 1850 – 2150 (reproduced from Dunn, 2002)

Since the mid-19th century, the world has been slowly shifting from one form of energy to another — from solids to liquids to gases, as shown in Fig. 1.1.

The move from solid to liquid to gas fuels involves another sort of transition: the less visible process of “decarbonization”. From wood to coal to oil to natural gas, the ratio of hydrogen (H) to carbon (C) in the molecule of each successive source has increased. Roughly speaking, the ratio is between 1–3 and 1–10 for wood; 1–2 for coal; 2–1 for oil; and 4–1 for natural gas. Between 1860 and 1990, the H–C ratio raised six fold. The trend toward ‘decarbonization’ is at the heart of understanding the evolution of the energy system (Carl-Jochen, 2005).

1.2 WHY HYDROGEN?

Hydrogen is the simplest and lightest atom consisting of a single proton and a single electron. Hydrogen is the cleanest, sustainable and renewable energy carrier. In many ways hydrogen seems to be an attractive replacement for existing fossil fuel system by their properties as given in Table 1.1. The most important properties as compared to other conventional fuels on the safety point are:

- **Density:** hydrogen is the lightest of all elements.
- **Diffusion:** hydrogen diffuses through air more rapidly than other gaseous fuels. In this regard, hydrogen rapid dispersion rate is its greatest safety asset.
- **Buoyancy:** hydrogen would rise more rapidly than methane, propane, or gasoline vapor.
- **Color, odor, taste, and toxicity:** hydrogen is colorless, odorless, tasteless, and non-toxic; similar to methane and gasoline.
- **Flammability:** flammability of hydrogen is a function of concentration level and is greater than that of methane and other fuels. Hydrogen burns with a low-visible flame.

- **Ignition energy:** hydrogen can be ignited by a very small amount of energy, if its concentration is neither lean nor very rich.
- **Detonation level:** hydrogen is detonable over a wide range of concentrations when confined. However, it is difficult to detonate if unconfined, similar to other conventional fuels.
- **Flame velocity:** hydrogen has a faster flame speed than other fuels provided its concentration is neither lean nor rich.
- **Ignition temperature:** compared to other fuels, hydrogen has higher ignition temperature.

Table 1.1 Properties of hydrogen compared to other fuel system

Property	Unit	Hydrogen H ₂	Methane CH ₄	Gasoline -(CH ₂)n-
Lower heating value	kWh kg ⁻¹	33.33	13.9	12.4
Self ignition temperature	K	858	813	498-774
Flame temperature	K	2318	2148	2473
Ignition limits in air	Vol %	4 - 75	5.3 - 15	1.0-7.6
Min. ignition energy	mW	0.02	0.29	0.24
Flame propagation in air	m s ⁻¹	0.02	0.4	0.4
Explosion energy	kg TNT m ⁻³	2.02	7.03	44.22
Diffusion coefficient in air	cm ² s ⁻¹	0.61	0.16	0.05
Toxicity		No	No	High

Although hydrogen appears to be a possible replacement for fossil fuels, it does not occur in nature as fuel. Rather, it occurs in the form of chemical compounds like water or hydrocarbons that must be transformed to yield hydrogen.

1.3 PRODUCTION OF HYDROGEN

There are various technical means to generate hydrogen, but none of them can yet compete with fossil fuels in cost, performance, or reliability. At present, most of the world's hydrogen is produced from natural gas by a steam reforming of naphtha. However, steam reforming does not reduce the use of fossil fuels but rather shifts them from end use to an earlier production step and it still releases CO₂ to the environment. Thus, to achieve the benefits of the hydrogen economy, one must ultimately produce hydrogen from non-fossil resources, such as water, using a renewable energy source. Methods of hydrogen production from water include electrolysis, direct thermal decomposition, photochemical and biochemical processes.

1.3.1 Electrolysis

Hydrogen production from water electrolysis is a mature technology, where one can obtain hydrogen and oxygen technically at a theoretical reversible applied potential of 1.23 V. But in practice, electrolysis takes place out at and above 1.7 V due to the over potentials at the respective electrodes (Vogel, 1961). Number of investigations have been carried out to reduce the over potentials of hydrogen and oxygen by suitably modifying the electrode materials or electrode surface. Further, the efficiency of the process was improved up to 90 % by employing Solid Polymer Electrolytic (SPE) process (which employs a proton-conducting ion exchange membrane both as electrolyte and as membrane that separates the electrolysis cell) (Dutta *et al.*, 1990). Advancement in the electrolysis process is by the use of coupling process with the renewable energy sources, particularly with photovoltaics (PV). Theoretical and experimental studies on the performance of photovoltaic-electrolyzer systems have been performed and they were still in the developmental stage (Hancock *et al.*, 1984).

1.3.2 Direct thermal decomposition of water

Direct decomposition of water to give hydrogen and oxygen occurs only at high temperatures above 4000 K, such a source of energy is not available. So attempts have been made to reduce the decomposition temperature by various thermo-chemical routes. Even then, the splitting of water by thermo-chemical methods requires temperatures around 1500 K. The thermochemical cycles include the following: (Wendt, 1987) sulfuric acid–iodine cycle, hybrid sulfuric acid cycle, hybrid sulfuric acid–hydrogen bromide cycle, calcium bromide–iron oxide cycle (UT-3), and iron - chlorine cycle. Only, limited heat sources are available like nuclear reactor, which can provide the required high temperature. The main problem of this method are related to materials required for extremely high temperatures, recombination of the reaction products at high temperatures, toxicity of some of the chemicals involved and separation of hydrogen.

1.3.3 Photocatalytic decomposition of water

Photocatalytic and photoelectrochemical splitting of water for hydrogen production are the other possible routes where one can use sustained energy source *i.e.* sunlight. Though it appears to be convenient, low cost and suitable method for hydrogen production, the maximum efficiency attained so far for this process is only around 18 % in the laboratory scale (Licht *et al.*, 2001). This can be improved by choosing a suitable photocatalyst. Various materials like CdS, TiO₂, Fe₂O₃, ZnO and SrTiO₃ have been investigated for this purpose (Litter, 1999; Kamat, 1993; Kato and Kudo, 1998; Chakrabarti and Dutta, 2004). The band gap and position of band edges with respect to the potential for the water decomposition reaction are the limiting factors that need

to be addressed for the success of this technology. In addition, the light absorption ability of these materials also plays an important role in the efficiency of the process.

1.3.4 Biological methods for decomposition of water

The biological or biochemical methods for the production of hydrogen by splitting water have also been under investigation (Rozendal *et al.*, 2006; Liu *et al.*, 2005). Micro organisms are capable of producing H₂ via either fermentation (Fumiaki *et al.*, 1996; Yokoi *et al.*, 1997) or photosynthesis (Lichtl *et al.*, 1997; Hansel and Lindblad, 1998; Matsunaga *et al.*, 2000). The former is generally preferred, because it does not rely on the availability of light sources and the transparency of the mixed liquor (Hart, 1997). Production of H₂ by fermentation process has been studied with a large group of pure fermentative bacteria, such as *Clostridia* (Heyndrickx *et al.*, 1991; Fumiaki *et al.*, 1993) and *Enterobacteria* (Rachman *et al.*, 1997; Kumar and Das, 2000). Since, the enzymes and bacteria are sensitive to pH and temperature, it is essential to maintain the required conditions to achieve water splitting. Generally, enzyme – hydrogenase, green algae *scenedesmus* (Gaffron and Rubin, 1942), cyanobacteria and *anabaena cylindrical* (Benemann and Weare, 1974; Stal and Moezelaar, 1979) are extensively studied for the splitting of water.

Although the technology for production of hydrogen from renewable sources is well understood, it is currently not utilized for producing hydrogen in large quantities. Hydrogen produced from renewable energy sources is currently too expensive. Production of significant quantities of hydrogen using such methods would take considerable time and investment to develop, to allow capital costs to be reduced to a satisfactory level. However, in the long term, hydrogen offers a potential route for gaining energy independence from fossil fuels.

Though the production of hydrogen is possible by various methods, the major difficulty of utilizing hydrogen as fuel or energy carrier has been the absence of a practical means for hydrogen storage. The storage of hydrogen is a critical component that the world faces today. Developing a high density hydrogen storage system is an essential component of hydrogen economy. Such a system should release hydrogen at room temperature and atmospheric pressure. The gap between the present and required states of art in hydrogen production, storage, and use, which is needed for a competitive hydrogen economy is too wide to bridge in incremental advances.

1.4 HYDROGEN STORAGE

The drawback of utilizing hydrogen as the alternative fuel is the absence of the appropriate storage medium. The challenges and demands faced for the storage of hydrogen can be surmounted if the following aspects are addressed

- Investigation and development of new materials for the storage of hydrogen.
- Developing suitable and reproducible experimental techniques to identify the storage capacity.
- The existing storage medium can be improved considerably and the cost and size of the storage medium can also be reduced. This will be one of the milestones towards the hydrogen economy.

1.4.1 Why should there be a target of hydrogen storage?

For stationary systems, the weight and volume of the system used for hydrogen storage is not a key factor. However, for mobile applications, such as fuel cell electric vehicles (FCEV) or hydrogen-fuelled (internal combustion) cars, hydrogen storage system has to be compact, lightweight, safe and affordable. In 1996, the International

Energy Agency (IEA) established the “hydrogen storage task force” to search for innovative hydrogen storage methods and materials (IEA, 1996). The US Department of Energy (DOE) Hydrogen Plan has set a standard for this discussion by providing a commercially significant benchmark for the amount of reversible hydrogen absorption. The benchmark requires system-weight efficiency (the ratio of stored hydrogen weight to system weight) of 6.5 weight % hydrogen and a volumetric density of 62 kg H₂/m³, since a vehicle powered by a fuel cell would require more than 3.1 kg of hydrogen for a 500 km range. Fig. 1.2. shows that various storage options that meet the long-term needs. The current high pressure hydrogen tanks and liquid hydrogen meet some, though clearly not all, of the near term (2007) targets (Hynek *et al.*, 1997). The hydrogen storage materials for 2007 targets are based upon systems such as, solid-state (e.g. metal hydride) or liquid (e.g. chemical hydride) systems. The focus of the DOE (US) is on materials-based technologies to meet 2010 targets and with potential to eventually meet 2015 targets as given in Table 1.2. The 2015 targets represent what is required based on achieving similar performance to today's gasoline vehicles (greater than 300 mile driving range) and complete market penetration across all light-duty vehicle platforms (Satyapal *et al.*, 2007). The targets include a 20% penalty for the assumption that hydrogen storage systems (unlike conventional gasoline tanks) are not conformable and have limitations on how they may be packaged within a vehicle. The targets also assume a factor of 2.5–3 in terms of efficiency improvement in using a fuel cell power plant as compared to a conventional gasoline internal combustion engine. If efficiency improvements are not as high as projected, this would clearly dictate even more challenging requirements for on-board hydrogen storage to achieve comparable driving range. Currently, extensive efforts have been made to develop methods for hydrogen storage, including

metal hydrides, porous solids and more recently, nano-structured carbons. The development of a high capacity, lightweight material that could be used to reversibly store hydrogen under ambient conditions, seems to be attainable.

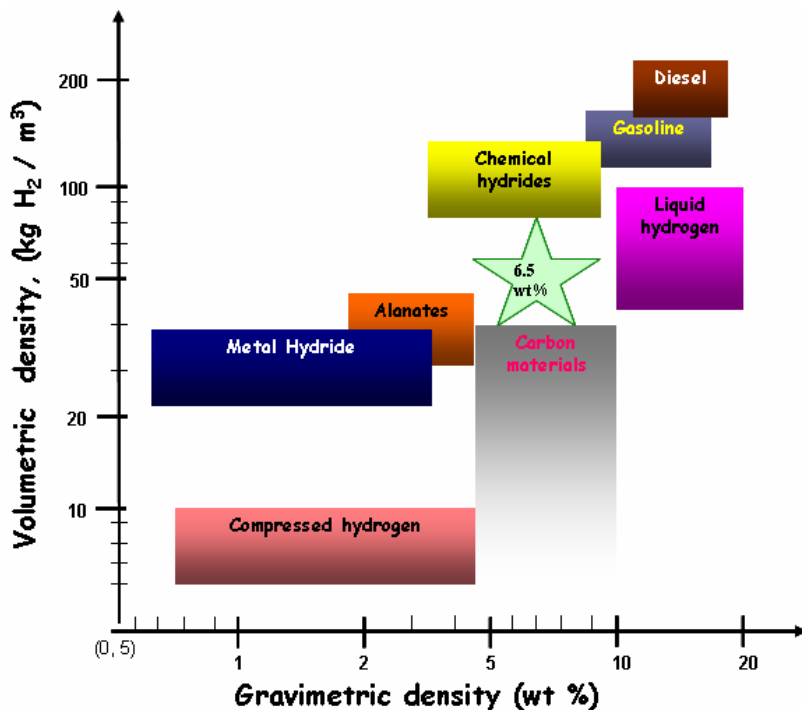


Fig. 1.2 A comparison of volumetric and gravimetric density of hydrogen with various storage media (reproduced from Hynek *et al.*, 1997)

Table 1.2 DOE targets for on-board hydrogen storage

Storage parameter	Unit	DOE technical targets		
		2007	2010	2015
Gravimetric energy density	MJ/kg	5.4	7.2	10.8
Gravimetric hydrogen density	wt. %	4.5	6	9
Volumetric energy density	MJ/L	4.32	5.4	9.72
Volumetric hydrogen density	kg H ₂ /m ³	36	45	81
Cycle life	Cycles	500	1000	1500
Min/max delivery temperature	°C	-20/85	-30/85	-40/85
Min H ₂ delivery pressure	atm	8	4	3
System fill time (5 Kg H ₂)	min	10	3	2.5

A viable on-board automotive hydrogen storage system must be compact, lightweight, low cost and safe. Moreover, it must be capable of storing enough hydrogen to provide a reasonable traveling range, and good dormancy (ability to retain hydrogen for a long period of time without leakage) (Berry and Aceves, 1998).

1.5 GASEOUS HYDROGEN STORAGE

The most traditional way of storing hydrogen is in the gaseous form in pressure vessels. Since, hydrogen behaves like an ideal gas at the ambient temperature (and the temperatures below) it satisfies the ideal gas law $PV = nRT$, where n is the amount of hydrogen in moles and R is the gas constant.

In a given volume and temperature, the energy density of storage is increased by increasing the pressure of storage vessel. The only problem of this are the safety features and regulations that limit the allowable pressure. But the gravimetric energy density of hydrogen storage is largely dependent on the material of the container since light materials usually do not tolerate high pressures. Today, modern storage tanks can be made with carbon fiber composite materials which are ultra light with permeation resistance with tough impact resistant reinforced shell. These are ten times stronger than steel allowing them to store hydrogen at pressures in excess of 350 bar, which can be safely used for over 100,000 refill cycles and withstand surface temperatures over 1073 K (Quantum, 2003). However, the potential risk associated with very high-pressure systems is the procedure of compressing hydrogen. This raises important practical problems as there is currently no practical solution to refilling cylinders in a domestic situation to such high pressures rapidly and safely.

1.6 LIQUID HYDROGEN STORAGE

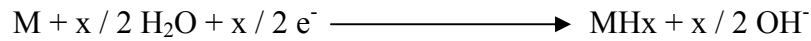
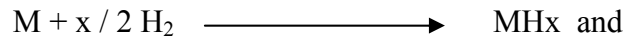
Liquid hydrogen has been used as a fuel in space technology for several years (Sherif, 1997). It is light and has less potential risks compared to the compressed gas in terms of storage pressure. However, hydrogen liquifies at 20.25 K (Greenwood and Earnshaw, 1997). Thus the storage vessels require sophisticated insulation techniques in order to minimize the unavoidable heat transfer leading to hydrogen loss via boil-off. Research in this area is currently focused on finding improved insulation and cooling methods (Wolf, 2002). Hydrogen boil-off and the high cost of sophisticated insulating techniques required for maintaining very low temperatures coupled with the initial energy cost to create liquid hydrogen, makes this method of hydrogen storage impractical for application in hydrogen fuel cell powered vehicles.

1.7 SOLID HYDROGEN STORAGE

Among various options of hydrogen storage, storage by the solid matrices alone appears to be appropriate. This method offers more safety and comfort for transport applications.

1.7.1 Metal hydrides

Hydrogen can be combined with many metals to form hydrides that will release hydrogen on heating (Bentzen *et al.*, 2001). Metal hydrides are composed of metal atoms that constitute a host lattice and hydrogen atoms that are trapped in interstitial sites. Since absorption of hydrogen increases the size of lattices, the metal is usually ground to powder in order to prevent the decrepitation of metal particles. There are two possible ways of hydriding a metal, direct dissociative chemisorption and electrochemical splitting of water. These reactions are, respectively



where M represents the metal. In the electrochemical splitting there has to be a catalyst, such as palladium.

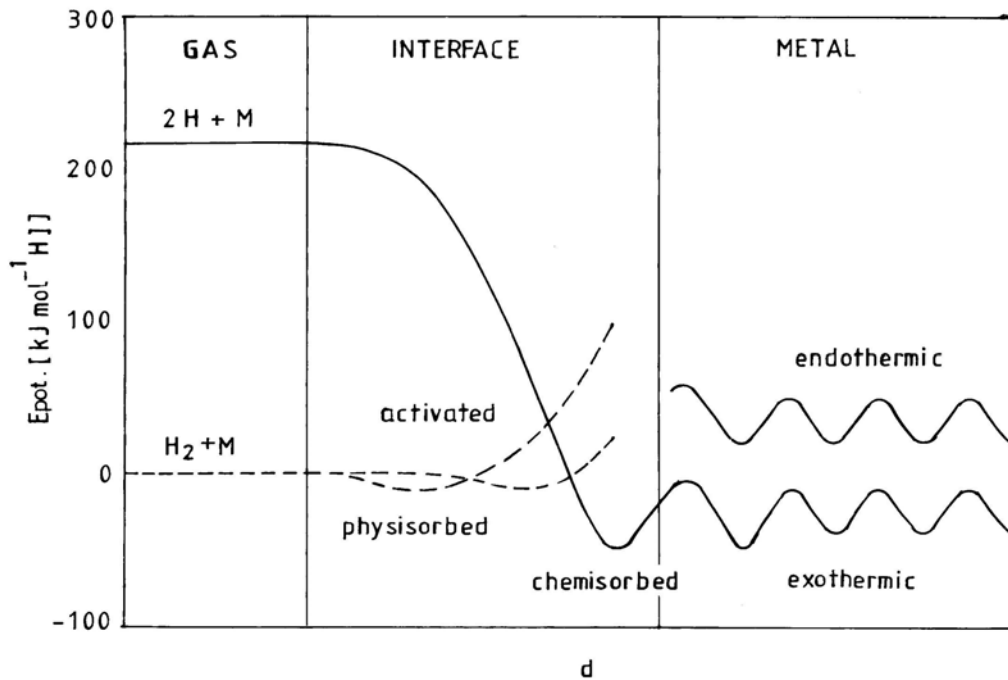


Fig. 1.3 Schematic of hydrogen chemisorption on metal (reproduced from Schlapbach, 1988; Christmann, 1981)

A schematic of hydrogen chemisorption is shown in Fig. 1.3. As shown in the figure, molecular hydrogen reaches a shallow potential minimum near the surface and the atomic hydrogen shows a deeper minimum almost at the surface. In the metal lattice, hydrogen has periodic potential minima in the interstitial sites. As the hydrogen molecule approaches the metal surface, weak van der Waal's forces begin to act upon the molecule, drawing it closer. The molecule reaches the potential well. Very large forces would be required to force it in molecular form. However, the dissociation energy of hydrogen molecule is exceeded by the chemisorption energy. Thus, the hydrogen molecule dissociates and individual hydrogen atoms are attracted to the

surface by chemisorptive forces and they reach the potential well. Even the thermal energy at the ambient temperature is sufficient to increase the vibrational amplitude of hydrogen atoms which can thus reach and enter the metal surface.

Metal and hydrogen usually form two different kinds of hydrides namely α -phase and β - phase hydride. In the α -phase there is only some hydrogen absorbed and in the β -phase the hydride is fully formed. For example, Mg_2Ni forms hydrides of $Mg_2NiH_{0.3}$ and Mg_2NiH_4 . When initially charged the α -phase of the hydride is formed. Subsequently charging and discharging cycles leads to β -phase.

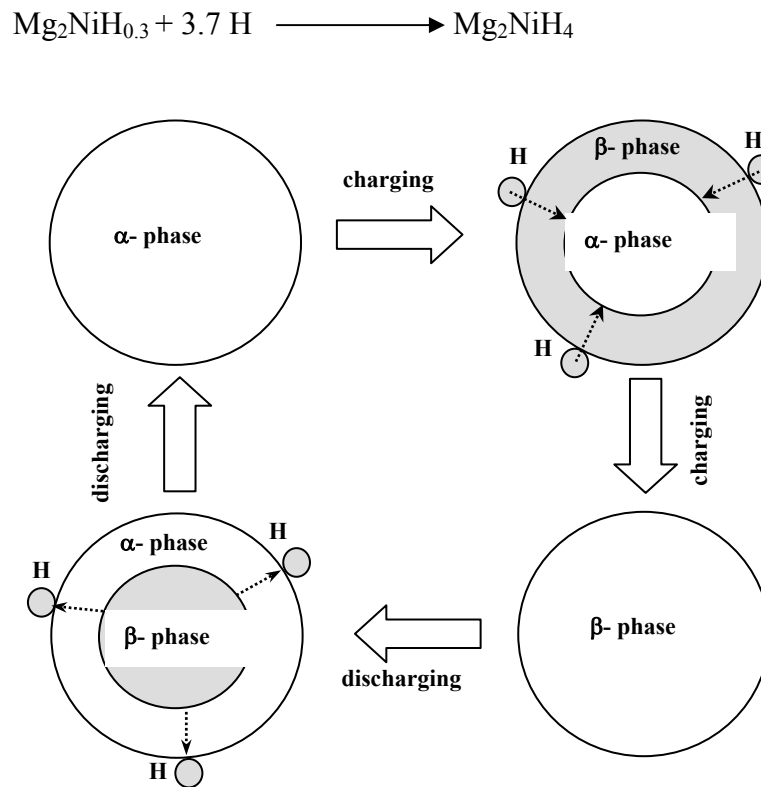


Fig. 1.4 Schematic of phase transition in the metal hydride (reproduced from Christmann, 1981)

A schematic of phase transition for metal hydride is presented in Fig. 1.4. During charging, hydrogen diffuses from the surface of the particle through the β -phase to the phase-transition interface and forms additional β -phase hydride (Chuang *et al.*, 2001). During discharging, hydrogen from the phase-transition interface diffuses through the α -phase to the surface of the particle where it is recombined to form molecular hydrogen. The studies of nano-scaled particles show that when the metal grains are in the range of 5 to 50 nm, the kinetics of both absorption and desorption is improved by an order of magnitude because of improved thermal conductivity. The kinetics of sorption can also be improved with a catalyst. These catalysts can be either in liquid or solid form. But, because the catalyst does not affect the overall reaction, its amount should be kept as low as possible in order to keep the storage capacity sufficient. The effect of the nanostructure and catalyst on the hydrogen absorption of LaNi_5 is shown Fig 1.5.

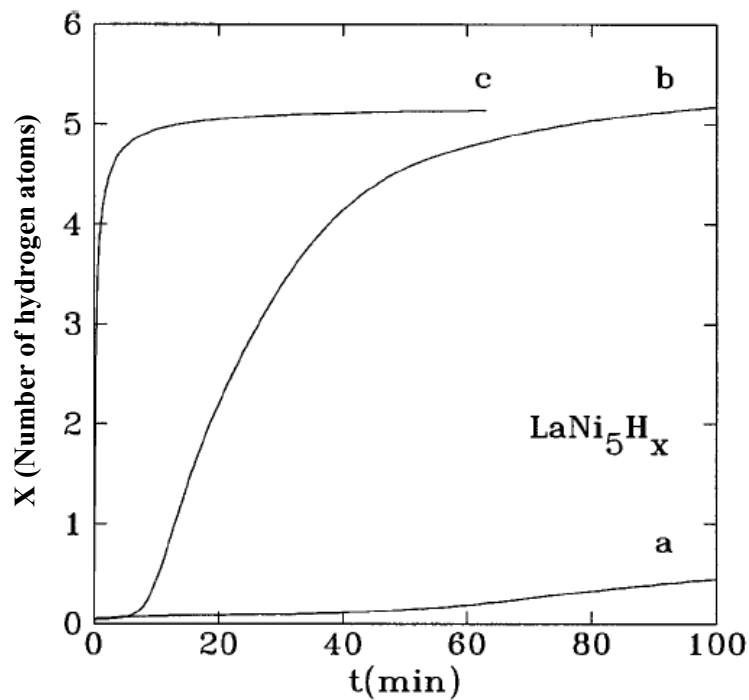


Fig. 1.5 Rate of hydrogen adsorption by LaNi_5 . a) Polycrystalline, b) Nanocrystalline, c) Nanocrystalline with catalyst (reproduced from Ström-Olsen *et al.*, 2001)

The most common characterization method of a metal hydride system is to trace the PCT (pressure – concentration – temperature) curve in the form of $P - C$ isotherms. A theoretical $P - C$ isotherm with α - and β -phases is shown in Fig. 1.6. The concentration, i.e. the hydrogen capacity, is usually defined as hydrogen atoms per metal species H/M . In order to characterize the metal hydride, it is convenient to use the maximum hydrogen capacity $(H/M)_{max}$. The reversible capacity $\Delta (H/M)$, defined as the plateau width, is also a useful tool while considering the hydrogen storage capacity of metal hydrides.

The thermodynamic reaction equilibrium is defined by the equilibrium constant K

$$RT \ln K = \Delta H - T\Delta S$$

Where, ΔH is the reaction enthalpy and ΔS , the reaction entropy. For a solid-gas reaction, the equilibrium constant reduces to the pressure of the gas. Thus the Van't Hoff equation is obtained.

$$\ln P = \Delta H / RT - \Delta S / R$$

Plotting the equilibrium (P, T) -values on $\ln P$ versus $1/T$ scale gives the Van't Hoff plot. The reaction enthalpy can be derived from the gradient of the plot and the plot indicates the suitability of $P - T$ behavior of a hydride for practical applications. The theoretical Van't Hoff plot usually describes the real properties of metal hydrides.

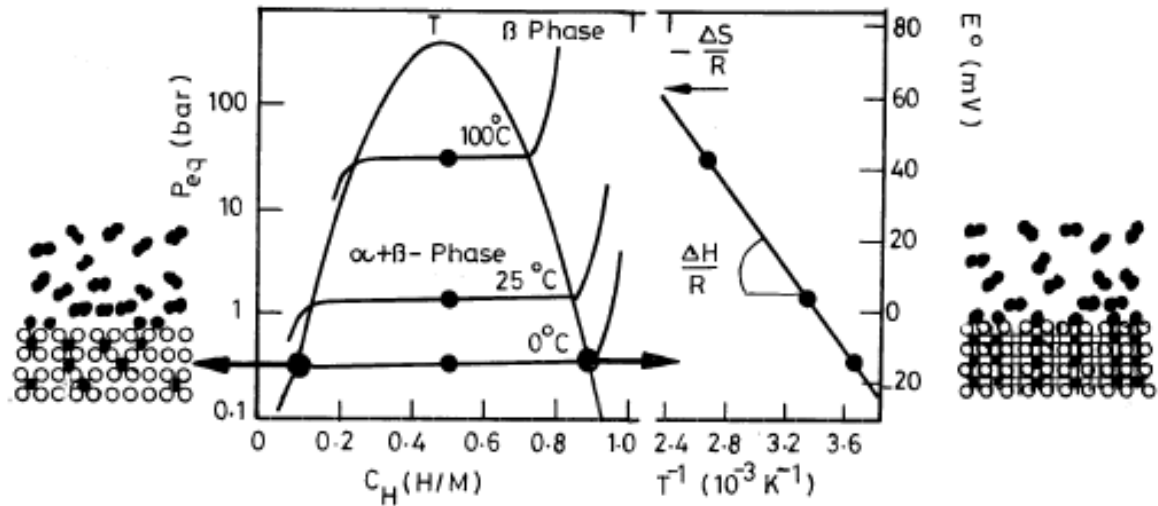


Fig. 1.6 Pressure composition isotherms for hydrogen absorption in a typical metal hydride (Schlapbach and Zuttel, 2001)

In Fig. 1.6. the solid solution (α -phase), the hydride phase (β -phase) and the region of the co-existence of the two phases are shown. The region of co-existence is characterized by the flat plateau and ends at the critical temperature T_c . The construction of the Van't Hoff plot is shown on the right hand side. The slope of the line is equal to the enthalpy of formation divided by the gas constant and the intercept is equal to the entropy of formation divided by the gas constant. The reaction enthalpy of hydride formation is an important quantity. It is usually negative, so the reaction is exothermic and thus the hydride formation releases energy. Therefore dehydration needs energy input. Since most of the applications are at ambient temperature, or at least in the range of 273-373 K, the reaction enthalpy should be quite small so that the hydride could take heat from the surroundings while releasing hydrogen. In some fuel cell systems, the hydride can take heat directly from the fuel cell. The reaction enthalpy also affects directly the stability of a hydride since the gas pressure varies exponentially. The essential requirements that should be satisfied by metal hydrides proposed for hydrogen storage application at a commercial level are summarized below.

- High content of hydrogen storage.
- Facile reversibility of formation and decomposition reactions. The hydride should be decomposable at moderate temperatures that can be provided from locally available heat sources, like solar, automobile exhaust and waste heat sources.
- Absorption-desorption kinetics should be compatible with the charge-discharge requirements of the system.
- The equilibrium dissociation pressure of the hydride at peak desorption rate should be compatible with the safety requirements of the hydride containment system. The hydride itself should have a high safety factor.
- The hydride should have a sufficient chemical and dimensional stability to permit its being unchanged over a large number of charge–discharge cycles.
- Minimal hysteresis in adsorption–desorption isotherms.
- The hydride should be reasonably resistant to deactivation by low concentrations such as O₂, H₂O, CO₂ and CO.
- The total cost of hydride (raw materials, processing and production) should be affordable for the intended application. Long term availability of raw materials (ie. the metal resources), must be ensured. The cost of the hydride system (which includes its containment) per unit of reversibly stored hydrogen should be as low as possible.
- The cost of storage vessel and ancillary equipment and the fabrication/installation costs should be moderate.
- Operating and maintenance costs and purchased energy requirements (that is, energy other than waste energy and energy extracted from the ambient air) per storage cycle should be low.

A careful combination of technical and economic considerations will determine the suitability of a hydride product for a given hydrogen storage or hydrogen containment application. Hydrogen storage capacity of some of the metal and intermetallics are given in Table 1.3.

Table 1.3 Hydrogen storage capacity of metallic and intermetallic systems

Material	P_{des} (atm)	T (K)	H-atoms/ $cm^3(x10^{22})$	Weight % of hydrogen
MgH_2	$\sim 10^{-6}$	552	6.5	7.6
Mg_2NiH_4	$\sim 10^{-5}$	528	5.9	3.6
$FeTiH_2$	4.1	265	6.0	1.89
$LaNi_5H_6$	1.8	285	5.5	1.37

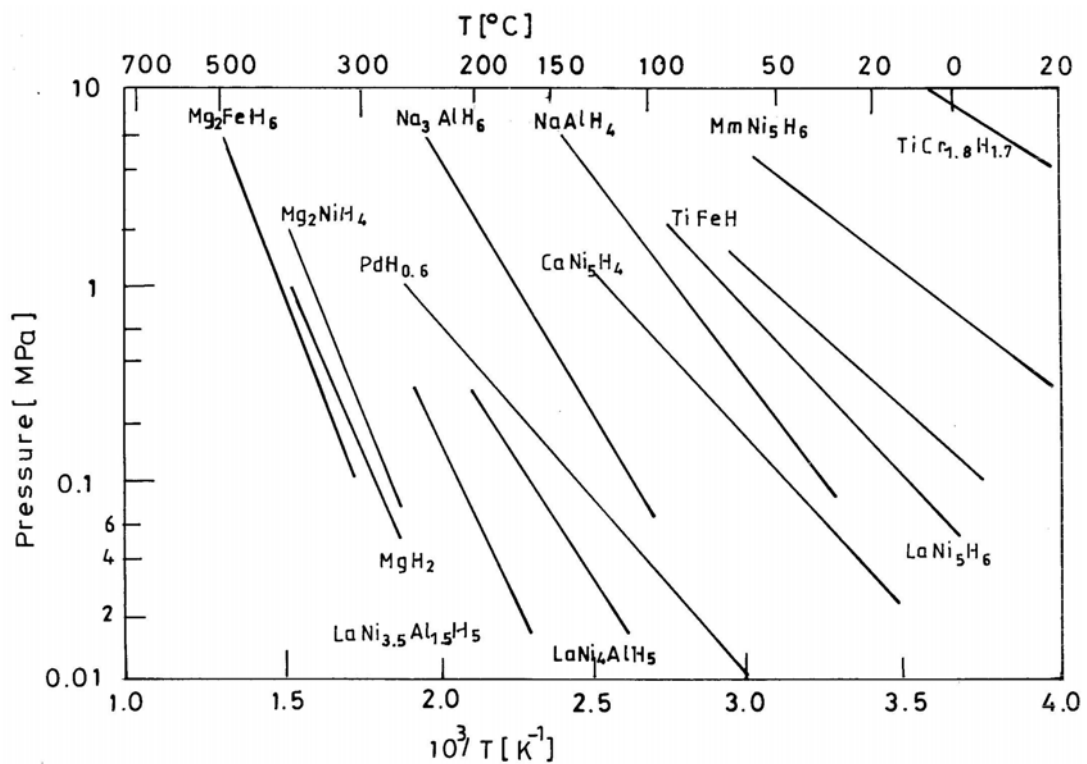


Fig. 1.7 Van't Hoff plot of some selected hydrides. The stabilization of the hydrides of $LaNi_5$ by the partial substitution of Ni with Al in $LaNi_5$ is shown, as well as the substitution of La with misch metal (example, 51% La, 33% Ce, 12% Nd, 4% Pr) (reproduced from Zuttel, (2004))

Metal hydrides are effective in storing large amounts of hydrogen in a safe and compact way. All the reversible hydrides working around ambient temperature and atmospheric pressure consist of transition metals; therefore, the gravimetric hydrogen density is limited to less than 3 mass %.

It remains a challenge to explore the properties of the lightweight metal hydrides. This is formed from palladium coated nanostructured magnesium films, which are reported to be able to adsorb approximately 5 wt% at 373 K under a hydrogen atmosphere of 1 bar and completely desorb below 373 K under vacuum (Yamamoto *et al.*, 1999). It has also been found that in some metal hydride systems, such as magnesium hydride, the adsorption could be drastically improved by ball milling magnesium with nanometer size catalysts of nickel and iron under a 10 bar argon atmosphere (Zaluska *et al.*, 1999 a-b). To date, the highest recorded hydrogen capacity for a metal hydride, applicable for fuel-cell electric vehicles is 2.6 wt%. This was recorded for a chromium-titanium-vanadium alloy at 313 K, under ambient pressure. Thus, with the promising results observed to date, metal hydrides clearly have potential as hydrogen storage systems, with the limits of this potential yet to be fully defined.

1.7.2 Complex metal hydrides

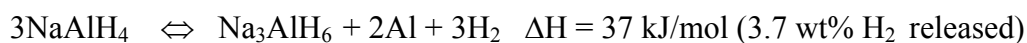
Non-transition metal hydrides, also known as complex metal hydrides, have been shown to have a high theoretical hydrogen storage capacity as indicated in Table 1.4. and are relatively inexpensive.

Table 1.4 Common complex hydrides for hydrogen storage applications

Hydride	^a H ₂ Content (wt %)
LiAlH ₄	10.5
NaAlH ₄	7.5
KAlH ₄	5.7
Be(AlH ₄) ₂	11.3
Mg(AlH ₄) ₂	9.3
Ca(AlH ₄) ₂	7.7
Ti(AlH ₄) ₄	9.3
LiBH ₄	18.0
NaBH ₄	10.4
Al(BH ₄) ₃	17.0

^aMaximum theoretical hydrogen storage capacity

Group I, II and III metals, e.g. Li, Na, Mg, B and Al give rise to a large variety of metal hydrogen compounds. They are especially interesting because of their lightweight and high hydrogen storage capacity. The hydrides of boron, tetrahydroborates M(BH₄)_x and the tetrahydroaluminates (Alanes) are interesting storage materials. E.g. LiAlH₄, NaAlH₄, Mg(AlH₄)₂, Ca(AlH₄)₂ and Ti(AlH₄)₄. Initial reports on some of these materials, such as aluminium hydrides, claimed that the hydrogen was bound irreversibly. Alanes can decompose to give the hydrogen through a series of reactions as follows.



The two above mentioned reactions occur at two different temperatures and the second step of decomposition requires temperatures above 373 K. The total hydrogen capacity is 5.6 wt%. Use of alanates as reversible hydrogen storage system has several advantages over other conventional metal hydride systems. The low molecular weight of the alanates allows for the greater amount of hydrogen storage per unit weight of storage materials. These potential benefits of using alanates as hydrogen storage systems were overshadowed by the fact that the synthesis of alanates is a difficult process and the kinetics of the reaction used to store the elemental hydrogen is slow. However in 1996, it was shown that by doping sodium alanate (NaAlH_4) with titanium catalyst, hydrogen binding of up to 4 wt% at 473 K could be made reversible with an enhanced kinetic release rate (Bogdanovic and Schwickardi 1997). Both ball milling and doping with transition metals like vanadium (V) result in a lowering of the decomposition reaction temperature. Several research groups are currently working on optimizing the system with metal catalyst (Gross *et al.*, 2002; Sandrock *et al.*, 2002). Another group has reported that milling, in the presence of carbon, also enhances the reversible hydrogen capacities of the sodium alanates. It was reported that storage capacities of 2.5-3.0 wt% have been achieved at 353-413 K and 4.5-5 wt% at 423-453 K (Zaluska *et al.*, 2000). The required temperatures and reaction rates for the operation of sodium alanates and variants, are however, still inadequate for applications and the exact mechanism of the catalyst is still unknown. In addition, the hydrogen release of the systems is still not optimized. It is because the full storage capacity is lost after the first cycle (Sandrock *et al.*, 2002). This leaves researchers working with sodium alanates with many questions to answer.

1.7.3 Zeolites

Zeolites are microporous inorganic compounds with an effective pore size of about 0.3 – 1.0 nm. At ambient temperatures, the pore entrances are not sufficient to allow hydrogen molecules into the structure. However, at elevated temperatures and pressures hydrogen molecules are forced to penetrate the cavities. Subsequent cooling to room temperature and release of excess pressure causes the hydrogen molecules to become encapsulated (or trapped) within the pores. When the zeolite is reheated the hydrogen molecules are released. Zeolites have structures based on TO_4 tetrahedra, where T is a silicon or aluminum atom. Depending on the structure, Si / Al – ratio, and substituting atoms, such as Na, K, and Pd, zeolites are named as zeolite A, X, Y, or mordenites etc (Langmi *et al.*, 2003). An example of the pore structure of zeolites is given in Fig. 1.8.

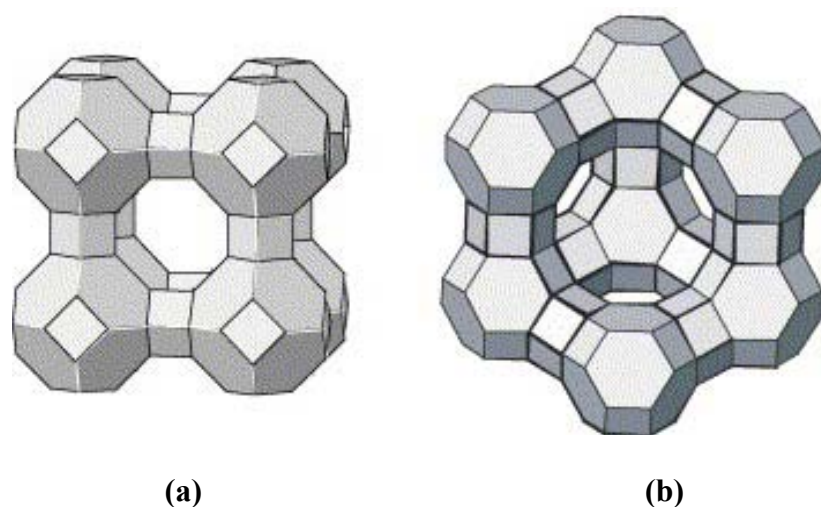


Fig. 1.8 Framework structures of zeolites: (a) zeolite A, (b) zeolites X and Y. The corners on each framework represent Si or Al and these are linked by oxygen bridges represented by the lines on the frameworks

The hydrogen storage capacity of zeolites is poor. At temperatures in the range of 473 – 573 K and pressures of about 100 – 600 bar about 0.1 – 0.8 wt% of hydrogen is stored. By modifying the zeolite (Fraenkel and Shabtai, 1977) hydrogen storage

capacity has been increased. One of the modifications is the increase in ionic radius from Na^+ to K^+ but decreased for larger Rb^+ and Cs^+ ions. The observed trend has been explained by the decrease in effective critical pore size as the ionic radius increases implying the increased ability for encapsulations while the available intracrystalline void volume per gram of zeolite decreased. Maximum storage capacity of $9.2 \text{ cm}^3 \text{ (STP) g}^{-1}$ (i.e. 0.08 wt.%) obtained for sodalite if loaded at 573 K and 100 bar, and concluded that hydrogen encapsulation capacity was generally higher for zeolites having a reasonable portion of small cavities in their structure (Weitkamp *et al.*, 1995). The stability of zeolites for cycling hydrogen storage has not been studied. Ernst *et al.*, suggested that there may be potential in zeolite by applying sophisticated techniques of synthesis and modification. (Ernst *et al.*, 1995). However, this is yet to be verified.

1.7.4 Glass spheres

Glass spheres are small hollow glass micro-balloons whose diameter varies from about 25 μm to 500 μm and whose wall thickness is about 1 μm . The microspheres are filled by heating in high-pressure hydrogen to temperatures sufficient for rapid diffusion of hydrogen into the microspheres. Upon cooling, the low diffusivity of hydrogen at ambient temperatures causes the gas to be retained in the microspheres. Hydrogen is then released when needed by reheating the microspheres (Schmitt *et al.*, 2006). Due to the inherently poor thermal conductivity of inorganic glasses, a problem further exacerbated by the morphology and size of hollow microspheres, poor hydrogen release rates have limited further development and implementation of this hydrogen storage method. A possible solution to the poor hydrogen release rates has been realized with the discovery of photo-induced

outgassing in which a high-intensity infrared light is used to elicit hydrogen release in selectively doped glasses (Rapp and Shelby, 2004). This process results in faster response times for the release of hydrogen in glasses than can be obtained by normal heating and may provide a path to superior performance for hydrogen storage in glass microspheres. However, high pressure and high temperature are stumbling blocks in the use of glass sphere as hydrogen storage medium for mobile applications. The storage capacity of spheres is about 5 – 6 wt% at 200 – 490 bar.

1.7.5 Metal organic frameworks (MOFs)

Recent studies have shown a promising new class of hydrogen storage compounds of porous metal coordination structures. The material is composed of a metal organic framework (MOFs) with a cubic, three-dimensional, extended porous structure. The open channels in MOFs are perfectly ordered allowing effective access of hydrogen to the interior space. The internal surfaces of MOFs can be modified to change the channel curvature thus enhancing the H₂ sorbent interactions. The “one-pot” synthesis is simple, cost effective, and reproducible. More importantly, the structures of these materials, including the metal building unit, pore dimension, shape, size, and volume, can be systematically tuned for the purpose of modifying and improving hydrogen uptake and adsorption/desorption properties. In particular, cubic frameworks consisting of tetrahedral [Zn₄O]⁶⁺ clusters linked by organic units were discovered to adsorb H₂ reversibly up to 1.6 wt % at 77 K and 1 atm (Rowsell *et al.*, 2004). The studies of Rosi *et al.*, through inelastic neutron scattering of molecular H₂ adsorbed in MOFs indicated that both the metal-oxide clusters and the organic units are the adsorption sites for hydrogen (Rosi *et al.*, 2003). Therefore, the hydrogen storage capacities of MOFs can be significantly modified by replacement of Zn²⁺ with other

similar metal ions, such as, Mg^{2+} , Ni^{2+} , or Cu^{2+} , or/and a variation of the organic linking units. Ferey *et al.*, reported a high hydrogen storage capacity of 3.8 wt % in the metal-benzendicarboxylate $\text{Al}(\text{OH})(\text{O}_2\text{C}-\text{C}_6\text{H}_4-\text{CO}_2)$, MIL-53, at 77 K and 1.6 MPa (Ferey *et al.*, 2003). However, no significant hydrogen uptake on the MOFs have been obtained at room temperature. Understanding the relationship between these structural factors and hydrogen uptake in a more quantitative way would be helpful for the development of MOFs as efficient hydrogen storage materials. As a potential hydrogen storage material MOFs are still in its infancy and the work is yet to be independently confirmed.

1.7.6 Chemical storage

Chemical hydrogen storage may offer options with high energy densities and potential ease of use, particularly if systems involve liquids that may be easily dispensed using infrastructure similar to today's gasoline refueling stations. Most of these reactions are irreversible. So the spent storage material would have to be regenerated off-board the vehicle because they cannot be reconstituted simply by applying an overpressure of hydrogen gas at modest temperature and pressure. A number of chemical systems, both exothermic and endothermic hydrogen release, are currently under investigation.

Chemical compounds containing hydrogen can also be considered as a kind of hydrogen storage. These include e.g. methanol (CH_3OH), ammonia (NH_3), and methyl cyclohexane ($\text{CH}_3\text{C}_6\text{H}_{11}$) (Hodoshima *et al.*, 2003). Under STP conditions all of these compounds are in liquid form and thus the infrastructure for gasoline could be used for transportation and storage of these compounds. There is a clear advantage compared to gaseous hydrogen, which demands leak-proof, preferably seamless, piping and vessels. The hydrogen storage capacity of these chemical compounds is

good – 8.9 wt% for CH₃OH, 15.1 wt% for NH₃, and 13.2 wt% for CH₃C₆H₁₁. These figures do not include the containers in which the liquids are stored. Because the containers can be made of light-weight composites or even plastic in some cases, the effect of the container is negligible especially with larger systems (Maria *et al.*, 1996).

Number of processes have been tried to release hydrogen from ammonia borane in the solid state and in solution. Catalysts, including a range of acids and transition metal complexes, have been demonstrated (Bluhm *et al.*, 2006) and are being optimized to enhance the amount of hydrogen released as well as the overall kinetics for hydrogen release. However, efficient and cost effective regeneration of the spent fuel resulting from the dehydrogenation of ammonia-borane is critical to the successful application of ammonia-borane as an on-board hydrogen storage material.

Chemical storage of hydrogen also got some disadvantages. The storage method is non-reversible, i.e. the compounds cannot be “charged” with hydrogen reproducibly. The compounds must be produced in a centralized plant and the reaction products have to be recycled somehow. This is difficult especially with ammonia, which produces highly environmentally unfavorable nitrogen oxides. Other compounds produce carbon oxides which are also unfavorable.

1.8 CARBON MATERIALS

1.8.1 Why carbon materials for hydrogen storage?

Carbon materials are attractive candidates for hydrogen storage, because of a combination of adsorption ability, high specific surface, pore microstructure and low mass density. Hydrogen sorption by carbon nanomaterials has assumed considerable importance in recent times especially from the context of following properties.

Coordination number is variable/expandable

The carbon cluster that can be formed can be varied with the cluster size starting from 2 – 2000 carbon atoms. The three well-known forms of carbon are diamond, graphite and fullerenes. In diamond each carbon has four bonds to its neighbours and forms a three-dimensional lattice. Graphite is built up of two-dimensional hexagonal sheets of carbon atoms where the carbon–carbon distance in the plane is 1.42 Å and the distance between the sheets is 3.35 Å.

Promote new morphologies

Various morphologies are promoted by carbon alone which form sheets in the case of graphite where hard crystalline solid form is seen in diamond. Carbon materials different morphologies namely cone, onion, belt, sphere are known.

Covalent character retention

In spite of a variety of morphologies being possible the covalency of the carbon atoms is maintained and retained in the structure. The strong covalent in-plane bonding and weak van der Waals interplane bonding result in anisotropic physical properties which are useful for applications in lubrication and other processes requiring ‘slippage’ between layers. The in-plane carbon–carbon bonds are shorter than those of diamond, but the interlayer distance is large.

Variable hybridization possible

Existence of variable hybridization states is possible in carbon from sp – sp^3 . Variable valency states of fractional values are also possible. The classical example of the difference between sp^3 and sp^2 bonding properties seen in diamond and graphite.

For diamond, the three-dimensional, four-fold coordinated sp^3 structure is rigid and almost isotropic in its properties. In contrast, the sp^2 bonding in graphite is planar and three-fold coordinated in the planes with weak bonding between the planes. Besides the usual hybridization (sp^3 , sp^2 , sp^1), structures involving more than single type of hybridization (mixed forms) and intermediate hybridization of type sp^n (with $3 > n > 1$, $n \neq 2$) are included. The former cover mixed short-range order carbon species with more or less randomly distributed C atoms, while the latter describe structure in which curvature introduces strains responsible for the mixture of different hybridization. For example the structure of fullerene C_{60} facilitates attribution of intermediate hybridization of sp^2 and sp^3 to the carbon atoms. These details are given in Table 1.5.

Table 1.5 Classification scheme for carbon allotropes, molecular crystals and derived forms

sp^3	sp^2	sp^1
Diamond Cubic Hexagonal	Graphite Hexagonal Rhombohedral	Carbyne α - Carbyne β - Carbyne Chaoite
$sp^3 + sp^2 + sp^1$	sp^n (with $3 > n > 1$, $n \neq 2$)	
Mixed forms of carbon Amorphous carbon Glassy carbon Carbon black Adamantine carbon	Intermediate forms of carbon	
	$3 > n > 2$ Fullerene, C_x $x = 60, 70, 84, \dots$ (when $x = \infty$, $n = 2$) Carbon onions Carbon nanotubes	$2 > n > 1$ Cyclo (N) carbons $N = 18, 24, 30, \dots$ (when $N = \infty$, $n = 1$)

Geometrical possibilities/size considerations

Various geometric forms can be obtained like platelet, sheet, and disk, flower, cones and ball shape

Metastable state

Carbon can form metastable compounds where the most stable form of carbon is graphite. However, the hardest substance with crystalline nature (diamond) is metastable state.

Similarity to biological architectures “Haeckelites”

The biological structures are formed by the carbon materials like helical structure as DNA and the equal number of hexagons and heptagons can lead to the formation of different morphology.

Boron and nitrogen doped graphitic arrangements promise important applications

The substitution in graphite is possible inspite of the fact that it is a more stable form of carbon. Subsequently, the substitution can be possible in all the metastable forms of carbon. The electronic properties of the materials can be drastically changed by the presence of impurities. When an impurity is added to a system, a slight modification is observed in the energy bands. From the electronic point of view, two types of impurities can be present, donor and acceptor impurity. In the former one, also called n-type doping, the impurity provides an extra electron, which can only be accommodated in the conduction band (for example N in carbon materials). The p-type doping impurity provides one electron less to the system and therefore leaves one state unoccupied in the valence band (B in C systems). Since a carbon

atom is small and the average C - C distance is only 1.41 Å in graphite, it is believed that the only likely substitution dopant in graphite is boron. However few studies have already been reported about N-doped graphite. Since diamond has a larger C-C distance equal to 1.54 Å, between the neighboring atoms both boron and nitrogen can enter in the diamond lattice substitutionally. Fullerenes and carbon nanotubes which are metastable can undergo substitution.

Usable Capacity Ratio (UCR)

The performance of a carbon sorbent to meet the requirement of storage property can be judged by usable capacity ratio (UCR). It is a measure of the effectiveness of sorption compared with gas compression at the same pressure. The UCR is defined as the mass of available fuel in an adsorbent-loaded vessel divided by the mass of available fuel in a vessel without adsorbent (compressed gas only). The available fuel, in this case hydrogen, is the mass of hydrogen in the vessel at the storage, or working pressure, minus the mass of hydrogen in the vessel at the discharge pressure. Various forms of carbon materials like activated carbon, fullerenes, carbon nanomaterials (fibers, plates and tubes) have shown UCR greater than unity. Extensive research has been carried to find out carbon materials who's UCR greater than unity.

1.8.2 Activated carbon

Activated carbon is a synthetic carbon containing very small graphite crystallites and amorphous carbon. The pore diameters are usually less than 1 nm and possess a specific surface area up to 3000 m² g⁻¹. Activated carbon is prepared from carbon-rich organic precursors by a thermal method (dry distillation) to form carbonized organic precursors, which can be activated to increase the pore volume either thermally or

chemically. Experimental results on activated carbons show a linear dependence of the excess hydrogen- adsorption capacity on the specific surface area of the activated carbons. In early 1980s first work has been started to investigate the potential of hydrogen storage in the capillary passages of activated carbon at low temperatures. Chahine and Bose (1994) reported hydrogen adsorption of 2 wt% at 77 K and room temperature on AX21 activated carbon, formed from chemical treatment of coke. Rzepka *et al.*, (1998) found that activated carbon exhibited hydrogen storage capacity of 0.7 wt%. The experiments were carried out by gravimetric method and the calculated specific surface area is 2600 m²/g. The atomic ratio of H/C = 0.085 means that 1 hydrogen atom is assigned to 11.8 atoms of carbon on average and one molecule of hydrogen is assigned to 23.6 C. This poor limit is attributed to lack of availability of ideal slit pores. Since any ideal solid for hydrogen storage could possess structure consisting of slit shaped layers having a width anywhere higher than the kinetic diameter of hydrogen namely 2.89 Å. It is difficult to obtain high surface area activated carbon adsorbent with small pore sizes with narrow pore size distributions. However high hydrogen adsorption capacity (4-6 wt %) can be obtained only at low temperatures such as cryogenic conditions.

1.8.3 Fullerene

Fullerene is a spheroidal or polyhedra shaped carbon molecule. It can be inscribed in a sphere and is composed of 20 triangular equilateral faces, with 12 apices, each at the junction of 5 triangles. Fullerene was discovered in 1984 by Harry Kroto and Richard Smalley at Rice University (Kroto *et al.*, 1985). Fullerene molecule closely resembles the soccer ball shape. It has 20 hexagons and 12 pentagons; structural studies of C₆₀ have shown it to possess a face centered cubic (FCC) lattice as shown in the Fig. 1.9.

The lattice parameter is $a = 14.17 \pm 0.001 \text{ \AA}$, with a van der Waals space of 2.9 \AA . Because of the high symmetry of the molecule, the ^{13}C NMR spectrum and the IR absorption spectrum are particularly simple. Doping the C_{60} crystals with a metal (M) changes the conductivity and yields a phase which is superconducting at temperature less than 18 K . The functionalization of C_{60} is relatively well known like reduction, oxidation, alkylation, and metal complex formation. Characteristics of fullerene are so close to those of graphite and that the molecules are hollow which leads to form inclusion derivatives ($\text{M}_x @ \text{C}_{60}$). $\text{M}_x @ \text{C}_{60}$ behaves as superconductor. Heating C_{60} at high pressures and temperatures leads to polymerization of the molecule by forming intermolecular bonds, as evidenced from a decrease in their distance from 2.9 \AA in pristine C_{60} to $1.64 - 1.68 \text{ \AA}$. The resulting three dimensional phase is found to be harder than diamond.

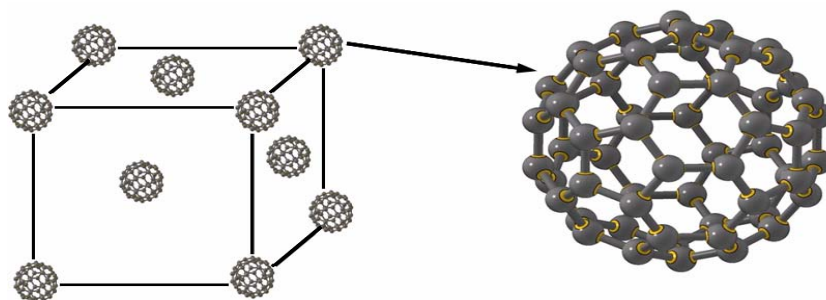


Fig. 1.9 FCC unit cell of the Buckminster fullerene crystal. Each lattice point has a C_{60} molecule

Fullerenes have been investigated as potential hydrogen storage material based on their ability to react with hydrogen via hydrogenation of carbon. Theory predicts that a maximum of 60 hydrogen atoms can be attached both to the inside (endohedrally) and outside (exohedrally) of the fullerene spherical surface and that a stable $\text{C}_{60}\text{H}_{60}$ isomer can be formed, which accounts for a storage capacity of $\sim 7.7 \text{ wt \%}$ hydrogen. The storage capacity is greater than the required amount for an economically viable

(6.5 wt %) storage medium. Even though the storage capacity of fullerenes is high, currently the hydrogenation of fullerene requires high pressures and temperatures for the reaction to take place by overcoming the reaction barrier (Jin *et al.*, 1994; Avent *et al.*, 1994; Zaginaichenko *et al.*, 2002). As shown in Fig. 1.10, hydrogenation of fullerenes involves the formation of C-H bonds as a result of breakage of C=C double bonds and dissociation of hydrogen molecule to form hydrogen atoms. From the experimental results, the activation energy for the hydrogenation was estimated to be 1.0 eV/H₂ and for dehydrogenation to form hydrogen molecule the activation energy is higher about 1.6 eV/H₂. To overcome this potential barrier high temperatures (> 673K) and pressures (> 60 MPa) are required.

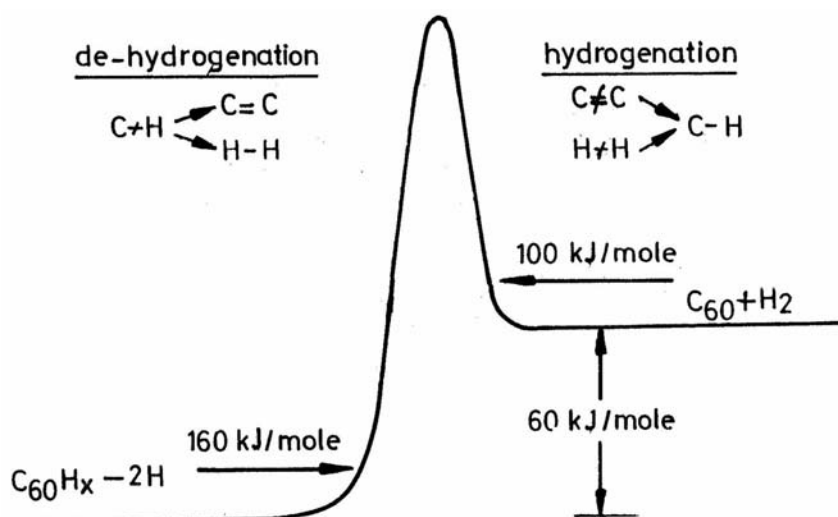


Fig. 1.10 The activation energy profile of fullerene to form hydrides

There have been number of attempts to prepare hydro-fullerenes. Initially experiments were carried out by direct gas phase hydrogenation of fullerenes under elevated temperatures and high pressures (673-723 K, 60-80 MPa) which resulted in the formation of compounds with hydrogen content up to 6.1 wt% (Loutfy and Wexler, 2001). In order to reduce the high energy required for the activation of hydrogen

molecule various approaches have been adopted like selecting and optimizing the metal catalyst for the reaction to take place. However addition of metal catalysts (Haufler *et al.*, 1990) resulted in a decrease in the temperature and pressure. But the storage capacity is not significant because of the high polarisability of the metal towards hydrogen when compared to carbon. Alternatively the reaction was carried out in the liquid phase, which involves the utilization of solvent molecules and by this process the experimental conditions required are the temperature in the range 453-523K and the pressure of 12 MPa (Meier *et al.*, 1994; Banks *et al.*, 1993; Attalla *et al.*, 1993). However the storage capacity of hydrogen decreased. The essential results of various methods of hydrogen stored in fullerene have been summarized in Table 1.6.

Table 1.6 Hydrogen storage capacity of fullerene determined by various methods

Method	Chemical reaction	Conditions: pressure (p) temperature (T)
Direct non-catalytic hydrogenation	$C_{60} + H_2 \Rightarrow C_{60} H_{2-18}$ (2.4 Wt%)	pH ₂ = 50–85 MPa, T = 573–623 K
Reaction of gaseous hydrogen with C ₆₀ Pd _{4.9}	$C_{60}Pd_{4.9} + H_2 \Rightarrow C_{60} H_{2-26}$ (3.48 Wt%)	pH ₂ = 2.0 MPa, T= 473–623 K
Catalytic hydrogenation in toluene solution in the presence of Ru/ C	$C_{60} + H_2 \Rightarrow C_{60} H_{36-48}$ (6.3 Wt%)	pH ₂ = 2-12 MPa, T= 383–553 K
Radical hydrogenation with promoter, C ₂ H ₅ I	$C_{60} + H_2 \Rightarrow C_{60} H_{\sim 36}$ (4.8 Wt%)	pH ₂ = 6.9 MPa, T= 723 K
Reduction with lithium in ammonia in the presence of t-BuOH	$C_{60} + H_2 \Rightarrow C_{60} H_{18-36}$ (4.8 Wt%)	T = 78 K
Reduction in toluene solution through hydro borating or hydrozirconating	$C_{60} + H_2 \Rightarrow C_{60} H_{2-4}$ (0.6 Wt%)	T = 278 K
Hydrogen transfer on the fullerene from the dihydroanthracene	$C_{60} + H_2 \Rightarrow C_{60} H_{18-36}$ (4.8 Wt%)	T = 623 K
Fullerene hydrogenation in the Zn–conc. HCl–toluene system	$C_{60} + H_2 \Rightarrow C_{60} H_{18-36}$ (4.8 Wt%)	T = 293 K
Electrochemical hydrogenation the 30% KOH solution	$C_{60} + x H_2 + xe \Leftrightarrow C_{60} H_{\sim x} + xOH$	Under normal conditions

1.8.4 Carbon nanofibres

Graphitic nanofibres (GNF) consist of graphite platelets stacked together in various orientations to the fiber axis with an interlayer spacing similar to bulk graphite. They are produced by decomposition of mixtures of ethylene, hydrogen and carbon monoxide on selective metal and alloy catalyst with three distinct structures such as tubular (90°), platelet ($\sim 0^\circ$) and herringbone (45°) in which the angle indicates the direction of the fiber axis relative to the vector normal to the graphene sheets (Fig. 1.11). The spacing between each layer is the same as in conventional carbon, $\sim 3.4 \text{ \AA}$ with diameter 5 - 500 nm. The length of these GNFs can vary between 5 and 100 μm .

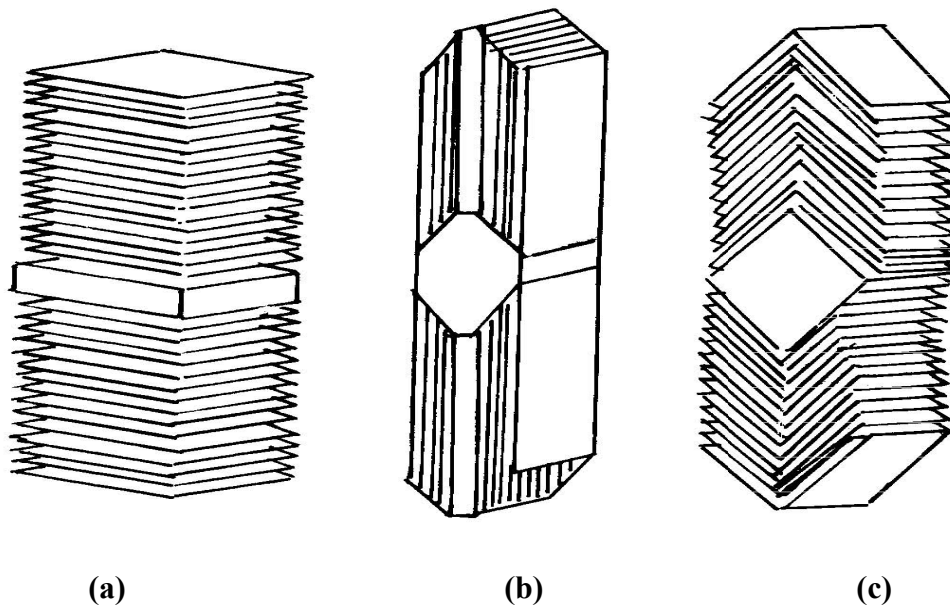


Fig. 1.11 The graphitic nanofibres (GNFs) (a) platelet (b) ribbon (c) herringbone structures

1.8.5 Carbon nanotubes

In 1991, Iijima described for the first time the new form of carbon called carbon nanotubes (CNT). CNTs are formed by rolled graphite sheets, with an inner diameter

starting from 0.7 nm upto several nm and a length of 10–100 μm as shown in Fig. 1.12.

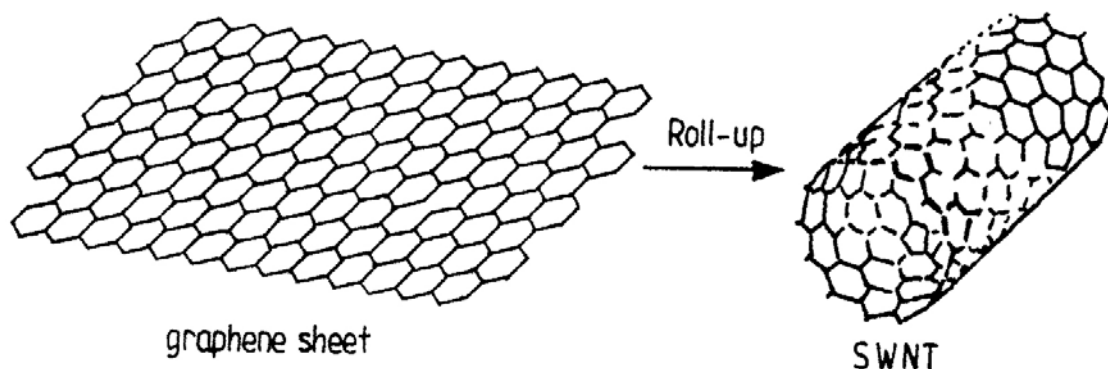
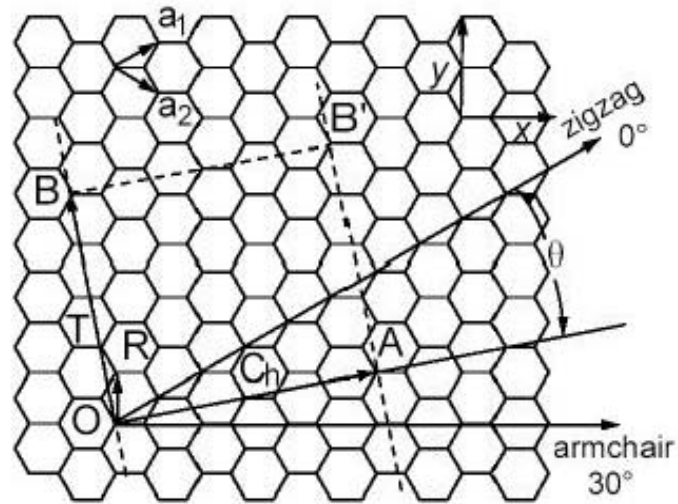


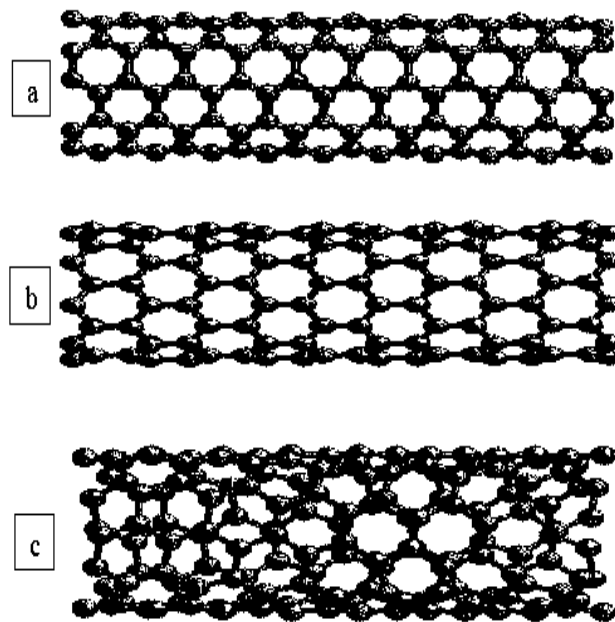
Fig. 1.12 The graphene sheet rolled to form cylindrical single walled nanotube (SWNT)

The CNTs are described as usually closed on both sides by a hemisphere, that is, half of a fullerene. Tubes formed by only one single graphite layer are called single wall nanotubes (SWNT); tubes consisting of multiple concentric graphite layers are called multi-wall nanotubes (MWNT). The interlayer distance in MWNTs is closer to the interlayer distance in graphite, which is equal to half of the unit cell parameter c ($0.5c = 0.3355 \text{ nm}$). The diameter of SWNTs varies from 0.671 to 3 nm, whereas MWNTs show typical diameters of 30–50 nm. The helicity of the nanotubes is usually described by the Hamada vector, (Hamada *et al.*, 1992) which indicates how the graphene sheet is rolled up along a lattice vector with components (n, m) . The values of the integers n and m identify the general geometry of SWNT. The tubes with $n = m$ are named ‘armchair’; tubes with either $n = 0$ or $m = 0$ are named ‘zigzag’; all others have chiral symmetry. The schematic representation is given in Fig. 1.13. One can view a single-walled carbon tube as a rolled up sheet or strip of sp^2 -bonded graphene. The atoms are located using a pair of integers (n, m) and the lattice vector $C = na_1 + ma_2$ as shown in Fig. 1.13a. A tube can be classified using the pair of integers by

viewing the rolling up of the sheet as the ‘placement’ of the atom at (0,0) on the atom at (n, m). Hence, different diameter tubes and helical arrangements of hexagons can arise by changing (n, m) as shown in Fig.1.13b.



(a)



(b)

Fig. 1.13 (a) Basic structure of a sheet of graphene. Consider the carbon atoms to be placed on each point on the edge of the hexagon. (b). Three different classification of nanotubes, (a) shows a (9,0) zigzag tube, (b) shows a (5,5) armchair tube and (c) shows a (6,4) chiral tube

1.8.5.1 Synthesis of carbon nanotubes

The carbon nanotubes were first noticed at the ends of the graphite electrodes used in an electric arc discharge employed in fullerene synthesis and the structures were examined by transmission electron microscopy (TEM). Decomposition of hydrocarbon gases by transition metal catalyst particles (Co, Fe, and Ni) has been used to produce carbon nanofibres that are similar in dimensions to the nanotubes, but far away in structural perfection. SWNTs were first made by the electric arc through the introduction of catalyst species (Fe, Co) into the carbon plasma. Several metal catalysts have been tried, but good yield of carbon nanotubes has been obtained with Co, Ni and bimetallic systems such as Co-Ni, Co-Pt, and Ni-Y as catalysts (Park and Keane, 2001). Another effective way to produce SWNTs is by using laser evaporation. It was shown that nanotubes could be obtained with good uniformity in size and structure (helicity). Depending on the temperature of the oven in which the nanotubes are grown, the diameter varied between 1 and 5 nm diameter; the higher the temperature (range between 1073 – 1473 K) the larger the nanotubes diameter. Other alternative strategies for the synthesis of nanotubes are through catalytic chemical vapor deposition (CVD) or using well defined porous inorganic membranes (such as alumina) as templates wherein a disordered form of carbon is deposited by CVD and graphitized further at higher temperature to yield nanotubes. The advantage of such template based methods is that the size of the particles and the pores, which determine the size of the nanotubes, can be controlled prior to the deposition of carbon. The length of the nanotubes formed can be controlled by adjusting the amount of carbon vapor feedstock supplied and the thickness of the membranes. By removing the templates after the nanotubes growth, freestanding arrays of highly graphitized nanotubes can be formed.

1.8.5.2 Hydrogen storage in carbon nanotubes

Among nanostructures, tubular materials are especially interesting because their morphology is assisted with an intrinsic multifunctionality that arises from four different contact regions as tube opening, outer surface, inner surface and interstitial region. These properties render nanotubes as promising candidates for the realization of highly functional, effective and resource saving nanodevices such as sensors, capacitors or storage and release systems. In contrast, in spite of their relatively small surface area and pore volume, carbon nanotubes and carbon nanofibers surprisingly may show high hydrogen storage capacity.

In recent years, interest in carbon nanomaterials for hydrogen storage applications has escalated, following claims of experimental results, made in 1997 by Dillon *et al.*, that CNT might be capable of 5-10 wt% hydrogen capacity (Dillon *et al.*, 1997). Storage of hydrogen in carbon materials took a dramatic turn in 1998-99, when Rodriguez *et al* reported exotic values of hydrogen absorption by carbon nano structures up to 10-12 hydrogen molecules per carbon atom, though in a sequent communication they have reduced this up to 4 molecules per atom of carbon (Chambers *et al.*, 1998; Park *et al.*, 1999). This is nearly twice (0.4 g H₂/g C) of the most hydrogenated carbon compound namely CH₄ where the hydrogen to carbon weight ratio is 0.25 g H₂/g C. Subsequently there have been various reports in literature to substantiate these observations (Ahn *et al.*, 1998; Ströbel *et al.*, 1999; Ye *et al.*, 1999; Liu *et al.*, 1999) and none of them in any way could realize the expected (DOE standards) 6.5 weight percent leave alone repeating the original adsorption capacity claimed. From the recent inelastic neutron scattering experiments by Schimmel *et al* showed that the pure carbon surface cannot activate hydrogen

molecule, which is concluded from the binding strength of hydrogen molecule is almost the same for all kinds of carbon materials and the magnitude of interaction is around 5 kJ/mol (Schimmel *et al.*, 2003; Ren and Price. 2001). Modifying the carbon surface has been advocated as one of the methods for higher hydrogen storage capacity. This is a potential field of research in recent times. However, the addition of metal or metal oxides as catalysts and as well as preparation of carbon in different forms (fibers and tubular forms) have not resulted in the enhancement of the storage capacity. Mainly the report by Chen *et al.* where the CNT has been doped with alkali metals could adsorb up to 20 wt% of hydrogen at 653 K and 10 bar (Chen *et al.*, 1999). However, it was later suggested that the presence of water might have influenced this result. Yang revisited these data by preparing the doped nanotubes following the same procedure and measured the adsorption-desorption using a comparable thermogravimetric analyzer (Yang, 2000). Moisture drastically increased the weight gain and lead to erroneous results, however in dry hydrogen adsorption only 2.5 wt% for lithium-doped nanotubes and 1.8 wt% for potassium-doped nanotubes were observed and these results were independently confirmed by Pinkerton *et al.* (Pinkerton *et al.*, 2000). These observations are also confirmed further by the investigation of Hirscher *et al.*, as they did not find any hydrogen desorption in graphite doped with Li or K (Hirscher *et al.*, 2001).

In all these hydrogen uptake studies, three common features exist: slow uptake, partial irreversibility of adsorbed species, and the use of transition metals in synthesis (Fe, CO, or Ni) that may not be completely removed by purification. Lueking and Yang experimentally showed that hydrogen storage on multiwalled nanotubes (MWNTs) was dependent on the degree of catalyst removal (Lueking and Yang,

2002). At atmospheric pressure, removal of the catalyst decreased the uptake from 0.6% to below detection limits.

By incorporating metal alloy $\text{TiAl}_{0.1}\text{V}_{0.04}$ to a purified laser-generated SWNT employing a high-power ultrasonic cutting procedure (Dillon *et al.*, 2000) and found the maximum adsorption capacity 7.0 wt % and the hydrogen adsorption occurs in two different sites approximately 2.5 wt % of hydrogen evolved at 300 K and the remainder desorbed between 475 to 850 K. However the uptake is not individually attributed to the presence of alloy but also to the associated electron transfer that is responsible for hydrogen storage. Hirscher *et al* reported 1.5 wt% storage capacity for SWNTs doped with alloy of Ti-6Al-4V by sonicating in 5M HNO_3 (Hirscher *et al.*, 2001). However the hydrogen uptake was explained with the assumption that the hydrogen is stored in Ti alloy particles only. This is possibly due to the different storage mechanism, as the metals involved form hydrides and the metal hydride could not store greater than its number atomic combinations. The summary of various reported hydrogen storage capacity are given in Table 1.7.

In spite of availability of enormous results on hydrogen uptake by carbonaceous materials the actual mechanism of storage is still a mystery. Scientists have employed different theoretical calculations and deductions in search of a reasonable interpretation. The intension of these theoretical studies is to find answers to the following questions:

- How do structural characteristics influence the physical/chemical process?
- Where does the absorption occur? In inner hollow cavities and in other pore space (inter-tube space) or in only one of them?

- In the absorption of hydrogen onto carbon nanotubes, what interaction—chemical or physical—occurs between the hydrogen and the carbon?
- What is the absorption mechanism?
- What is the maximum absorption capacity?

Table 1.7 Summary of reported hydrogen storage capacities in carbon nanostructures

Adsorbent	Hydrogen storage (Wt %)	Conditions	References
		Temperature (K) / Pressure (MPa)	
SWNT(low purity)	5-10	273/0.04	Dillon <i>et al.</i> , 1997
SWNT(high purity)	3.5-4.5	298/0.04	
SWNT(high purity)	8	80/8	Ye <i>et al.</i> , 1999
SWNT(50% purity)	4	300/12	Liu <i>et al.</i> , 1999
SWNT	2	80/10	Wang and Johnson, 1999a
SWNT	11	80/10	Wu <i>et al.</i> , 2000
SWNTs	~0.1	300-520/0.1	Hirscher <i>et al.</i> , 2002
SWNT	6.5	300/16	Yin <i>et al.</i> , 2000
SWNT	10	300/0.04	Dillon <i>et al.</i> , 1999
Li doped MWNT	20	200-400/0.1	Chen <i>et al.</i> , 1999
K doped MWNT	14	300/0.1	
Li doped MWNT	2.5	200-400/0.1	Yang, 2000
K doped MWNT	1.8	<313/0.1	
MWNT	5	300/10	Zhu <i>et al.</i> , 2001
K doped MWNT	1.8	300/0.1	Pinkerton <i>et al.</i> , 2000
GNFs (tubular)	11.26	298/11.35	Chambers <i>et al.</i> , 1998
GNFs (herring bone)	67.55	298/11.35	
CNFs	~10	300/10.1	Fan <i>et al.</i> , 1999
CNFs	~5	300/10.1	Cheng <i>et al.</i> , 2000
Nano-structured graphite	7.4	~300/1.0	Orimo <i>et al.</i> , 1999
SWNT-Fe	-	300/0.08	Hirscher <i>et al.</i> , 2001
SWNT-Ti-6Al-4V	1.47	300/0.08	
SWNT-TiAl _{0.1} V _{0.04}	~7	300/0.067	Dillon <i>et al.</i> , 2000

The interaction may be either based on van der Waals attractive forces (Physisorption) or on the overlap of the highest occupied molecular orbitals of carbon with the occupied electronic wave function of hydrogen electron, overcoming the activation energy barrier for hydrogen dissociation (Chemisorption). Physisorption of hydrogen limits the hydrogen to carbon ratio to less than one hydrogen atom per two carbon atoms (i.e., 4.2 mass %), while in chemisorption the ratio of two hydrogen atoms per one carbon atom is realized similar to the case of polyethylene. Physisorbed hydrogen has a binding energy normally of the order of 0.1 eV, while chemisorbed hydrogen has C-H covalent bonding, with a binding energy of more than 2-3 eV.

Several reports, both experimentally and theoretically attribute the uptake of hydrogen atom to physisorption of hydrogen on carbon. The mechanism of hydrogen storage on carbon nanomaterials that explains the higher storage capacity than the expected value reported uptake by several groups remains unclear. According to Chambers *et al.* the interlayer spacing of CNT and CNF produces an array of nanopores which are accessible to hydrogen, directly from the edge of the material (Chambers *et al.*, 1998; Park *et al.*, 1999). Hydrogen penetrates into the nanopores formed by the layers of CNF and the interior of CNT forming an intercalated layer of hydrogen (Cao *et al.*, 2001b; Chen *et al.*, 2001; Dillon *et al.*, 1997; Gadd *et al.*, 1997; Ma *et al.*, 2002; Meregalli and Parrinello, 2001). In addition to this, the nanopores could undergo expansion in order to accommodate hydrogen in a multilayer configuration (Park *et al.*, 1999). However, there is no evidence found for the influence of the geometric structures of the nanostructured carbon on the amount of hydrogen adsorbed. Further, all attempts to open the nanotube and adsorb hydrogen inside the tube did not result in increase of adsorption of hydrogen molecule, a conclusion drawn by Zuttel and Orimo (Zuttel and Orimo, 2002). Theoretical studies beyond well known physisorption lead

to a large set of various maximum hydrogen adsorption capacities. Most of the results were obtained under special conditions such as at 0 K or with high energy hydrogen atom implantation. No evidence was found for a higher density of hydrogen in and on carbon nanostructures, as compared to liquid hydrogen at ambient conditions. On the other hand, Browning *et al.*, proposed that the exposed edge sites of the graphene sheets act as catalytic site for the dissociation of hydrogen followed by intercalation of the graphene layers (Browning *et al.*, 2002). Another theory is that the hydrogen dissociates on the metal catalyst with the CNF and CNT left from their preparation and spills over in the carbon structure (Lueking *et al.*, 2003). The presence of functional groups has also been attributed to the enhancement of hydrogen storage capacities, by facilitating stronger bonding (Badzian *et al.*, 2001; Bai *et al.*, 2001; Wang *et al.*, 2002; Zhu *et al.*, 2003). Many reports showed large hydrogen storage capacities of CNT and CNF but they are yet undefined with uptake mechanism (Cheng *et al.*, 2000; Hwang *et al.*, 2002; Liu *et al.*, 1999; Strobel *et al.*, 1999). However, until reliable and repeatable results are obtained the question of the mechanism of hydrogen storage cannot be conclusively answered.

In the literature, the concept of interaction of atomic hydrogen is not clearly dealt with and if it becomes a facile process, one can achieve higher storage capacities. In order to achieve atomic hydrogen adsorption an activator is essential to dissociate the incoming hydrogen molecule and the dissociated hydrogen atoms can move on to carbon surfaces (spill over route). Therefore it is clear that carbon material cannot activate hydrogen in catalytic style in its pure form. Metal or metal oxide doped carbon material offer high sorption capacities than their pure counterparts may fit into this concept. Though the metal and metal oxide doped carbon nanotubes offer higher sorption capacities (~ 5-6 wt %), but desorption process occurs in two steps as

mentioned earlier, consequently leading to lower usable capacity. This is due to the fact that M-H bonds are stronger than C-H bonds. In order to increase the user capacity ratio of carbon nanomaterials, one has to find suitable activator that could split the incoming hydrogen gas molecules and transfer them to carbon sites. A rationale is evolved for the research of a suitable activator, and the essential criteria for such an activator are:

- Must possess equi-potential sites with that of carbon.
- These sites themselves should be easily hydridable
- They should act as *catalytic sites* rather than mere *reactive sites* that lead to stoichiometric reaction

Heteroatoms such as N, P, S and B are identified by us as activators fulfilling the above desirable attributes.

1.9 WHAT ALTERNATIVES?

Hydrogen adsorption on carbon materials especially nanotubes, is possible only when it contains some sites wherein hydrogen molecule can be activated. Taking the clue from nature, it is postulated that the presence of heteroatoms in the carbon nanotubes may be appropriate sites for activation of hydrogen. In nature, the high percentage of hydrogen is stored mainly in the form of hydrocarbon (petroleum) formation is mainly facilitated by the presence of heteroatom containing compounds like pyridine, thiophene and pyrrole, since the heteroatoms plays important role in hydrogen storage in carbon. We followed the nature's path by substituting the heteroatom in carbon nanotubes and studied the effect in hydrogen storage. Where the heteroatom has the high polarizability that can alter the Fermi level of the carbon network there by one

can tune the redox potential by substituting the appropriate heteroatom like nitrogen, boron, phosphorus and sulphur with required atomic weight percentage. The hydrogenation behavior of carbon is well established potentially where in heteroatom substituted carbon nanotubes are hydrided by the electro negativity difference between them. The alteration in electro negativity makes the molecule to be polarized and behaves differently from unsubstituted carbon nanotubes. The hydriding property of heteroatom is well explainable by the redox potential (Fig. 1.14) and by the Ellingham diagram like the formation of N-H, B-H bonds (Fig. 1.15). By the heteroatom substitution one can exploit the manipulation of electronic and structural perturbation resulting in the carbon lattice for the hydrogen storage applications.

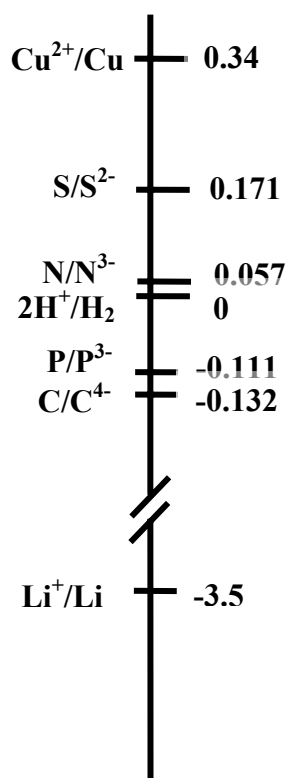


Fig. 1.14 Standard redox potential (V) values of some selected species

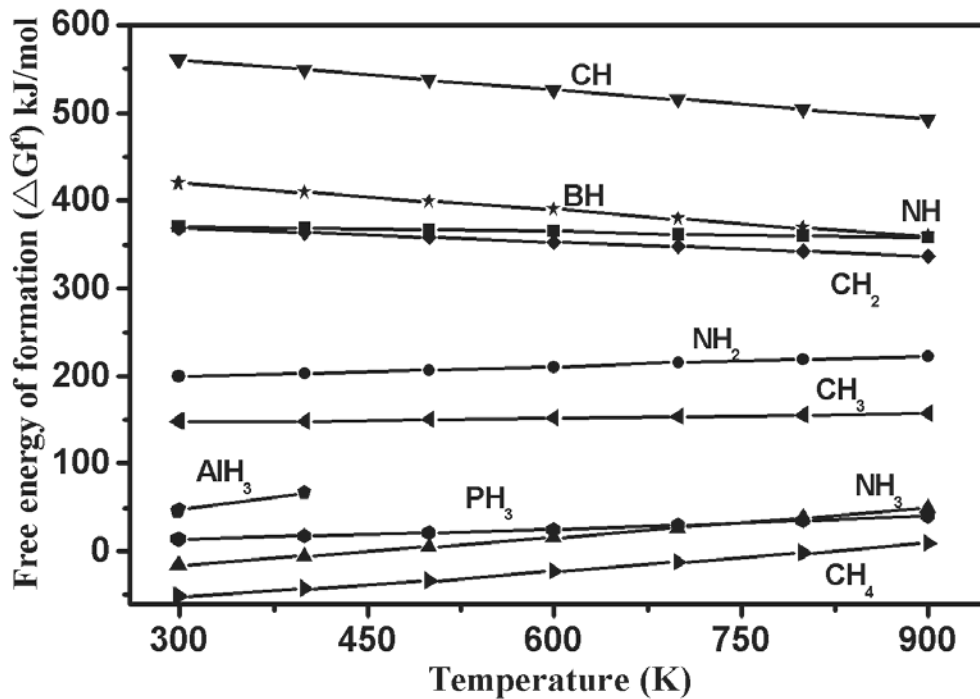


Fig. 1.15 Ellingham diagram for various heteroatoms (hydriding property)

1.10 OBJECTIVES AND SCOPE OF THE PRESENT INVESTIGATION

Against this background, the need for an activator for hydrogenation in carbon materials is realized, which should be easily hydridable than carbon and facilitate migration of the dissociated hydrogen to equipotential carbon surface. While considering these aspects heteroatoms like N, P, S and B seem to be promising as activators due to their properties like higher redox potential than that of carbon. This can result in the tuning of the electronic property of the carbon materials. Therefore, the present study is aimed at establishing the role of heteroatom for hydrogen storage in the carbon materials, both by theoretical and experimental methodology.

The study reported in this thesis is focuses on the following aspects:

- ❖ To develop suitable theoretical models for identifying the activation sites for hydrogen.
- ❖ To prepare carbon nanomaterials of various types and examine their hydrogen storage characteristics.
- ❖ To synthesize heteroatom containing carbon nanomaterials by various methods and evaluate their hydrogen storage characteristics.
- ❖ To evolve conditions for the formation of substituted carbon nanomaterials and also evaluate their hydrogen storage capacity under ambient conditions.

CHAPTER 2

MATERIALS AND METHODS

2.1 CHEMICALS AND MATERIALS USED

The Whatman Anodisc Membrane Filters (Alumina) with pore diameter, thickness and percentage porosity of 200 nm, 60 μm and 65 % respectively were purchased from Whatman Inc. U.S.A. The Glassy Carbon (GC) disc (0.07 cm^2) and polishing kit were purchased from Bio Analytical System. U.S.A. H-zeolite-Y was obtained from Sud-Chmie Pvt Ltd., India.

The chemicals used and the sources from which they were obtained are as follows:

Pyrrole (Sisco Research Laboratory, India) used after distillation and stored in dark in nitrogen atmosphere. 1, 4 Divinyl benzene and Hydrofluoric acid were received from E. Merck, India. These chemicals were used as such without further purification. Tetrahydrofuran was dried over sodium and distilled prior to use. All other chemicals used in the investigation were of analytical reagent (AR) grade and were obtained from Qualigens, India and S.D. Fine Chemicals, India. These chemicals were used as such without further purification.

2.2 PURIFICATION OF HYDROGEN

Hydrogen gas obtained from M/s. Indian Oxygen Ltd., was purified through another heated trap containing reduced copper powder kept at 623 K followed by a trap containing potassium hydroxide pellets fused calcium chloride and silica gel. Then it was followed by passing through liquid nitrogen trap, evacuated and cooled at liquid

nitrogen temperature of activated carbon trap. Hydrogen of high purity is thus obtained for adsorption experiment.

2.3 PREPARATION OF THE CATALYST

2.3.1 Preparation of nickel supported on activated carbon

Various percentages (2, 5 and 20 wt %) of nickel have been loaded on commercial activated carbon (calgon) by physical impregnation method. In this method the acetate salt of nickel is taken with calgon carbon ground for 30 min. The physical mixture was calcined in N₂ atmosphere at 573 K for 2 h and then in H₂ atmosphere at 723 K for 6h followed by cooling to room temperature. The sample is used for absorption studies immediately after removing from the furnace.

2.3.2 Chemical treatment of activated carbon

Acid and amine treatments have been carried out on the commercial activated carbon (CDX-975). During acid treatment CDX-975 carbon refluxed with 1 M HNO₃ acid for 3 h at 333 K and cooled to room temperature. The treated sample is washed with distilled water and dried at 373 K (TCDX). Amine treatment has been carried out using triethylene tetra amine. CDX carbon was refluxed with amine in a round bottom flask in an oil bath at 473 K for 4 h, followed by cooling to room temperature, washed with distilled water and dried in air at 373 K (ACDX). Both acid and amine treatment have been carried out for the CDX carbon. Acid treatment was carried out first followed by amine treatment (TACDX).

2.3.3 Preparation of Polymer Derived Carbon (PDC) with nitrogen content

Polymer was used as the structure directing agent as well as carbon source for the preparation of nitrogen containing carbon nanomaterials. Synthesis has been carried by following the gel composition out of 1.2 SiO₂: 0.005 PVP: 4.2 HCl: 126 H₂O in acidic medium. Polyvinyl pyrrolidone was taken as the carbon source and structure directing agent, where the polymer has been dissolved in acid solution and the silica source TEOS (tetra ethyl ortho silicate) solution, was added slowly with heating at 318 K for 4 h. The precipitate was washed with distilled water and dried at 373 K over night. The white powder obtained was ground and carbonized in Ar atm for 6h at 1173 K. After carbonization the carbon/silica has been treated with 48% HF solution for 24 h to remove the silica. The carbon obtained was washed with distilled water and dried at 373 K thus polymer derived carbon (PDC) is synthesized.

2.3.4 Preparation of microemulsion mediated synthesis of nitrogen containing carbon (MEC)

Microemulsion polymerization has been utilized to prepare nitrogen containing carbon nanomaterial and in this method polyacrylonitrile has been synthesized in micelle core environment. In this method sodium di (2-ethyl hexyl) sulfosuccinate commercially called AOT, anionic surfactant has been taken in hexane stirred together to get a clear solution. Acrylonitrile with AIBN radical initiator has been added. 2M PTSA (para-toulene sulphonic acid) was added with continuous stirring followed by slow addition of TEOS drop by drop, which leads to the formation of white precipitate. This white precipitate has been washed with hexane and dried in oven. It has been carbonized in Ar atm for at 1173 K for 6 h. After carbonization the carbon/silica composite has been treated with 48% HF for 24 h. The carbon thus

obtained was washed with hot distilled water and dried at 373 K, characterized and used for hydrogen absorption studies (MEC).

2.3.5 Preparation of nitrogen containing carbon nanotubes using polypyrrole as carbon source

Polypyrrole (PPY) coatings were applied by a reaction coating approach (Han and Im, 1998) by suspending alumina template membrane in an aqueous pyrrole (0.1 M) solution containing 0.2 M ferric chloride hexahydrate. Added 0.2 M p-toluene sulphonic acid slowly and polymerization was carried out for 3 h. This leads to the black coating of polypyrrole on the template membrane. The surface layers were removed by polishing with fine neutral alumina powder and ultrasonicated for 20 min. to remove the residual alumina used for polishing. The polypyrrole coated alumina membrane was characterised by IR- spectroscopy, the characteristic –NH- stretching frequencies were observed at 1540, 1460 and 1312 cm^{-1} for polypyrrole they match with those reported in literature (Selampinar *et al.*, 1994). The membrane was then dried and placed in a quartz boat and carbonized in Ar atmosphere (at different temperature and time intervals). The resulting curled carbon / alumina composite was immersed in 48 % HF for 24 h to remove the template. The residue was thoroughly washed with water to remove HF and dried at 373 K for 10 min.

2.3.6 Preparation of carbon nanotubes without nitrogen content

Polyphenyl acetylene is used as carbon source for the preparation of carbon nanotubes. It contains only carbon – hydrogen bonds. The polyphenyl acetylene/alumina composite was prepared by adding 10 ml of 5 % w/w polyphenyl acetylene in dichloromethane to the alumina membrane (Whatmann, 200 nm pore diameter, 60 μm thick) applying vacuum from the bottom. The entire polymer solution penetrates

inside the pores of the membrane by the suction applied. The solvent was evaporated slowly and the membrane was dried in vacuum at 373 K for 10 min. The composite was then polished with fine neutral alumina powder to remove the surface layers and ultrasonicated for 20 min to remove the residual alumina powder used for polishing. The FT-IR spectrum of the composite membrane confirms the presence of polyphenyl acetylene in the membrane. The composite was then carbonized by heating in Ar atmosphere at 1173 K for 6 h at a heating rate of 10 K/min. This resulted in the deposition of carbon on the channel walls of the membrane. The carbon/alumina composite was then placed in 48 % HF to free the nanotubes. The tubes were washed with distilled water to remove HF.

2.3.7 Preparation of pillared clays

Montmorillonite $[(\text{Na}_{0.35}\text{K}_{0.01}\text{Ca}_{0.02})(\text{Si}_{3.89}\text{Al}_{0.11})^{\text{tet}}(\text{Al}_{1.60}\text{Fe}_{0.08}\text{Mg}_{0.32})^{\text{oct}}\text{O}_{10}(\text{OH})_2 \cdot n\text{H}_2\text{O}]$ was used for the preparation of Al-pillared clays. The pillaring solution was prepared by the partial hydrolysis of an aluminum salt solution using sodium hydroxide as base. NaOH was added drop wise into a stirred solution containing $\text{AlCl}_3 \cdot 6\text{H}_2\text{O}$ in order to obtain OH/Al molar ratio of 2.0. The resulting solution was aged for five days at room temperature and warmed at 333 K for 2 h before using the pillaring process. In pillaring procedure, Na-montmorillonite was dispersed in 200 ml of deionised water to form 1.0 wt% of clay slurry. The slurry was stirred at room temperature for 2 h and sonicated for 15 min for better dispersion of the clay particles. The pillaring solution was then added drop wise (50ml/h) to the clay slurry to finally obtain Al /montmorillonite ratio 20 mmol/g. During the process of addition of the pillaring solution, the clay suspension was stirred vigorously. The mixture was kept at constant stirring for 24 h at room temperature, then washed with deionised water until free

from chloride ions (AgNO_3 test), centrifuged and dried in air, and calcined at 773 K for 2 h in air (Vaccari, 1998; Figueras, 1988).

2.3.8 Preparation of carbon nanotubes by chemical vapor deposition (CVD) method

Calcined H-Y-Zeolite and Al-pillared clay were taken as the template and acetylene as carbon precursor and pyridine as nitrogen source for the preparation of nitrogen containing carbon nanotubes. Acetylene was passed at a flow rate of 5 ml/min to the reaction chamber of horizontal tubular furnace with quartz tube and the quartz boat in the middle containing the template. The reaction chamber was heated to 1173 K in Ar atmosphere and subsequently the carbon source is carbonized. After carbonization the carbon/ template has been subjected to 48% HF treatment to remove the silica matrix. Carbon nanotubes obtained were washed with distilled water and heated to 393 K to remove the water. In the chemical vapor deposition method hydrocarbon is used as carbon precursor. Metal catalyst has been used to produce carbon nanotubes with controllable size (Colomer *et al.*, 1999; Satishkumar *et al.*, 1998; Ci *et al.*, 2001; Cheng *et al.*, 1998; Lyu., 2003). Subsequently doped carbon nanotubes especially nitrogen doped CNTs are produced by this method using different nitrogen precursors (Sen *et al.*, 1998; Nath *et al.*, 2000; Liu *et al.*, 2006; Carrol *et al.*, 1998). In the present case metal or metal oxide catalyst were not used and this will avoid the presence of metal impurities in carbon nanotubes and facilitates the study of the effect of heteroatom alone.

2.4 CHARACTERIZATION

2.4.1 UV-Visible absorption studies

UV-Visible absorption spectra were recorded using a CARY 5E UV-Vis-NIR spectrophotometer in the spectral range of 200-800 nm.

2.4.2 Powder X-ray Diffraction (XRD)

X-ray diffraction patterns of various samples were recorded using SHIMADZU XD-D1 diffractometer using Ni-filtered Cu K α radiation ($\lambda = 1.5418 \text{ \AA}$) in the range of 10 - 80 degrees at a scan rate of 2 degrees per minute using Bragg-Brantán configuration.

2.4.3 Transmission Electron Microscopic studies (TEM)

Transmission electron micrographs were recorded with a PHILIPS CM12/STEM microscope, working at a 100 kV accelerating voltage. Samples for TEM were prepared by dispersing the powdered sample in acetone by sonication and then drop drying on a copper grid (400 mesh) coated with carbon film.

2.4.4 Scanning Electron Microscopic studies (SEM)

Scanning electron micrographs were recorded using JEOL, JSM5610LV microscope (acceleration voltage 15 kV). The sample powders were deposited on a carbon tape before mounting on a sample holder.

2.4.5 X-ray Photoelectron Spectroscopy (XPS)

Chemical nature of N and S in TiO $_2$ has been studied using X-ray photoelectron spectroscopy in a VG Microtech Multilab ESCA 3000 spectrometer with a non-monochromatized Al K α X-ray ($h\nu = 1486.6 \text{ eV}$). The catalyst pellet surface was scraped *in situ* to remove any surface contamination that could arise from atmospheric

components like water, CO₂ etc. The energy resolution of the spectrometer was set at 1.1 eV at pass energy of 50 eV. BE was calibrated with respect to Au 4f_{7/2} core level at 83.9 eV.

2.4.6 Thermogravimetric Analysis (TGA)

Thermogravimetric analyses of catalyst precursor, metal complexes were performed to know the calcination temperatures. TGA analyses were performed for the calcined catalyst also to confirm complete decomposition of precursor materials. The analyses were done using Perkin Elmer TGA (Delta series TGA7) instrument with a heating rate of 20 K min⁻¹ under air atmosphere.

2.4.7 Infrared (IR) studies

FT-IR absorption spectra of the samples were recorded using a Bruker FT-IR spectrometer (Model IFS 66v) at room temperature in the range 4000-400 cm⁻¹. The powdered samples were ground with KBr and pressed into pellets (5 ton/cm²) for recording the spectra.

2.4.8 Raman spectral studies

The Raman studies for all the carbon nanomaterials prepared were characterized to see the nature of carbon. WiTec GmbH, micro Raman instrument, 514.5 nm excitation laser, 600 grooves/mm grating, back scattering geometry has been used. 100x objectives was used to focus the laser on the sample.

2.4.9 Elemental analysis

The C, H and N analysis of the carbon nanotubes has been carried out using Perkin-Elmer 2400 Series II.

2.4.10 Cyclic Voltammetric measurements

Cyclic voltammograms were recorded for nitrogen containing carbon nanotubes (NCNT) and nanotubes (CNT) without nitrogen to study the hydriding property of carbon nanotubes. Cyclic voltammograms were measured at the scan rate of 25 mV/s using potentiostat Wenking (POS 73) with Philips digital X-Y recorder (PM 8033). The working electrodes for electrochemical measurements were fabricated by dispersing the CNT in 0.5 ml deionised water. To the catalyst suspension 5 μ l Nafion (5 wt %) solution was added and ultrasonicated for 20 min. A known amount of suspension was added on the glassy carbon (GC) electrode and solvent was slowly evaporated which results in CNT on GC electrode. Pt foil (1 cm²) was used as counter electrode and Ag/AgCl/KCl (saturated) was used as reference electrode 6 M KOH has used as the electrolyte.

2.4.11 Evolved Gas Analysis (EGA)

Hydrogen absorption characteristics were evaluated by evolved gas analysis technique. In a typical experiment, the sample was loaded in the EGA chamber (Balzer, GAM 440) and was evacuated to 10^{-6} Torr. The sample was then heated to 300 °C. Hydrogen was then admitted into the chamber while the sample was heated at a rate of 20 °C /min to 673 K. The chamber was then cooled to room temperature and the chamber was again evacuated to 10^{-6} Torr followed by heating at the same heating rate up to 693 K while simultaneously monitoring the gas evolved by quadruple mass spectrometer with a Faraday cup detector.

2.4.12 Hydrogen storage apparatus

2.4.12.1 Low pressure absorption apparatus

Volumetric low pressure and high pressure hydrogen adsorption was carried out using custom build Seivert's apparatus. The low pressure home made glass apparatus (Fig 2.1) was utilized for the adsorption measurements in the pressure range of 0 – 760 Torr. Hydrogen adsorption was evaluated with respect to change in pressure vs the volume adsorbed. A plot was obtained for equilibrium pressure with the volume of hydrogen adsorbed per gram of the sample. Helium gas was used to find the dead space at room temperature and various temperatures. Nitrogen gas was used as the adsorbent to determine the specific surface area (SSA) by using the BET equation at 77 K.

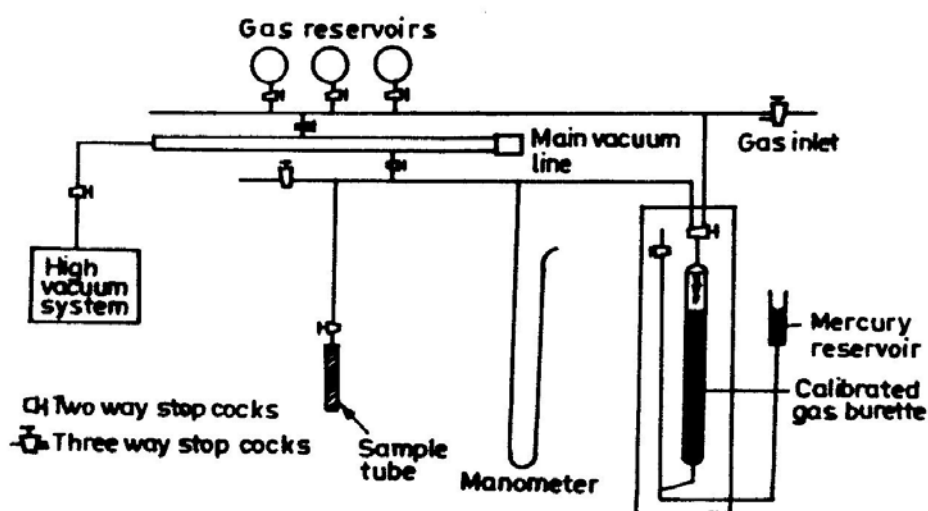


Fig. 2.1 Low pressure volumetric hydrogen absorption apparatus (glass)

2.4.12.2 High pressure apparatus

The high-pressure hydrogen absorption experimental setup shown in Fig.2.2 consists of reference cell, sample cell and measuring unit (pressure transducer). The experimental setup consists of seamless stainless steel tubes (SS 316), elbow joints, needle valves and the filter is of sintered SS-316, with 2-micron pore size procured from Swagelok Bangalore, India. The tubings can withstand up to a maximum pressure of 200 bar. The sintered SS-316 filter of 2 μm is used to ensure the purity in hydrogen supply during absorption process. The piezo resistive type pressure transducers procured from Syscon Bangalore, India were used to monitor the hydrogen pressure in the range 0-200 bar. The pressure transducer has been calibrated using dead weight tester. The test pressures are varied in steps to cover the complete pressure range of pressure transducer to be calibrated. Metal-sheathed “K” type quick sensing thermocouples of 0.2 mm wire diameter with ground bead end has been used for measuring the reaction sample temperature during the absorption processes. The details of design and development of the apparatus are described in Fig. 2.2.

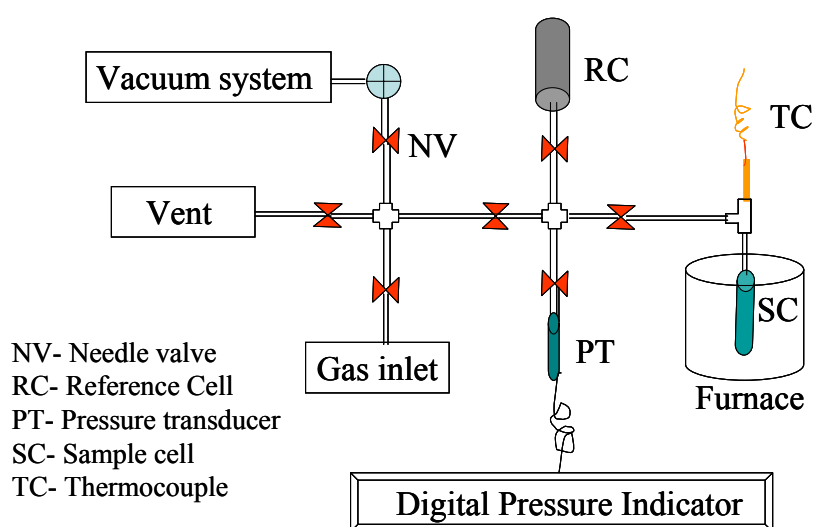


Figure 2.2 High pressure hydrogen absorption apparatus

Volumetric high pressure hydrogen adsorption measurements have been carried out using custom built volumetric and Seivert's apparatus. The high pressure adsorption apparatus consists of reservoir cell and a cylindrical sample cell of known volume (33.8 cm³). A leak proof connection is obtained by tightening the inner and outer flanges with a soft copper gasket kept in between the sample cell. All possible care for the possible sources of leak was taken and long blank run tests were carried out. Care has been taken to avoid the errors due to factors such as temperature instability, leaks and additional pressure and temperature effects caused by the expansion of hydrogen from the reservoir to the sample cell. The volume of the system was determined by measuring accurately those of the single components at lower pressures using helium gas. The measurements were carried out by utilizing the systematic procedure as follows: Typically the mass of the carbon samples used for hydrogen storage measurements is in the region of 100–300 mg. Prior to measurement, the samples are degassed and heated at 573 K for approximately 6 h in vacuum of 10⁻⁵ Torr. The whole system has been pressurized at the desired value by hydrogen and change in pressure was monitored. The change in the pressure was recorded by a pressure transducer, after the equilibrium is reached. All the hydrogen adsorption measurements have been carried out at room temperature. The experiments have been repeated under the same conditions for various pressures. The hydrogen compressibility factors were utilized for the calculations.

$$P_i V_i = P_f (V_1 + V_2 + V_3 + V_{\text{ads}})$$

[P_i =Initial pressure, P_f = Final pressure]

$$V_{\text{ads}} Z = V_{\text{correct}}$$

where Z = Compressibility factor of hydrogen.

CHAPTER 3

THEORETICAL STUDIES ON CARBON NANOTUBES AND FULLERENES

3.1 THEORETICAL STUDIES ON CARBON NANOTUBES

3.1.1 Introduction

Hydrogen has been recognized as an ideal energy carrier; however the transition towards hydrogen economy mainly depends on the efficient storage medium. After the discovery of carbon nanotubes (Iijima, 1991), there has been considerable interest in using carbon nanotubes as appropriate hydrogen storage medium. Carbon nanotubes, which have diameters of typically a few nanometers, have been suggested as suitable materials for gas storage (Dillon *et al.*, 1997, Liu *et al.*, 1999). In the beginning, pure single-walled-carbon-nanotubes (SWNTs), carbon nanofibers and graphite were investigated and shown to possess high hydrogen storage capacity. (Chambers *et al.*, 1998; Fan *et al.*, 1999). Soon it has been realized that even these do not provide sufficient storage and the results are also not reproducible in any other laboratories. By modifying the carbon nanomaterials by doping with a metal or metal oxide or phase modification has been carried out. This stimulated many experimental studies (Chen *et al.*, 1999 and Yang, 2000). However the target has not been achieved. There are a number of theoretical studies probably aimed at resolving these contradictory reports on the quantity of hydrogen uptake by carbon nanotubes. Unfortunately, even though various model calculations have been carried out using a variety of computational techniques, the results have not yet converged.

Essentially all the theoretical calculations so far reported in literature address one or the other aspects of the problem as follows.

- Whether hydrogen adsorption takes place inside the tube or outside the tube. Calculations seem to favour adsorption in between the tubes rather than inside the tubes. There are also indications that the arrangement of the tube also has an influence on the hydrogen adsorption. (Bauschlicher and Christopher, 2002; Lee and Lee, 2000; Froudakis 2001; Wang and Johnson, 1999a; Ye *et al.*, 1999).
- The reports dealing with adsorption of hydrogen inside the tubes, consider various types of sites like, zigzag, armchair, chiral show that hydrogen adsorption is favored only in some specific sites. (Lee *et al.*, 2001; Dodziuk and Dolgonos, 2002; Yang and Yang, 2002).
- There are also reports which deal with tube diameter, tube geometry like (5,5), (10,10) arrangements which show that adsorption is not only dependent on tube diameter, but also on the structural arrangements of the carbon nanotubes. (Lee and Lee, 2000; .Ma *et al.*, 2002; Lee *et al.*, 2000; Arellano *et al.*, 2002).
- There are a few studies on the evaluation of interaction potential, which show that the adsorption strength is not adequate to account for any substantive chemisorption on carbon nanotubes. (Stan and Cole, 1998; Wang and Johnson, 1999b; Gordon and Saeger, 1999).
- There are a few studies relating to effect of experimental variables like pressure and temperature as well as inclusion of hydrogen in the carbon frame work and the resultant effect of alteration of the carbon nanotube geometries (Chan *et al.*, 2001; Yin *et al.*, 2000).

The essence of these studies is:

- The studies could not establish whether carbon nanotubes could adsorb hydrogen up to the extent of DOE standards 6.5wt% or 62% in terms of volumetric density.
- They are unable to unequivocally state whether hydrogen adsorption is preferred inside the nanotube or adsorption takes place in the interstices between the tubes.
- Above all, these studies have been somewhat silent on the sites on which hydrogen activation takes place before they are adsorbed by the carbon atoms of the nanotube. It is generally believed that the carbon sites present are unable to activate the hydrogen molecule.

The present investigation has therefore been undertaken with the following objectives and postulates.

1. Hydrogen adsorption on carbon materials especially nanotubes, is possible only when it contains some sites wherein hydrogen molecule can be activated. Taking the clue from nature, it is postulated that the heteroatoms present in the carbon nanotubes may be the appropriate sites for activation of hydrogen.
2. If heteroatom containing carbon nanotubes were to be one of the appropriate materials for hydrogen storage, then what is the gradation of materials containing various heteroatoms as well as their geometrical positions in the nanotubes.

In order to understand the interaction of hydrogen molecule in pure carbon nanotubes and heteroatoms like nitrogen, phosphorus, sulphur and boron (N, P, S and B)

substituted carbon nanotubes, cluster model calculations were carried out using Density Functional Theory (DFT).

Molecular modeling provides a rapid means of assessing the potentiality of the new materials developed and used. Mainly in the case of adsorption application by parameterizing the description of the adsorbate and adsorbent interactions, one can estimate the adsorption capacity as a function of the system temperature and pressure. In general, more complicated descriptions of these features will require more computational effort. Thus, it is important to choose a model simple enough to perform calculations quickly and efficiently yet with sufficient rigour to provide reliable estimates for potential applications. Molecular modeling is one of the best tool to understand the fundamental science. This technique is used in the fields of computational chemistry, computational biology and materials science for studying molecular systems ranging from small chemical systems to large biological molecules and material assemblies.

3.1.2. Computational models

A theoretical model for any complex process is an approximation but well-defined mathematical procedure of simulation. When applied to chemistry, the task is to use the input information on the number and character of component particles (nuclei and electrons) to derive information and understanding of resultant molecular behaviour. Even very complex systems can be modeled and the activity can be found.

3.1.2.1. An overview of computational chemistry

There are two broad areas within computational chemistry devoted to the structure of molecules and their reactivity: molecular mechanics and electronic structure

theory, (Forsman and Frish, 1996). Both perform the same basis types of calculations:

- Computing the energy of a particular molecular structure (spatial arrangement of atoms or nuclei and electrons). Properties related to the energy may also be predicted by some methods.
- Performing geometry optimisations, which locate the lowest energy molecular structure in close proximity to the specified starting structure. Geometry optimisations depend primarily on the gradient of the energy – the first derivative of the energy to atomic positions.
- Computing the vibrational frequencies of molecules resulting from interatomic motion within the molecule. Frequencies depend on the second derivative of the energy with respect to atomic structure, and frequency calculations may also predict other properties, which depend on second derivatives. Calculations aimed at predicting frequencies of vibrational modes are not possible or practical for all computational chemistry methods.

3.1.2.2 Methods for electronic structure

Electronic structure methods use the laws of quantum mechanics rather than classical physics as the basis for their computations. Quantum mechanics states that solving the Schrodinger equation, for the smallest systems may yield energy and other related properties of a molecule, however, exact solutions to the Schrodinger equation are not computationally practical. Electronic structure methods are characterised by their various mathematical approximations to its solution. There are two major classes of electronic structure methods, (Foresman and Frish, 1996):

- Semi-empirical methods, such as AM1, MINDO/3 and PM3, which use the parameters derived from experimental data to simplify the computation. Plugged parameters are taken into consideration during calculation.
- *Ab- initio* methods, unlike either molecular mechanics or semi-empirical methods, use no experimental parameters in their computations. Instead, their computations are based solely on the laws of quantum mechanics – the first principles referred to in the name of *ab initio*- and on the values of a small number of physical constants: the speed of light, the masses and charges of electrons and nuclei and Planck's constant.

Semi-empirical and *ab- initio* methods differ in computational cost and accuracy of result. Semi-empirical calculations are relatively inexpensive and provide reasonable qualitative descriptions of molecular systems and fairly accurate quantitative predictions of energies and structures for systems where good parameter sets exist. (Foresman and Frish, 1996).

Quantum chemical cluster calculations are widely employed to study the hydrogen storage capacity in carbon nanomaterials. Several non-empirical and semi-empirical calculations are reported to study the storage capacity. The non-empirical methods especially the conventional Hartree Fock plus correlation energy method is associated with sharp increase in the computer time requirement with increase in the size of the cluster or basis set. For example, a wave function for an N electron system contains 3N coordinates (three for each electron, four if spin is included.). For larger carbon clusters of carbon nanotubes, (number of electrons is high), calculation of electronic properties by conventional *ab-initio* method is not desirable. Moreover to solve the HF equations, assumptions have to be made that the electron interacts with average

potential coming from other electrons. In reality, electronic correlation with their movements and try to avoid each other, so there is least amount of electrostatic repulsion. To account for the dynamic correlation, one has to go to correlation methods, which use multi determinant wave functions and their scales are of fifth or greater power with size of a system. In order to avoid these complexities and difficulties, Density Functional Theory (DFT) is used to describe the electron systems.

3.1.2.3 Density Functional Theory (DFT)

The basis of DFT method is that the ground state electronic energy is determined completely by electron density 'ρ'. In other words there exists one to one correspondence between the electron density of a system and energy. The electron density is the square of wave function, integrated over N-1 electron coordinates. This depends only on three coordinates independent of the number of electrons. The complexity of the wave function increases with the number of electrons, the electron density has same variables independent of the size of the system.

For a system of M nuclei and N electrons, the electronic Hamiltonian operator contains the following terms.

$$H_e = -\sum 1/2 \nabla_i^2 - \sum \sum Z_A / |R_A - r_i| - \sum \sum 1 / |r_i - r_j| + \sum \sum Z_A Z_B / |R_A - R_B|$$

The first term represents the kinetic energy in atomic units, the second term represents the nuclear potential, third term represents the inter-electronic repulsion and last term corresponds to the inter nuclear repulsion. According to Born-Oppenheimer approximation the last term is a constant. It is seen that the Hamiltonian operator is uniquely determined by the number of electrons and the potential created by the

nuclei V_{nc} . This means that the ground-state wave function (and thereby electron density) and ground state energy are also given exclusively by these quantities. The goal of DFT method is to design the functions connecting the electron density with energy.

The field of rigorous DFT theory was born in 1964 with the publication of Hohenberg and Kohn (Hohenberg and Kohn 1964). The aspects on which this theory is based are:

1. Every observable of a stationary quantum mechanical system (including energy) can be calculated in principle exactly from the ground state density alone. Every observable can be written as a function of ground state density.
2. The ground state density can be calculated in principle exactly using the variational method.

3.1.2.4 KOHN and SHAM Method.

The expression relating kinetic energy to density is not known with satisfactory accuracy. The current expressions even those improved upon from the original Thomas-Fermi theory are quite crude and quite unsatisfactory for atoms and molecules in particular. On the other hand, the kinetic energy is easily calculated from the wave function, provided it is known. For that reason, Kohn and Sham (1965) proposed an ingenious method of merging wave function and density approach. They repartitioned the total energy function into the following parts:

$$E[\rho]=T_0[\rho]+ \int [V_{ext}(r) +U_{el}(r)] \rho(r) dr + E_{xc}[\rho]$$

where $T_0[\rho]$ is the kinetic energy of the electrons in a system which has the same density ρ as the real system, but in which there is no electron-electron interaction. This is frequently called a system of noninteracting electrons. But it may be misunderstood, since electrons still interact with nuclei. $U_{el}(r)$ is a pure Coulomb ('classical') interaction between electrons. It includes electron self-interaction explicitly. $V_{ext}(r)$ is the external potential, i.e. potential coming from the nuclei.

The last function $E_{xc}(\rho)$ is called exchange correlation energy. It includes all the energy contributions, which are not accounted for by previous terms. (i.e.)

1. Electron exchange
2. Electron correlation since non-interacting electrons do need to correlate their movements
3. A portion of the kinetic energy which is needed to correct $T_0(\rho)$ to obtain true kinetic energy of a real system $T(\rho)$
4. Correction for self-interaction introduced by the classical coulomb potential

However, better approximations for this function are being available. Derivation of Kohn-Sham equations by assuming energy function to apply this in variational principle and obtain

$$\mu = \delta E[\rho(r)] / \delta \rho(r) = \delta T_0[\rho(r)] / \delta \rho(r) + V_{ext}(r) + U_{el}(r) + \delta E_{xc}[\rho(r)] / \delta \rho(r)$$

$$\mu = \delta E[\rho(r)] / \delta \rho(r) = \delta T_0[\rho(r)] / \delta \rho(r) + V_{eff}(r)$$

where all terms are lumped together, except noninteracting electron kinetic energy, into an effective potential depending upon r :

$$V_{\text{eff}}(\mathbf{r}) = V_{\text{ext}}(\mathbf{r}) + U_{\text{el}}(\mathbf{r}) + V_{\text{xc}}(\mathbf{r})$$

where the exchange correlation potential is defined as a functional derivative of exchange correlation energy:

$$V_{\text{xc}}(\mathbf{r}) = \delta E_{\text{xc}}[\rho(\mathbf{r})] / \delta \rho(\mathbf{r})$$

The form of equation asks for a solution as a Schrodinger equation for non-interacting particles:

$$[-1/2\nabla_i^2 + V_{\text{eff}}(\mathbf{r})]\phi_i^{\text{KS}}(\mathbf{r}) = \epsilon_i \phi_i^{\text{KS}}(\mathbf{r})$$

It is similar to the eigen equation of the Hartree-Fock method, with one difference it is simpler. The Fock operator in Hartree Fock Roothan method contains the potential, which is non local. i.e. different for each electron. The Kohn-Sham operator depends only on r , and not upon the index of the electron. It is the same for all electrons. The Kohn-Sham orbitals, which are quite easily derived from this equation, can be used immediately to compute the total density

$$\rho(\mathbf{r}) = \sum |\phi_i^{\text{KS}}(\mathbf{r})|^2$$

which can be used to calculate an improved potential $V_{\text{eff}}(\mathbf{r})$, that can lead to a new cycle of self-consistent field. Density can also be used to calculate the total energy from equation in which the kinetic energy $T_0(\rho)$ is calculated from the corresponding orbitals, rather than density itself.

$$T_0(\rho) = 1/2 \sum \langle \phi_i^{\text{KS}} | \nabla_i^2 | \phi_i^{\text{KS}} \rangle$$

The key to Kohn-Sham theory is the calculation of the kinetic energy under the assumption of non-interacting electrons. In reality, electrons are interacting. Kohn-Sham theory does not provide the true kinetic energy. The difference between the exact kinetic energy and that calculated by assuming non-interacting electron orbitals is small. The remaining kinetic energy is absorbed in to an exchange –correlation term E_{xc} . However, the exchange correlation energy was partitioned into two parts.

$$E_{xc}[\rho] = E_x[\rho] + E_c[\rho]$$

The exchange energy and correlation energy. This partition is quite arbitrary, since exchange and correlation have slightly different meaning than in *ab-initio* approaches. The exchange energy in LDF/LSD was approximated with the homogenous gas exchange result given by equation

$$E_{X\alpha}[\rho\uparrow, \rho\downarrow] = -9/4\alpha(3/4\pi)^{1/3} \int [\rho\uparrow^{4/3}(r) + \rho\downarrow^{4/3}(r)] dr$$

where $\alpha=2/3$

The correlation energy is expressed as

$$E_c[\rho] = \int \rho(r) \epsilon_c[\rho\uparrow(r)\rho\downarrow(r)] dr$$

where $\epsilon_c[\rho\uparrow(r)\rho\downarrow(r)] dr$ is the correlation energy per one electron in a gas with spin densities $\rho\uparrow(r)$ and $\rho\downarrow(r)$. This function is not known analytically, but is constantly improved on the basis of quantum Monte Carlo simulations and fitted to analytical expansions (Vosko and Wilk, 1980; von Barth, 1979). The local functions derived from electron gas data worked surprisingly well, taking into account that they substantially underestimate the exchange energy (by as much as 15%) and grossly

overestimate the correlation energy, sometimes by 100%. The error in exchange is however larger than the correlation error in absolute values. LSD/LDF is known to overbind normal atomic bonds, on the other hand, it produces too weak hydrogen bonds.

Early attempts to improve functions by GEA (Gradient Expansion Approximation), in which $E(\rho)$ was expanded in Taylor series versus ρ and truncated at a linear term, did not improve results too much (Langreth and Vosko, 1990). Only GGA (Generalized Gradient Approximation) provided notable improvements by expanding $E(\rho)$. The expansion is not a simple Taylor expansion, but tries to find the right asymptotic behavior and right scaling for the usually nonlinear expansion. These enhanced functions are frequently called non-local or gradient corrections, since they depend not only upon the density, but also on the magnitude of the gradient (i.e. first derivative) of density at a given point. Probably the most frequently used functions today are: For exchange B88 (Becke, 1988), PW86 (Perdew and Wang 1986) For correlation P86 (Perdew, 1986), LYP (Lee, Yong, Parr) (Lee *at al.*, 1988)

Connection can be made between the exchange-correlation energy and the corresponding potential, connecting the non-interacting reference and the actual system. The resulting expansion is called adiabatic connection formula. These methods are called hybrid methods. B3LYP is one of the widely used hybrid method in literature for calculating electronic properties of carbon clusters (carbon nanotubes, fullerenes).

B3LYP is Becke 3 parameter function, which has the form:

$$A * EX_{\text{Slater}} + (1-A) * EX_{\text{HF}} + B * EX_{\text{Becke}} + EC^{\text{VWN}} + C * EC_{\text{non-local}}$$

where the non-local correlation is provided by the LYP expression. The constants A, B, and C are those determined by Becke by fitting to the G1 molecule set. Becke determined the values of the three parameters by fitting to the 56 atomization energies, 42 ionization potentials, 8 proton affinities, and 10 first-row atomic energies in the G1 molecule set computing values of A=0.80, B=0.72, and C=0.81. He used LDA densities and the Perdew/Wang 1991 correlation functions rather than VWN and LYP.

Since LYP includes both local and non-local terms, the correlation functions used are actually: $C \cdot E_{\text{CLYP}} + (1-C) \cdot E_{\text{CVWN}}$. In other words, VWN is used to provide the excess local correlation required, since LYP contains a local term essentially equivalent to VWN.

3.1.2.5 Basis set

There are two types of basis functions commonly used in electronic structure calculations: Slater Type Orbitals (STO) and Gaussian Type Orbitals (GTO). Slater type orbitals has the functional form

$$\chi_{\zeta,n,l,m}(r,\theta,\varphi) = N Y_{l,m}(\theta,\varphi) r^{n-1} e^{-\zeta r}$$

where N is normalization constant and $Y_{l,m}$ is the usual spherical harmonic functions. The exponential dependence on the distance between the nucleus and the electron mirrors the exact orbitals for the hydrogen atom. However, STOs do not have any radial nodes; Nodes in the radial part are introduced by making linear combinations of STOs. The exponential dependence ensures a fairly rapid convergence with increasing number of functions, however, the calculation of three and four center two electron integrals cannot be performed analytically. STOs are primarily used for atomic and

diatomic systems where high accuracy is required and in semi empirical methods where all three and four center integrals are neglected.

Gaussian type orbitals can be written in terms of polar or Cartesian coordinates.

$$\chi_{\zeta,n,l,m}(r,\theta,\varphi) = NY_{l,m}(\theta,\varphi) r^{2n-2-l} e^{-\zeta r^2}$$

$$\chi_{\zeta,n,l,m}(x,y,z) = N x^{l_x} y^{l_y} z^{l_z} e^{-\zeta r^2}$$

Where the sum of l_x , l_y and l_z determines the type of orbital (for example $l_x + l_y + l_z$ is a p orbital). Although a GTO appears similar in the two sets of coordinates, there is a subtle difference. A d-type GTO written in terms of the spherical functions has five components ($Y_{2,2}$, $Y_{2,1}$, $Y_{2,0}$, $Y_{2,-1}$, $Y_{2,-2}$) but there appear to be six components in the Cartesian coordinates (x^2 , y^2 , z^2 , xz , yz , xy). The latter six functions however, may be transformed to the five spherical d-functions and one additional s-function ($x^2 + y^2 + z^2$). Having decided on the type of function (STO/GTO) and the location (nuclei), the most important factor is the number of functions to be used. The smallest number of functions possible is a minimum basis set. Only enough functions are employed to contain all the electrons of the neutral atom(s). For hydrogen (and helium) this means a single s-function. For the first row in the periodic table it means two s-functions (1s and 2s) and one set of p-functions ($2p_x$, $2p_y$ and $2p_z$). Lithium and beryllium formally only required two s-functions, but a set of p-functions is usually also added. For the second row elements, three s-functions (1s, 2s and 3s) and two sets of p-functions (2p and 3p) are used.

The next improvement in the basis sets is a doubling of all basis functions producing a Double Zeta (DZ) type basis. A basis set which doubles the number of functions in the minimal basis set is described as a *double zeta basis*. The term zeta stems from the

fact that the exponent of STO basis functions is often denoted by the Greek letter ζ . A DZ basis thus employs two s-functions for hydrogen (1s and 1s') four s-functions (1s 1s' 2s and 2s') and two p-functions (2p and 2p') for first row elements and six s-functions and four p-functions for second row elements.

The chemical bonding occurs between valence orbitals. Doubling the 1s-functions in for example carbon allows for a better description of the 1s-electrons. However, the 1s-orbital is essentially independent of the chemical environment, being very close to the atomic core. A variation of the DZ type basis only doubles the number of valence orbitals, producing a split valence basis. In actual calculations, a doubling of the core orbitals would rarely be considered and the term, DZ basis is also used for split valence basis sets (or sometimes VDZ for valence double zeta). Example 3-21G in this basis set three Gaussian functions are used to describe the core orbitals. The valence electrons are represented by three Gaussians: the contracted part by two Gaussians and the diffuse part by one Gaussian. The most commonly used split valence basis sets are 3-21G, 4-31G and 6-31G.

The next step up in basis set is a Triple Zeta (TZ). Such a basis contains three times as many functions as the minimum basis (i.e. six s-functions and three p-functions) for the first row elements. Some of the core orbitals may again be saved by only splitting the valence producing a triple split valence basis set. Again the term TZ is used to cover both cases. The names Quadruple Zeta (QZ) and Quintuple Zeta (5Z) for the next levels of basis sets are also used, but large sets are often given explicitly in terms of the number of basis functions of each type.

Polarization functions are added to the chosen sp-basis. Adding a single set of polarization functions (p-functions on hydrogen s and d-functions on heavy atoms) to

the DZ basis forms a Double Zeta plus Polarization (DZP) type basis. The use of polarization basis function is indicated by an asterisk (*). There is a variation where polarization functions are only added to non-hydrogen atoms. This does not mean polarization functions are not important on hydrogen. However, hydrogen is often has a passive role, sitting at the end of bond, which does not take an active part in the property of interest. The errors introduced by not including hydrogen polarization functions are often rather constant and as the interest is usually in energy differences, they tend to cancel out. Thus, 6-31G* refers to a 6-31G basis set with polarization function on the heavy (i.e. non-hydrogen) atoms. Two asterisks (e.g. 6-31G**) indicates the use of polarization (i.e. p) function on hydrogen and helium. The 6-31G** basis sets is particularly useful where hydrogen acts as a bridging atom.

3.1.2.6 Effective core potential basis sets

For systems involving elements from the third row or higher in the periodic table, there is a large number of core electrons which in general are unimportant in a chemical sense. However, it is necessary to use a large number of basis functions to expand the corresponding orbital. Otherwise the valence orbital will not be properly described (due to a poor description of the electron-electron repulsion). In the lower half of the periodic table, relativistic effects furthermore complicate matter. These two problems may be solved simultaneously by introducing an Effective Core Potential (ECP) (also called Pseudopotential) to represent all the core electrons. This is in the spirit of semi empirical methods, the core electrons are modeled by a suitable function, and only the valence electrons are treated explicitly. In many cases this gives quite good results at a fraction of the cost of a calculation involving all electrons. Part of the relativistic effects may also be taken care of especially the scalar effects without

having to perform the full relativistic calculation. ECPs have also been designed for second row elements, although the saving is only marginal relative to all electron calculations.

There are four major steps in designing ECP type basis sets. First a good quality all electron wave function is generated for the atom. This will typically be a numerical Hartree-Fock or a relativistic Dirac-Hartee-Fock calculation. The valence orbitals are then replaced by a set of nodeless pseudo-orbitals. The regular valence orbitals will have a series of radial nodes in order to make them orthogonal to the core orbitals, and the pseudo-orbitals are designed so that they behave correctly in the outer part, but do not have a nodal structure in the core region. The core electrons are then replaced by a potential so that solution of the Schrodinger (or Dirac) equation produces valence orbitals matching the pseudo-orbitals. Since relativistic effects are mainly important for the core electrons, this potential effectively includes relativity. The potential will be different for each angular momentum, and will normally be obtained in a tabulated form. In the final step, this numerical potential is fitted to a suitable set of analytical functions, normally a set of Gaussian functions.

$$U_{\text{ECP}}(r) = \sum a_i r^{n_i} e^{-\alpha_i r^2}$$

The parameters ‘n’ and ‘a’ depend on the angular momentum (s-, p.- d- etc.) and are determined by least squares fit. Typically between two and seven Gaussian functions are used in the fit, (and consequently the resulting orbitals) at the price of increased computational time.

3.1.2.7 Molecular Mechanics

For calculation of ground state electronic properties of molecules, the geometry of a molecule should be at global minimum. The given geometry of a molecule has to be optimized in any theoretical method to get a global minimum. The

geometry optimization of simple molecules like methane and water can be carried out easily by quantum mechanical method. For a larger cluster of carbon atoms (carbon nanotubes and higher fullerenes) the geometry optimization by quantum mechanical method is not reliable, because it will take four or five months to get an optimized geometry for a given large cluster model. In order to get an optimized geometry for large clusters, force field method is usually employed. In the force field method the molecules are modeled as atoms and held together by bonds. The molecule is described by a ball and spring model. Force field methods are also referred to as molecular mechanics methods. Molecular mechanics calculations don't explicitly treat the electrons in a molecular system. Instead, they perform computations based on the interactions among the nuclei. Electronic effects are implicitly included in force fields through parameterisation (Foresman and Frish, 1996). In addition to by passing the solution of the Schrodinger equation, quantum aspects of the nuclear motion are also neglected. This means that the dynamics of the atoms are treated by classical mechanics, i.e. Newton's second law.

The force field energy is written as the sum of the terms, each describing the energy required for distorting a molecule in a specific fashion.

$$E_{FF}=E_{str}+ E_{bend}+ E_{tors}+ E_{vdw}+ E_{el}+ E_{cross}$$

E_{str} is the energy function for stretching bond between two atoms. E_{bend} represents the energy required for bending an angle, E_{tors} is the torsional energy for rotation around a bond. E_{vdw} and E_{el} are describing the non-bonded atom-atom interactions and finally E_{cross} describes the coupling between the first three terms. Stable molecules

corresponding to minimum on the potential energy surface can be located by minimizing E_{FF} as a function of the nuclear coordinates.

There are many different force fields in use. They differ in three main aspects

1. The functional form of each energy term
2. The number of cross terms included
3. The type of information used for fitting the parameters.

Advantages of UFF include the fact that it uses a 'first-principles approach', where the atomic parameters are based only on the element, its hybridization and its connectivity. This is the most promising full periodic table force field available at this time.

3.1.3 Heteroatom containing CNTs - their relevance

In order to understand the interaction of hydrogen molecule in pure carbon nanotubes and heteroatom (N, P, S and B) substituted carbon nanotubes, cluster model calculations have been carried out using Density Functional Theory (DFT). To study the activation of hydrogen molecule by heteroatom containing carbon nanotubes, a combined Universal Force Field (UFF) and Density Functional Theory (DFT) method has been used. In the later stage, DFT method has been utilized to study the reaction mechanism of hydrogenation by using a simple cluster model chosen from the reactive part of the CNT to get the accurate results.

3.1.4 Model design and methodology

Typically three Single Walled Carbon nanotubes (SWNTs) of armchair type (4, 4) with each tube having 32 carbon atoms making tube diameter of 5.56 Å have been

considered. First full geometry optimization has been carried out to one SWNT with DFT by using Becke's three parameter hybrid functional with LYP correlation functional (B3LYP) and 6-31G (d, p) basis set (Becke, 1993; Lee *et al.*, 1988). The terminal sites of the CNT cluster are saturated with hydrogen atoms in order to avoid the edge effect (Yang *et al.*, 2002). This optimized SWNT has been utilized to construct an interface with three nanotubes of interstitial site 3.64 Å (the distance between two tubes) as shown Fig 3.1(a). The valency of each element is taken into consideration for the calculations. It is reported in literature that the hydrogen molecule has preferential interaction at the interface of the carbon nanotubes (Chan *et al.*, 2001). The model describes the interface of the three carbon nanotubes that has been optimized with Universal Force Field parameter (UFF 1.02) (Rappe *et al.*, 1992) in Cerius² software.

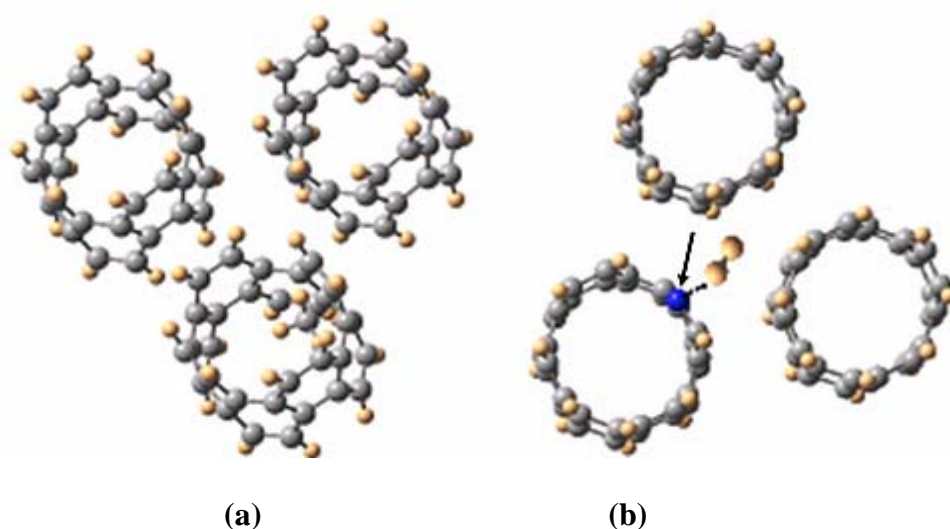


Fig. 3.1 (a) The side view of the UFF optimized CNT (4, 4) cluster taken for the study, where the terminal positions are saturated with hydrogen (b) Top view of the heteroatom (arrow indicated ball) containing CNT cluster with the hydrogen molecule interaction

The geometric parameters of the cluster models minimized by force field method (Table 3.1) coincide well with the normal bond length values. The intermolecular

torsions are all zero indicating that the cluster model minimized by Force field method can be reliable. Hydrogen molecule is allowed to interact at the top of cluster as shown in Fig. 3.1. The interactions are found to be effective on the top of carbon atoms rather than on the top of carbon hexagon cluster (Froudakis, 2001). Computations using DFT have been carried out on optimized configuration obtained using UFF. The single point energy and bond population analysis were carried out by DFT on the optimized configurations by using B3LYP/ 6-31g (p, d) basis set. To reduce the computational cost combined UFF / DFT method has been utilized to find the effect of heteroatom on hydrogen activation as this combined method has been effectively utilized for such large systems (Froudakis, 2001). The substitutional positions for heteroatoms in the CNT cluster model have been chosen based on the fact that the interstitial position offers minimum potential energy for the cluster and our calculations also show the same. The stability of the substituted CNT plays a crucial role in hydrogenation reaction and they seem to be stable by showing the minimum energy difference between pure CNT and the substituted CNT.

Table 3.1 Geometric parameters of the CNT cluster optimized by employing Universal Force Field (UFF 1.02) method

Cluster model	Average bond length (Å)			Average bond angles (°)			
	C-C	X-C		<C-X-C		<X-C-C	<C-C-C
		Reported	Observed	Reported	Observed		
CNT	1.416	1.385	1.396	120.0	120.9	123.0	123.0
N CNT	1.409	1.336	1.359	117.4	122.1	121.0	121.6
P CNT	1.417	1.768	1.710	104.6	103.0	119.2	122.4
S CNT	1.416	1.790	1.736	99.6	103.2	118.8	122.4
B CNT	1.420	1.486	1.431	106.6	109.6	120.5	120.8

To study the reaction mechanism a simple cluster model with 14 carbon atoms has been taken which is the terminal and reactive part in the SWNT for the hydrogen interaction and hydrogenation as shown in Scheme 3.1. The ends of the cluster are saturated with hydrogen in order to avoid the boundary effect (Yang *et al.*, 2002). The cluster was fully optimized with density functional B3LYP method with 6-31g (p, d) basis set. The geometrical parameter of the simple cluster shows planar nature. This simple cluster has been considered only to study the reaction of hydrogen with the carbon surface and the structural effects like tube curvature are not taken into the consideration. The nature of stationary points thus obtained was characterized by frequency calculations. All the transition states corresponding to hydrogen migration were located and characterized as saddle points using the frequency calculations. It was found to possess one imaginary frequency at the same levels of theory. The geometric parameters and the nature of the imaginary frequencies were examined using the graphical interface program, Gauss View 03 (Dennington II *et al.*, 2003). All the DFT calculations were performed using Gaussian 03 in a cluster of IBM Linux machine (Frisch *et al.*, 2004).

3.1.5 Results and Discussion

The total energy, hydrogen bond distance and the dissociation energy of hydrogen molecule obtained are given in Table 3.2. The points that emerge out of the results are: (i) Hydrogen activation has been favoured by a decrease in the hydrogen dissociation energy in the case of substitution of heteroatoms like N, P and S. The dissociation energy of hydrogen in its free state is 4.76 eV, and remains unaltered when it is placed in between the pure carbon nanotubes (4.51 eV). Whereas it is altered to 0.13, 0.22 and 2.33 eV for S, N, and P substituted CNTs respectively. Though the calculated dissociation energy values are unrealistically small, they

definitely indicate that the dissociation of hydrogen molecule is a facile process on heteroatom substituted carbon nanotubes. Even though the calculated dissociation energy is small, the process of hydrogen storage may involve other barriers including mass transport and hence could not be achieved at such low energies.

The lowering of this dissociation energy of hydrogen molecule can be explained on the basis of redox potential values of the respective redox couples involved. For instance, redox potentials (Fig 1.3) of heteroatoms are higher than that of carbon (S/S^{2-} , N/N^{3-} , P/P^{3-} , C/C^{4-} are respectively, 0.171, 0.057, -0.111 and -0.132 V vs SHE). The same fact can be further independently supported by the Ellingham diagram which indicates that free energy of formation of N-H bond is more favourable than that of C-H bond.

Table 3.2 Bond length and dissociation energy of hydrogen on the CNTs calculated using B3LYP with 6-31g (p, d) basis set on the UFF optimized structure

Substitution	Total energy (Hartrees)	Bond length H_1-H_2 (Å)	Dissociation energy (eV)
Hydrogen	-1.175	0.708	4.76
CNT	-3686.5502	-	-
CNT + H ₂	-3687.7161	0.776	4.51
N CNT	-3702.5908	-	-
N CNT + H ₂	-3703.5989	0.835	0.22
P CNT	-3989.1694	-	-
P CNT + H ₂	-3990.2550	0.815	2.33
S CNT	-4046.0020	-	-
S CNT + H ₂	-4047.0067	0.817	0.13
B CNT	-3671.7254	-	-
B CNT + H ₂	-3672.9440	0.818	5.95
2B CNT (adjacent)	-3658.6666	-	-
2B CNT (adjacent) + H ₂	-3659.8092	0.913	3.88
2B CNT (alternate)	-3659.3491	-	-
2B CNT (alternate) + H ₂	-3660.3594	0.928	0.28

The bond length of the hydrogen molecule is elongated in heteroatom substituted CNT compared to that of pure CNT, indicating that there is considerable amount of activation of hydrogen molecule in heteroatom containing CNTs. (ii) Substitution of boron atom in the CNT shows interesting results. Single boron substitution cannot activate the hydrogen molecule. Two boron atoms are essential for the hydrogen activation. The dissociation energy of hydrogen for single boron substitution is 5.95 eV where as when two boron atoms are substituted in adjacent positions the dissociation energy is reduced to 3.88 eV. It is further decreased to 0.28 eV when two boron atoms are substituted in the alternate positions. This implies substitution of boron at alternate positions is more favourable for hydrogen activation rather than substitution at adjacent positions. It can be substantiated that boron - boron bond length is the key factor for hydrogen – hydrogen bond activation. Substitution of B at alternate position seems to be favorable for the activation of hydrogen, where in bonding appears to be similar to that of diborane (Weast. 1978). Orbital contributions have been analyzed by taking the HOMO (Highest Occupied Molecular Orbital) level of CNT cluster. In the case of unsubstituted CNT, the main contribution to the HOMO level is from 2p orbital of carbon (Table 3.3). There is no contribution from the terminal hydrogen present in the cluster which clearly shows that terminal hydrogen used to saturate the valency will not affect the results obtained.

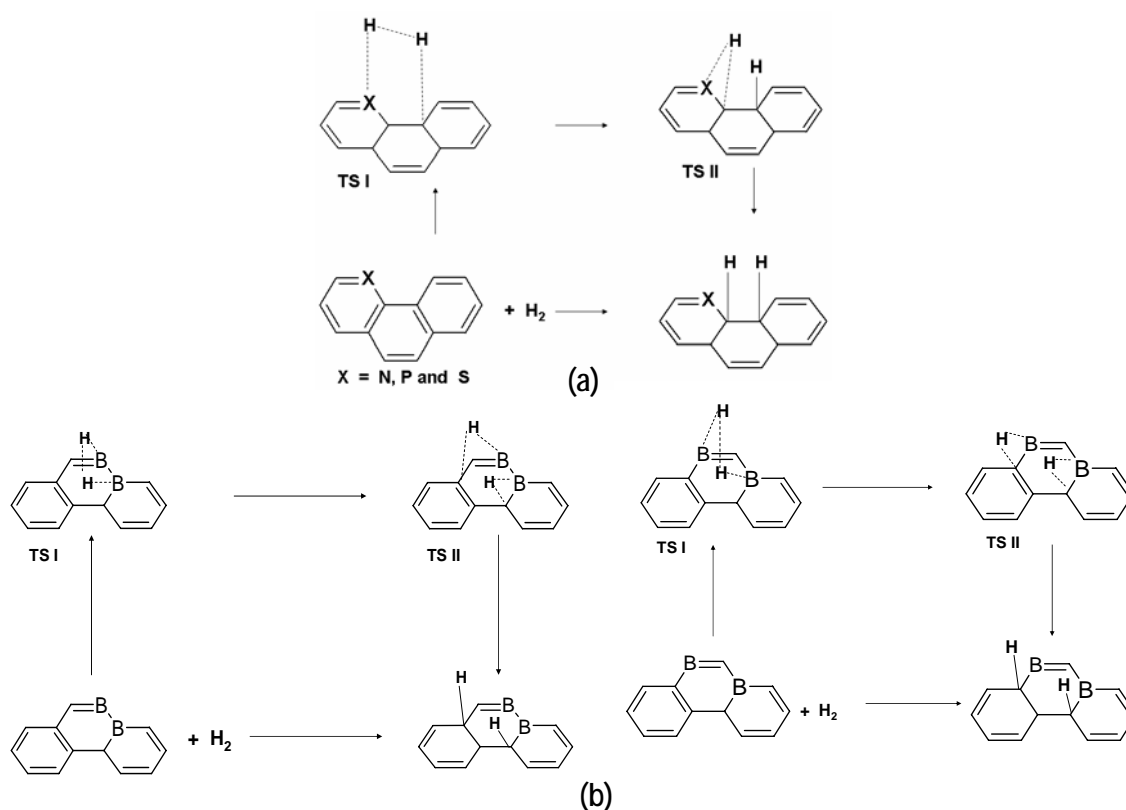
Table 3.3 Percentage orbital contribution of the HOMO level of the pure CNT and heteroatom substituted CNT before and after hydrogen interaction

% of orbital contribution from HOMO level (energy in Hartrees)	Carbon		Heteroatom		Hydrogen	
	S	p	s	p	b ^a	t ^a
Contribution	S	p	s	p	s	s
CNT (-0.1612)	0	100	-	-	-	-
CNT + H ₂ (-0.1613)	0	100	-	-	0	0
N CNT (-0.1617)	1	98.30	0	0.18	-	0.56
N CNT + H ₂ (-0.1371)	0.52	37.39	1.37	31.91	26.66	2.15
P CNT (-0.1611)	1	96.85	0	1.71	-	0.53
P CNT+ H ₂ (-0.1516)	1	85.62	0.04	8.06	4.83	0.49
S CNT (-0.1375)	1	76.87	0	21.17	-	1.16
S CNT + H ₂ (-0.1207)	0.45	41.80	0.35	41.65	14.87	0.88
B CNT (-0.1576)	1	94.87	0	3.59	-	0.5
B CNT + H ₂ (-0.1534)	1	96.26	0.10	1.12	1	0.54
2B CNT (adjacent) (-0.1568)	1.01	96.98	0	1.53	-	0.5
2B CNT (adjacent) + H ₂ (-0.1564)	6.26	88.34	0.10	4.67	0.28	0.4
2B CNT (alternate) (-0.1540)	12.56	80.41	0.60	5.49	-	1
2B CNT (alternate) + H ₂ (-0.1572)	14.67	73.93	0.73	4.48	5.32	0.86

^a where b- bonded hydrogen to heteroatom and t- terminal hydrogen in the cluster

On interaction of hydrogen molecule with CNT cluster, there is no contribution of H 1s orbital to HOMO values. This indicates that there is no bond formation between the CNT and hydrogen molecule. In the case of heteroatom-substituted CNT, the HOMO level contribution is from 2p orbital of the carbon. Upon interaction with hydrogen molecule, the contribution to HOMO level comes from both hydrogen 1s orbital and the p orbitals of heteroatom, which unambiguously shows that there exists bond formation between the heteroatom and hydrogen molecule. The valuable information obtained is that the in-coming hydrogen molecule is activated at the heteroatom sites and further gets transferred to the carbon sites as in the case of spill over mechanism. This is due to the fact that the existence of equipotential sites favours such a facilitating situation. It is deduced from the bond length, bond energies

and wave function values that the presence of heteroatoms in carbon nanotubes activates hydrogen and lead to adsorption of hydrogen.



Scheme 3.1 (a) The proposed mechanistic path way for hydrogenation of heteroatom substituted CNTs. (b) Mechanistic pathway for the hydrogenation of boron substituted CNTs in adjacent and alternate positions

Calculation of transition state parameters show that the reaction proceeds from one minimum to another minimum via an intermediate maximum. The movement of hydrogen from the heteroatom can be conceived by the transition state theory calculation as shown in Scheme 3.1. The activation energy (ΔE_a) for this process has been obtained using the calculated parameters. The results are given in Table 3.4 and the energy profile diagram of the mechanistic path ways for the substitution of heteroatoms like N, P and S is given in Fig. 3.2.

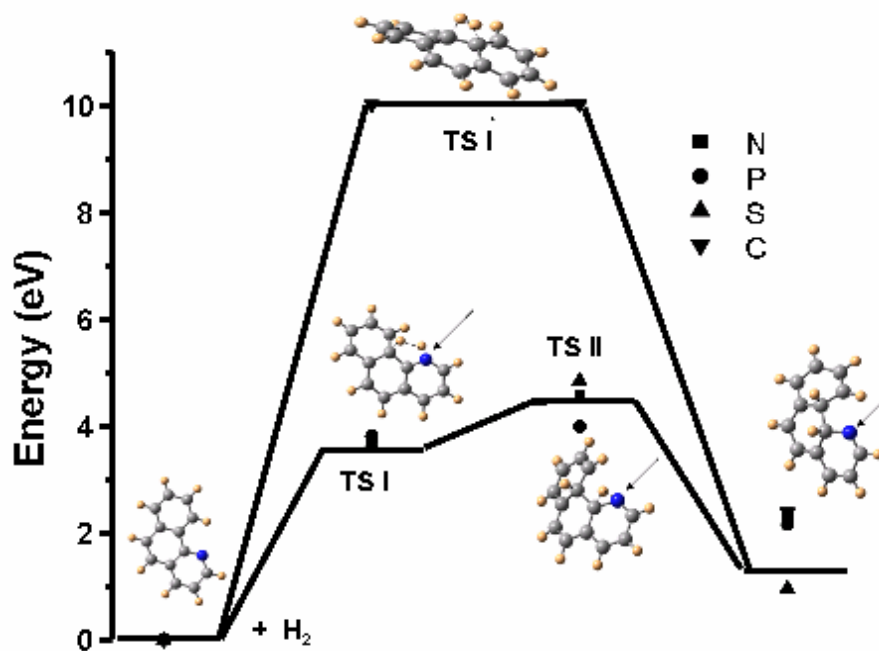


Fig. 3.2 The transition state energy profile of the heteroatom substituted CNTs cluster calculated by DFT method (B3LYP) with 6-31g (p, d) basis set (the balls indicated by arrows are heteroatoms like N, P and S)

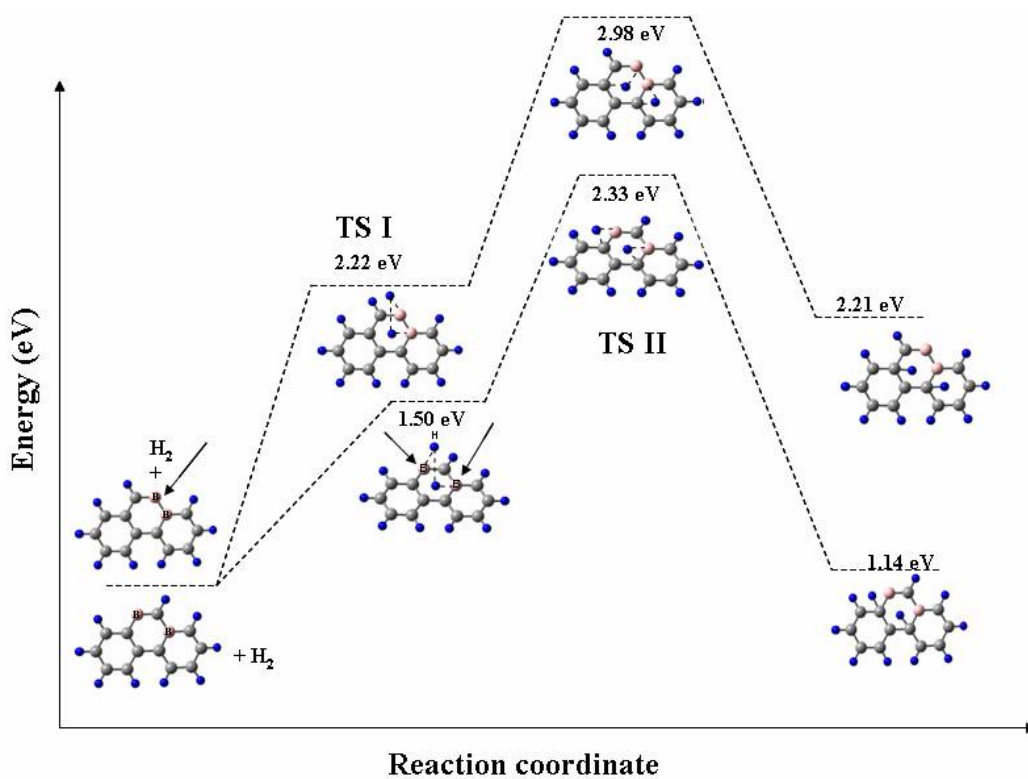


Fig. 3.3 The transition state energy profile of boron substituted CNTs cluster calculated by DFT method (B3LYP) with 6-31g (p, d) basis set (the balls indicated by arrows are boron atoms)

Table 3.4 Transition state optimized parameters of the cluster and the value of the activation energy calculated by B3LYP with 6-31g (p, d) basis set

Substitution	Ea I (eV)	Ea II (eV)	H ₁ -H ₂ (Å)	X-H (Å)	C-H ₁ ^b (Å)	C-H ₂ ^b (Å)
CNT cluster	10.02	-	0.71	-	-	-
N CNT cluster	3.84	4.58	1.45	1.11	1.70	1.94
P CNT cluster	3.81	3.99	1.51	1.61	1.27	2.33
S CNT cluster	3.65	4.85	1.50	1.75	1.24	2.40
2B CNT cluster (adjacent)	2.22	2.98	1.95	1.31	2.59	2.72
2B CNT cluster (alternate)	1.5	2.33	2.95	1.47	1.47	2.34

where Ea = E(transition state) – E (reactant) and ^b Shortest C-H bond distance

From the results, it is clear that the energy for the activation of hydrogen in the first transition state is lower for the heteroatom containing CNT compared to pure CNT. In addition, subsequent transfer of hydrogen to carbon is a facile process in the presence of heteroatom. Boron containing CNT with boron atom located at alternate positions show considerable reduction in the overall activation barrier compared to the system with boron located at adjacent positions (Fig. 3.3). The proposed mechanism is given in Scheme 3.1(b). These results support the contention that heteroatoms are the appropriate sites for hydrogen activation. In recent results it has been shown that high hydrogen adsorption is possible by the substitution of heteroatom like nitrogen in the carbon frame work (Zhu *et al.*, 2005). These results further support the present theoretical calculations.

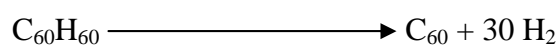
The present studies thus have shown that hydrogenation of CNTs requires activation centers and the heteroatom containing CNTs are able to activate the hydrogen in a facile manner compared to pure CNTs. For the effective hydrogenation and hydrogen

storage these heteroatoms should be incorporated geometrically and chemically into the carbon network.

3.2 THEORETICAL STUDIES ON FULLERENES

3.2.1 Introduction

The objective is to focus the logic behind this contention that carbon materials may be the possible candidates for hydrogen storage applications as well as to outline the fullerene and fullerene – based materials as promising media for hydrogen storage. Fullerenes have received attention due their unusual hydrogen – sorbing properties and the process of reversible reaction with hydrogen. Fullerenes, a new form of carbon with a closed-caged like molecular structure was first detected by Smalley (Kroto and Smalley, 1985). The theory predicts that maximum of 60 hydrogen atoms can be attached both to the inside (endohedrally) and outside (exohedrally) of the fullerene spherical surface via hydrogenation of carbon to form a stable $C_{60}H_{60}$ isomer. This is equal to ~7.7 wt.% hydrogen storage capacity. Since many of the fullerene reactions appear to be reversible, if a 100% conversion of $C_{60}H_{60}$ is achieved, 30 moles of H_2 gas would be liberated from each mole of fullerene hydride:



Since 1 mole of H_2 gas can produce 67.25 W·hr of electric power, 30 moles of H_2 generated by 1 mole of $C_{60}H_{60}$ should produce 2017.5 W·h of electricity resulting in 2.6 kW·h/kg or 4.4 Wh/m³ power density (density of $C_{60}H_{60}$ is ~1700 kg/m³). Even though the storage capacity of fullerenes is high, currently the hydrogenation of fullerene requires high pressure and temperature for the reaction to take place to overcome the reaction barrier (Jin *et al.*, 1994; Avent *et al.*, 1994). Hydrogenation of

fullerenes involve formation of C-H bonds as a result of breakage of C=C double bonds and dissociation of hydrogen molecule to form hydrogen atoms. From the experimental results, the activation energy for the hydrogenation was estimated to be 1.0 eV/H₂ and for dehydrogenation to reestablish C=C and reforming hydrogen molecule is higher about 1.6 eV/H₂. To overcome this potential barrier, high temperatures (> 673 K) and pressures (> 60 MPa) are required.

The process of hydrogenation of fullerenes involve formation of C-H bonds as a result of breakage of C=C double bonds of fullerenes and H-H bonds of molecular hydrogen to form hydrogen atoms. Although the hydrogenation reaction is exothermic (heat is released as a result of reaction), additional energy is required to break these bonds. Besides the thermodynamics involved in this process, a certain energy barrier has to be overcome for the reaction to occur. From the experimental results of solid state hydrogenation of fullerenes in gaseous hydrogen atmosphere at temperatures ranging between 673 – 723 K and pressures ranging between 60 to 80 MPa, the activation energy for the hydrogenation was estimated to be 100 kJ/mole (1.0 eV/H₂). Considering the dehydrogenation process, the potential barrier, associated with the breakage of C-H bonds, reestablishing C=C double bonds and forming molecular hydrogen, is even higher - about 160 kJ/mole (1.6 eV/H₂).

There have been a number of attempts to prepare hydro-fullerenes. Initially the experiments were carried out by direct gas phase hydrogenation of fullerenes under elevated temperatures and high pressures (673 - 723 K, 60 – 80 MPa) which resulted in the formation of compounds with hydrogen content up to 6.1 wt% (Loutfy and Wexler, 2001). In order to reduce the high energy required for the activation of hydrogen molecule, various approaches have been adopted like, selecting and

optimizing the metal catalyst for the reaction to take place. However, the addition of metal catalysts (Haufler *et al.*, 1990) shows decrease in the temperature and pressure. But the storage capacity is not significant because of the high polarisability of the metal towards hydrogen when compared to carbon. Alternatively the reaction was carried out in the liquid phase, which involves the utilization of solvent molecules and for this process the experimental conditions required are temperatures in the range 453-523 K and pressure of 12 MPa (Meier *et al.*, 1994; Banks *et al.*, 1993; Attalla *et al.*, 1993) However, the storage capacity of hydrogen decreased.

In a recent study Schimmel *et al* have shown that low temperature adsorption of hydrogen on carbon materials is related to the surface area. Carbon nanotubes with relatively low accessible area do not take up hydrogen as much as high surface area activated carbon (Schimmel *et al.*, 2003). A number of inelastic neutron scattering experiments have been carried out to identify the sites and the strength of bonding of hydrogen molecule with various types of carbon materials at low temperatures. These studies essentially consider the dynamics, especially the rotational features of the physisorbed hydrogen molecule either entrapped inside the C₆₀ network (FitzGerald *et al.*, 1999) or in the interstitial tunnels of the SWNT bundles (Ren and Price, 2001). These studies essentially lead to the conclusion that the binding strength of hydrogen molecule is almost the same for all kinds of carbon materials and that the magnitude of interaction is nearly around 5 kJ/mol.

In order to establish the feasibility of hydrogenation of fullerene molecules, number of theoretical calculations has been carried out various levels and the results essentially indicate that the fullerenes are capable of forming stoichiometric hydrides (C₆₀H_{12n} series). Among all the stoichiometric hydrides the C₆₀H₃₆ seems to be stable

one and has the lowest enthalpy of formation (Hall *et al.*, 1993; Rathna and Chandrasekhar, 1993; Hendrson and Cahill, 1992). By lowering the activation energy reversible hydrogenation of fullerenes is thermodynamically feasible at low temperatures. In order to lower the activation energy for the hydrogenation, other approaches are modifying the electronic structure of the fullerenes. In this approach, doping the fullerene with alkali metals (Na, K and Li) resulted in the formation of fulleride anions (Schur *et al.*, 2003). However it improves the hydrogenation process at lower temperatures and pressures but the dehydrogenation of hydrides is difficult and also the storage capacity is low. Though the metal sites are capable of activating hydrogen, the transport to the carbon surface is not a facile process and also the carbon surface by nature is not heterogeneous so as to promote the migration of hydrogen species from the metallic sites. In order to achieve high storage capacity there must be an activator, which should be easily hydridable than carbon and the dissociated hydrogen should then migrate to carbon surface (equipotential). While considering these aspects, heteroatoms like N, P and S seem promising to function as activator. The heterofullerenes may show higher hydrogen storage capacity.

The present investigation therefore has been undertaken with the following objectives

1. Hydrogenation of fullerenes is possible only in presence of activators, which can activate the hydrogen molecule. Taking the clue from nature, it is postulated that the presence of heteroatoms in the Fullerene may be the appropriate sites for activation of hydrogen.
2. If heterofullerenes were to be one of the materials appropriate for hydrogen storage, then the questions to be addressed are: (a) what is the gradation of

materials containing various heteroatoms? (b) What are the geometrical positions in the fullerene that are active?

In order to understand the interaction of hydrogen molecule in pure fullerene and heteroatom (N, P, S and B) substituted fullerene, cluster model calculations have been carried out using Density Functional Theory (DFT).

3.2.2 Theoretical methods and model

Typical C₆₀ model has been chosen for the study. The hydrogen molecule is allowed to interact as shown in Fig. 3.4 for substituted and unsubstituted fullerene. The stability of the substituted fullerene plays a crucial role in the hydrogenation reaction and they seem to be stable by showing the minimum energy difference between virgin C₆₀ and the substituted C₆₀ molecules (Andreoni *et al.*, 1992; Kurita *et al.*, 1992). The Density Functional computations have been carried out on the optimized configuration obtained using Universal Force Field (UFF 1.02) parameter (Rappe *et al.*, 1992). Cerius² software was used for the force field calculations and the single point energy calculations on the optimized configurations obtained from force field have been carried out using Gaussian 98W (Frisch *et al.*, 1998) with Becke's three parameter hybrid functional with LYP correlation functional (B3LYP) and 6-31G(d) basis set. The total energy, H-H bond distance as well as the dissociation energy obtained from the single point calculations is given in the Table 3.5. To study the reaction mechanism of hydrogenation of substituted fullerene, a simpler cluster model of pyracyclene ring structure has been taken, which is the subunit of C₆₀ molecule consisting of two pentagons and two hexagons and shows fulvalene like character and is responsible for the facile reaction to take place in fullerene molecule. The geometrical parameters of the cluster used for proposing the mechanism are listed in

Table 3.6 and are similar to that of fullerene molecule (C_{60}). The ends of the cluster were saturated with hydrogen in order to avoid the edge effect (Yang and Yang, 2002) and the simple cluster selected in the present study, was fully optimized with hybrid density functional B3LYP method with 6-31G (d) basis set. The nature of stationary points thus obtained was characterized by frequency calculations. All the transition states corresponding to hydrogen migration were located and characterized as saddle points using the frequency calculations and were found to possess one imaginary frequency at the same levels of theory. The geometric parameters and the nature of the imaginary frequencies were examined using the graphical interface program, GaussView 03. The optimized geometrical parameters obtained from DFT calculations are given in Table 3.7. Essentially the hydrogen activation and subsequent hydrogenation of carbon atoms of fullerenes are conceived by the pathways shown in Fig 3.6.

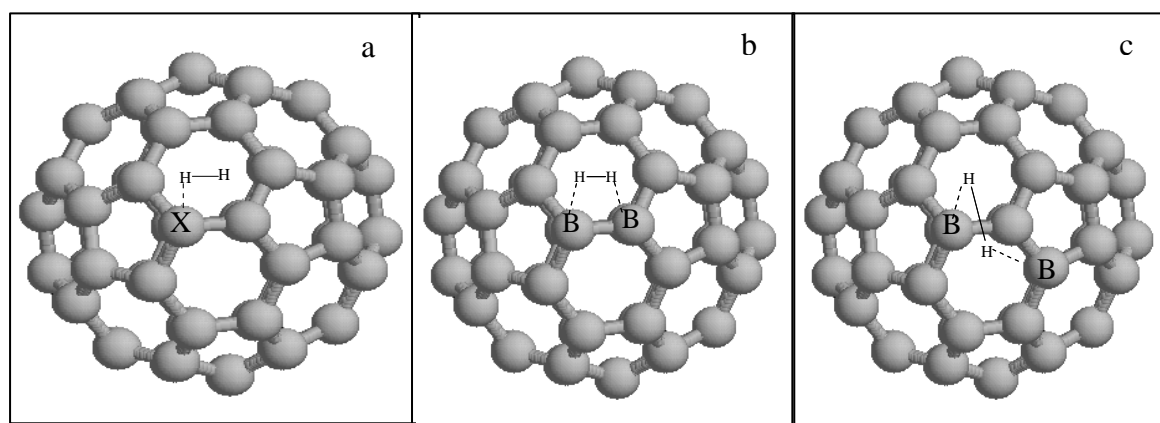


Fig. 3.4 Cluster model chosen for hydrogen activation study in substituted and un substituted fullerene (C_{60}): (a) heteroatom ($X = N, P, S$ and B) substituted fullerene with hydrogen interaction (b) boron atoms substituted in adjacent positions (c) boron atoms substituted in alternate positions

3.2.3 Results and Discussion

The hydrogen molecule is allowed to interact with the carbon atoms of the unsubstituted fullerene and the dissociation energy of hydrogen was calculated (Table 3.5). The dissociation energy of hydrogen in its free state is 4.74 eV, and remains unaltered when it is allowed to interact with pure fullerene (4.61 eV).

Table 3.5 Bond length and dissociation energy of hydrogen molecule upon interaction with fullerene molecule is calculated using B3LYP with 6-31g (p, d) basis set on the UFF optimized structure

Substitution	Total energy (Hartrees)	H ₁ -H ₂ (Å)	Dissociation energy (eV)
H ₂	-1.175	0.708	4.76
C ₆₀	-2286.042	-	-
C ₆₀ + H ₂	-2287.211	0.707	4.61
N C ₅₉	-2302.653	-	-
N C ₅₉ + H ₂	-2303.640	0.831	0.36
P C ₅₉	-2589.253	-	-
P C ₅₉ + H ₂	-2590.276	0.813	0.64
S C ₅₉	-2646.036	-	-
S C ₅₉ + H ₂	-2647.013	0.815	0.62
B C ₅₉	-2272.764	-	-
B C ₅₉ + H ₂	-2273.908	0.818	3.92
2B C ₅₈ (adjacent)	-2259.506	-	-
2B C ₅₈ + H ₂ (adjacent)	-2560.567	1.126	1.662
2B C ₅₈ (alternate)	-2259.487	-	-
2B C ₅₈ + H ₂ (alternate)	-2260.477	1.016	0.276

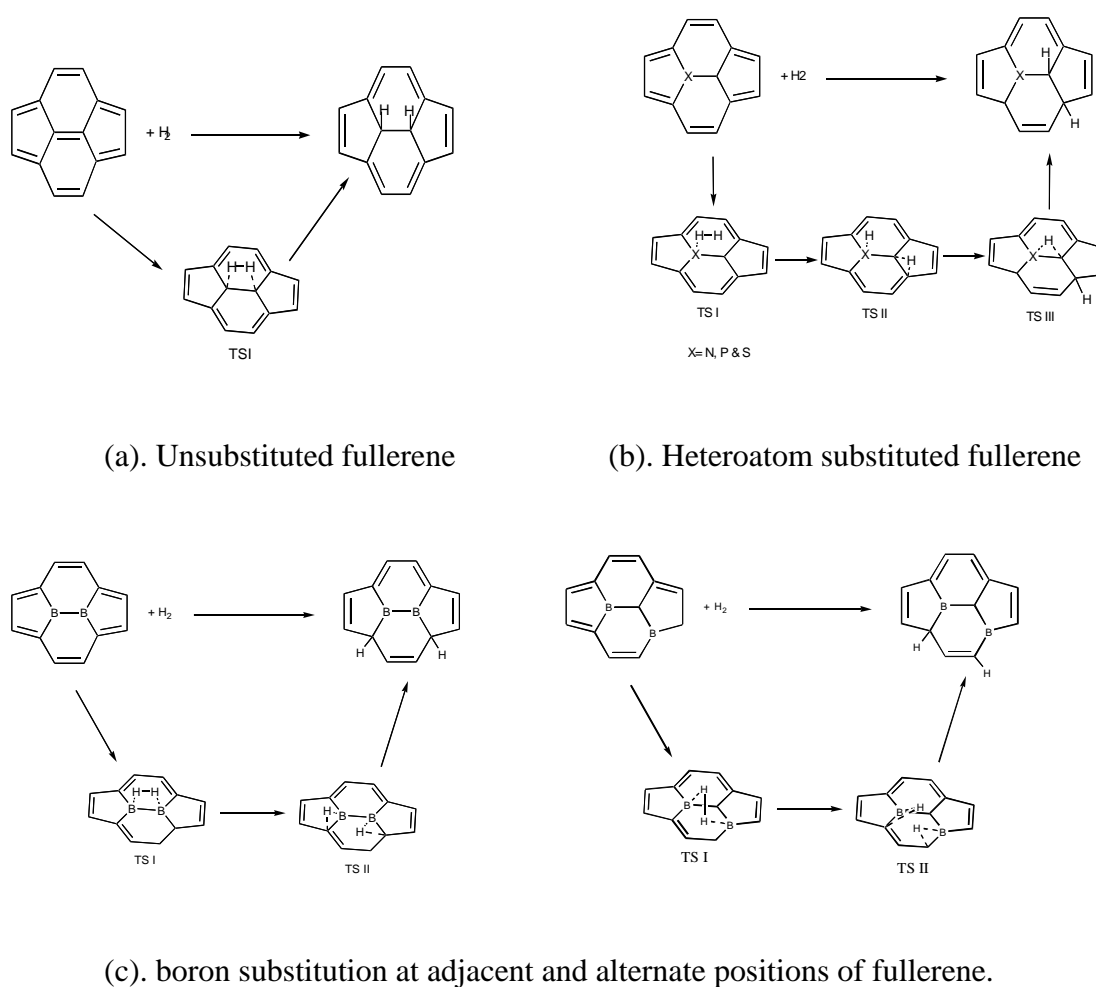
In order to study the influence of heteroatoms towards the activation of hydrogen, various heteroatoms (N, P, S and B) are substituted at different positions of the fullerene showing the minimum potential energy and the hydrogen interaction is monitored. In the presence of heteroatom the dissociation energy of hydrogen molecule is considerably decreased compared to that of pure fullerene as can be seen

from the values presented in Table 3.5. The points that emerge out of the results given in the table are:

- 1) Substitution of carbon by heteroatoms (N, P, S and B) appears to favor the activation by decreasing the dissociation energy of hydrogen molecule. However the dissociation energy is decreased from 4.74 eV to 3.9 eV, when one boron is substituted and to 1.67 eV when two boron atoms are substituted in adjacent positions and to 0.3 eV when the two boron atoms are substituted in alternate positions.
- 2) The bond length of H-H increased when hydrogen activation is carried out on heteroatom substituted fullerenes.
- 3) Heteroatom substitution favours hydrogen activation, moreover the boron substitution in alternate positions is more favorable than substitution at adjacent sites. This result is similar to what has been observed on boron substituted carbon nanotubes. However, the bond length elongation is higher for H-H bond in the case of the systems where the boron atoms are substituted at adjacent positions.

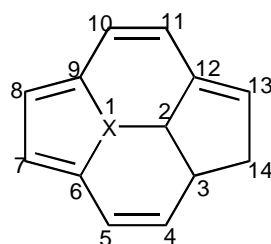
The reasons for these observations have been examined by the calculation of transition state parameters, which show that the reaction proceeds from one energy minimum to another via an intermediate maximum. From the transition state configuration one can predict the feasibility of the reaction. The hydrogen movement from the heteroatom can be conceived by the transition state theory calculation. Using the calculated property of transition state, the activation energy for the reaction is evaluated. The optimized geometrical parameters obtained from DFT calculations

given in Table 3.6 show the model chosen is reasonably good to study the reaction mechanism. Essentially the hydrogen activation and subsequent hydrogenation of carbon atoms of fullerenes are conceived by the pathways shown in Scheme 3.2 and the values of activation energy for each of the steps of hydrogen activation and migration of hydrogen have been calculated within the framework of transition state theory by using Density Functional Theory (DFT) and the same are summarized in Table 3.7.



Scheme 3.2 Proposed transition state pathways for hydrogen storage in fullerene and heteroatom (N, P, S & B) containing fullerene

Table 3.6 Geometrical parameters of the simple cluster considered for the mechanistic pathway employing hybrid density functional B3LYP method with 6-31g (d) basis set



Cluster	X-C ₁ Å	X-C ₂ Å	X-C ₃ Å	C ₄ -C ₁ -X deg	C ₂ -X-C ₁ deg	C ₄ -C ₁ -X-C ₂ deg	C ₄ -C ₁ -X-C ₂ deg
UNSUB	1.35	1.43	1.43	122.63	122.63	0.00	0.00
N-SUB	1.35	1.42	1.40	124.54	120.31	-8.83	9.28
P-SUB	1.60	1.68	1.69	124.90	101.48	-32.59	34.25
S-SUB	1.58	1.70	1.70	124.38	101.49	31.73	-31.73
B-SUB	1.65	1.59	1.58	116.4	108.6	7.1	-7.3

Table 3.7 Transition state optimized parameters of the cluster and the value of the activation energy calculated by B3LYP with 6-31g (p, d) basis set

Cluster	E _a I (eV)	E _a II (eV)	H ₁ -H ₂ (Å)	X-H (Å)	C-H ₁ ^b (Å)	C-H ₂ ^b (Å)
Carbon cluster	18.49	-	0.70	-	-	-
N substituted	3.24	3.15	1.85	1.04	1.44	1.50
P substituted	1.73	1.52	1.85	1.26	1.48	1.62
S substituted	2.56	6.48	1.13	1.60	1.70	1.70
2B substituted (adjacent)	2.26	2.68	1.98	1.19	2.52	1.43
2B substituted (alternate)	0.5	2.03	2.95	1.27	1.25	1.97

E_a = E (transition state) – E (reactant) and ^b Shortest C-H bond distance

From the values of activation energy given in Table 3.7, one can deduce that the heteroatoms are favourable for the hydrogen interaction and dissociation and possibly favour subsequent migration to the carbon surface. These results support that

heteroatoms are the appropriate sites for activation of hydrogen on fullerene. In the configuration where in the two boron atoms are substituted at alternate positions and the overall activation barrier is considerably reduced to nearly 0.5 eV, whereas in the case of substitution at adjacent positions the activation barrier is of the order of 2.26 eV. This is an indication that substitution at alternate position is geometrically favourable for the hydrogenation of carbon atoms of fullerenes, while the C-H is not that much favorable for the system where boron substitution is located at adjacent positions. The results substantiating these statements are given in Table 3.7. Theoretical calculations have shown that substitution of heteroatom in fullerenes seems to be one of the methods suitable for hydrogen storage applications. The heteroatom containing fullerenes are able to activate the hydrogen compared to unsubstituted fullerene. This activated hydrogen can then migrate to other sites. The implications of these results for hydrogen storage applications are yet to be realized. In summary, these studies thus show that hydrogenation of carbon materials (carbon nanotubes or fullerenes) requires activation centers and geometrically and chemically these activation sites have to be incorporated in to the carbon net work for effective hydrogenation and hydrogen storage applications.

CHAPTER 4

HYDROGEN STORAGE IN ACTIVATED CARBON

4.1 INTRODUCTION

The choice of an appropriate medium to store hydrogen is not yet rationalized and it is posing challenges to the scientific community for the past several decades. Among the various options for hydrogen storage, only storage in solid state materials seems to be promising. Scientific community in their anxiety and enthusiasm has come up with remarkable but not reproducible results for hydrogen storage in solid state. The desirable storage capacity for viable commercial exploitation of hydrogen as energy source is 6.5 weight % as originally postulated by US-DOE. Recently, lightweight carbon absorbent materials have become interesting for possible use in a hydrogen-storage system. Early work in this area focused on the H₂-absorption properties of various activated carbon materials which were prepared from mineralogical or organic precursors. Activated carbons are broadly defined as porous, non-graphitizable and manufactured to exhibit a high degree of porosity and surface area (McEnaney, 2002). These materials were typically obtained by thermochemical processing and contained many different types of carbon structures that provided a variety of environments for binding hydrogen. Unfortunately, the vast majority of the sites for absorption could not stabilize hydrogen above cryogenic temperatures (Chahine and Bose, 1994; Aceves *et al.*, 2000; de la Casa-Lillo *et al.*, 2002; Zhou *et al.*, 2004). Hydrogen absorption in carbon materials depends on the applied pressure and the temperature. Various studies have been carried out to study the interaction of hydrogen with various forms of carbon materials. From these experiments, it has been claimed that

activated charcoal had the largest hydrogen storage capacity, in amounts up to 2 wt% at low temperatures (Nijkamp *et al.*, 2001; Takagi *et al.*, 2004). The absorption isotherms of hydrogen on activated carbon (AX-21, BET surface area: 3000 m²/g) and multi-walled carbon nanotubes (MWNT, BET surface area: 137 m²/g), revealed a common mechanism of absorption, however, the amount of H₂ absorbed on MWNT is 3–5 times less than that on activated carbon. Other reports on activated carbon showed 0.35–0.41 wt% of hydrogen storage capacity which is similar to that of SWNT (Texier-Mandoki *et al.*, 2004; Rzepka *et al.*, 1998; Terres *et al.*, 2005; De la Casa-Lillo *et al.*, 2002). Activated carbon prepared by simple activation method provides hydrogen storage values at 125 bar of 1 to 1.6 wt% at ambient temperature (Ströbel *et al.*, 1999; Panella *et al.*, 2005). Hence, considering the high absorption under ambient conditions, low cost, easy handling and the high surface area, activated carbon seem to be promising carrier of hydrogen for practical applications. In literature, there is a correlation between surface area and hydrogen storage capacity of carbon materials. If this situation is true then to meet the DOE target of 6.5 wt % of hydrogen storage capacity at ambient condition requires 10 times higher surface area of activated carbon available at present (3000 m²/g). Recently, studies have shown that as such pure carbon materials show no interaction with the hydrogen molecules and the interaction energy of few kJ/mol of hydrogen (Schimmel *et al.*, 2003). For the storage application there should be optimum interaction of hydrogen with the storage medium, for this the carbon materials should be modified to have appreciable interaction for good storage property. One of the ways is to activate hydrogen by the metal loading (transition metals). It is believed that by the nickel support to the carbon can activate hydrogen (Challet *et al.*, 2004; Kim *et al.*, 2005). Another method is the surface modification by introducing the functional groups through chemical treatment

(Zhao *et al.*, 2005; Raymundo-Pinero *et al.*, 2005). Various weight percentage of nickel supported on commercial Calgon activated carbon and the chemical treatments like acid and amine treatments employed on commercial CDX-975 activated carbon have been examined in the present study.

4.2 EXPERIMENTAL METHODS FOR HYDROGEN STORAGE DETERMINATION IN CARBON MATERIALS

To determine the hydrogen storage capacity of a carbon material, three main methods have been utilized namely, volumetric, gravimetric and temperature programmed desorption (TPD) (Kiyobayashi *et al.*, 2002; Zhang *et al.*, 2004).

4.2.1 Volumetric method

Volumetric method measures the pressure drop owing to hydrogen absorption. When a degassed carbon sample, in a container of known volume, is exposed to a known amount of hydrogen at high pressures there will be reduction in pressure. Furthermore, any leakage or temperature instability of the apparatus may give rise to large experimental errors. The advantage of this technique is that both, absorption and desorption can be measured and that the conditions are similar to usage in a storage tank.

4.2.2 Gravimetric method

The gravimetric method measures the weight changes of the carbon due to absorption or desorption of hydrogen. However, this method is sensitive to all gases sorbed, since it is purely based on weight. The sample was then exposed to hydrogen at the desired pressure and the change in weight was then monitored and used to calculate the hydrogen storage capacity of the material.

4.2.3 Temperature programmed desorption (TPD)

Temperature programmed desorption experiments were carried out in an ultra-high-vacuum chamber equipped with a cryostat and a mass spectrometer. Throughout the process the presence of hydrogen was monitored by mass spectrometry. From this, the amount of hydrogen desorbed can be quantitatively calculated. This greatly enhances the sensitivity as water and other hydrogen containing- molecules provide additional source of hydrogen, which can hinder accurate results. The sensitivity and selectivity can even be improved by using deuterium loaded specimens.

Among all the methods, storage capacity determined by volumetric method seems to be more appropriate to real hydrogen storage application.

4.3 RESULTS AND DISCUSSION

4.3.1 Metal loading in Calgon carbon

Various percentages of nickel were loaded by physical impregnation method on commercial Calgon carbon. XRD studies (Fig 4.1) showed a predominant peak for Ni (111) at $2\theta = 44.42^\circ$ for all the weight percentages of nickel and a peak at 54.75° corresponds to Ni (200). Ni (220) was present at $2\theta = 76.34$ which matches with JCPDS (87-0712) for metallic Ni. The peak at $2\theta = 25.22$ corresponds to carbon (002) plane of graphitic carbon. From XRD analysis, it was found that the prepared nickel supported activated carbon contain metallic nickel after calcination in the hydrogen atmosphere.

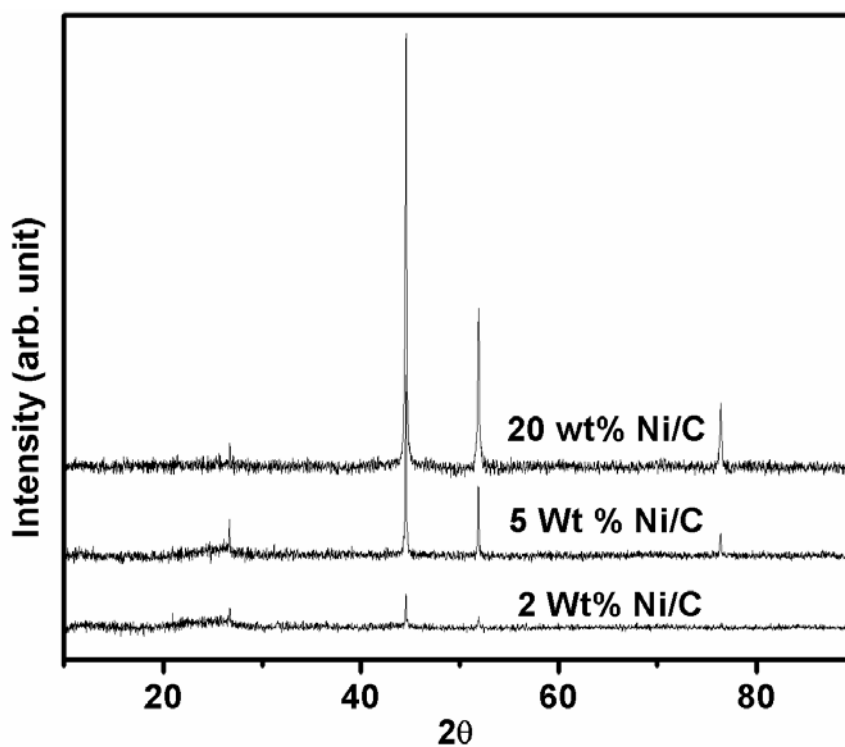


Fig. 4.1 XRD patterns of various percentages of nickel supported on Calgon carbon

SEM analysis of the nickel supported carbon (Fig 4.2) showed variation of particle size with respect to the amount of metal loading. 20% Ni/C carbon shows a maximum particle size and the dispersion of metal particle is uniform in the case of 2 wt % Ni loaded carbon. SEM and EDAX analysis confirmed the presence of nickel in the carbon. The percentage of metal present is estimated and given in Table 4.1. From the results, it is found that the amount of Ni loaded and the actual amount present were comparable.

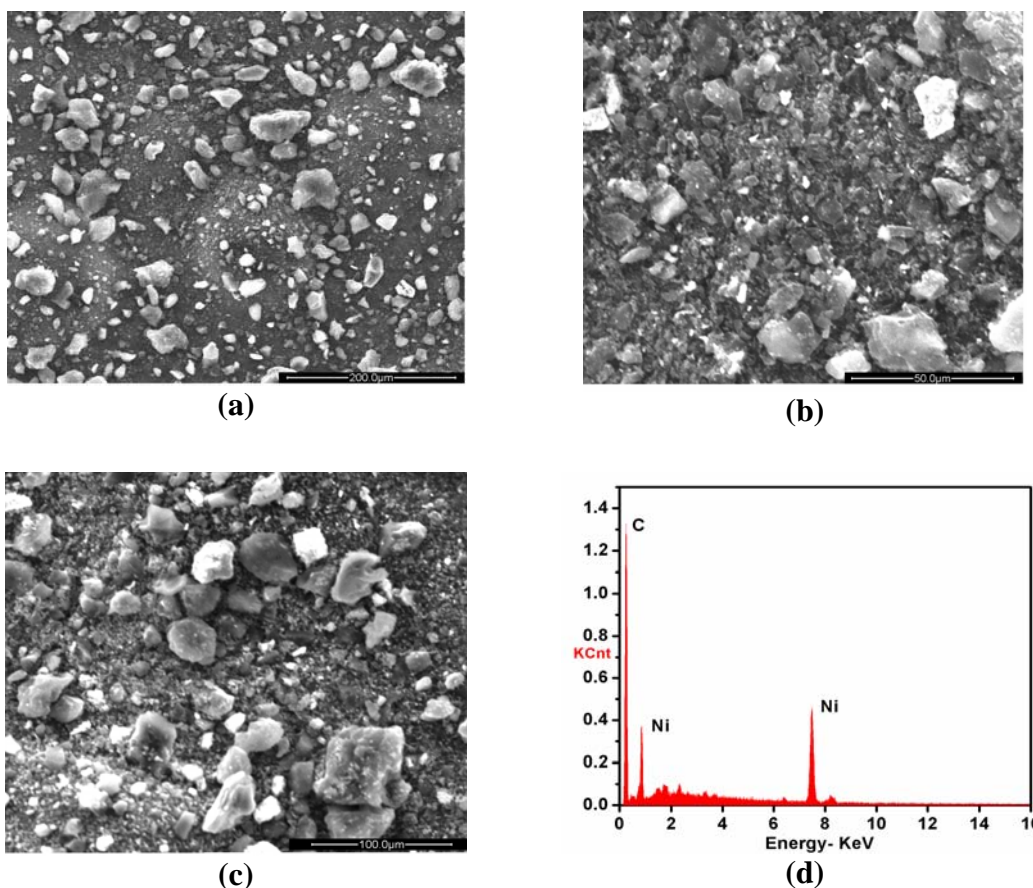


Fig. 4.2 SEM images of various weight percentages of nickel loaded on Calgon carbon (a) 2 wt%, (b) 5 wt%, (c) 20 wt% and (d) SEM EDAX of 20 wt% Ni/C

Table 4.1 Comparison of amount of nickel loaded and the nickel determined from the SEM / EDAX analysis

Samples	Weight % of nickel loaded on carbon	Presence of Nickel determined by SEM / EDAX
2 wt % Ni supported on carbon (Calgon)	2 %	1.72 %
5 wt % Ni supported on carbon (Calgon)	5 %	4.66 %
20 wt % Ni supported on carbon (Calgon)	20 %	16.45 %

The hydrogen absorption activity of the Calgon carbon and the various weight percentages of nickel loaded on Calgon carbon have been studied from 0 to 760 mm Hg of hydrogen pressure. The Specific Surface Area (SSA) values for all the carbon materials have been determined by the N₂ absorption at 77 K using BET equation.

From the studies, it is seen that the hydrogen absorption capacity of the Calgon carbon decreases with increase in the temperature. The isotherms were obtained for various temperatures (77, 298, 323, 348 and 373 K). The hydrogen absorption at 77 K showed a maximum value of hydrogen absorption of 1.23 wt% for granular commercial Calgon carbon. However, the absorption decreased with an increase in the temperature (Fig. 4.3a). The Van't Hoff plot (plot of $\ln p$ vs $1/T$) gave a value for the heat of absorption of 5.69 kJ/mol of hydrogen (Fig. 4.3b). This showed that the interaction of hydrogen is negligible and the interaction energy value is comparable to the value obtained by neutron inelastic scattering experiments (Schimmel *et al.*, 2003) for pure carbon materials.

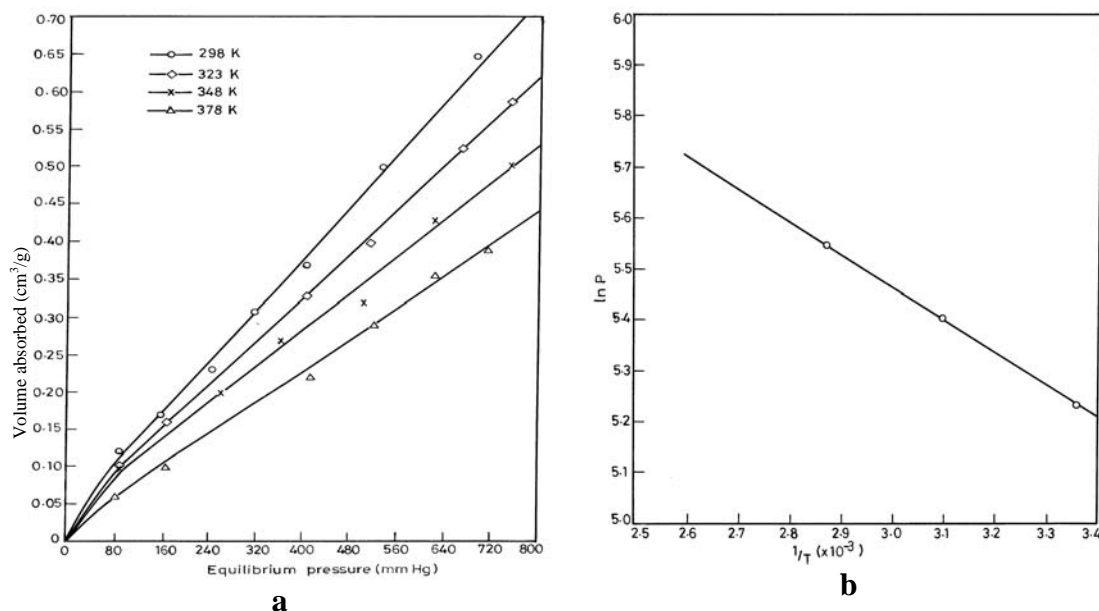


Fig. 4.3 Hydrogen absorption activity of Calgon carbon at various temperatures (a) Hydrogen absorption isotherms at different temperatures (b) Van't Hoff plot of Calgon carbon

Increase in the wt % of Ni loading in carbon showed a reduction in the surface area of the carbon from 930 to 650 m²/g for the 20 wt % Ni/Calgon sample. This is due to the blocking of accessible pores by the metal particles. Hydrogen absorption activity does not enhance significantly as a result of metal loading. The hydrogen absorption activity of 20 wt% Ni on C showed a maximum absorption at 77 K and decreases with

increase in temperature. The hydrogen absorption activity increases from 298 K to 373 K and exhibited a maximum at 373 K then subsequently decreased with an increase in the temperature (Fig 4.4a and b). The value of heat of absorption calculated from the Vant's Hoff plot is 59.2 kJ/mol (Fig. 4.4c). This can be attributed to the metal hydride bond formation.

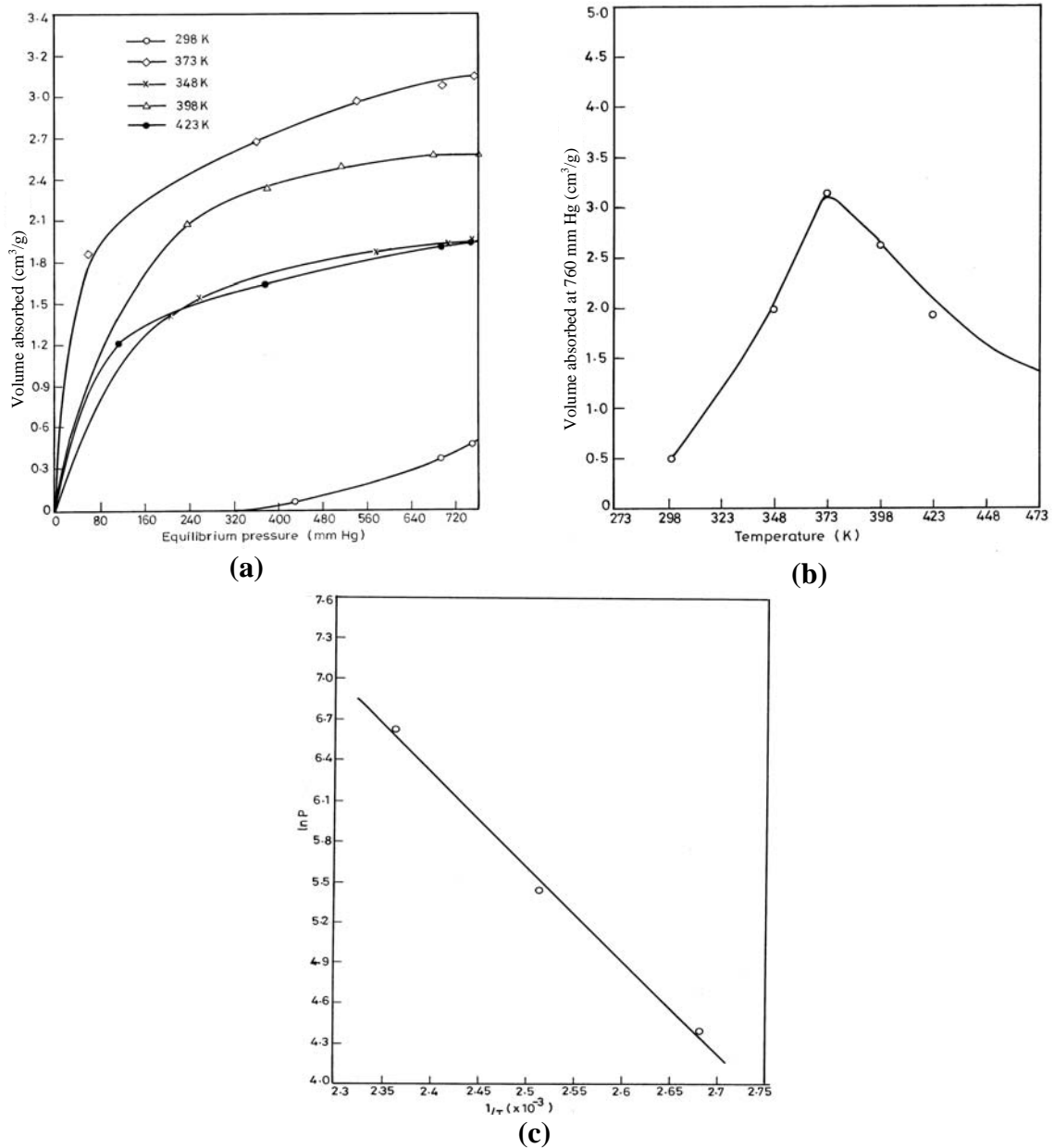


Fig. 4.4 (a) Hydrogen absorption activity of 20 wt% Ni/C at various temperatures (b) hydrogen absorption activity at 1 atm and at various temperatures (c) Van't Hoff plot for 20 wt % Ni supported on Calgon carbon

However, 2 wt % of metal loaded on the carbon showed different trend in hydrogen absorption activity. By increasing temperature, the absorption activity increased (Fig. 4.5). It is because of the transition state in the absorption process and there is no appreciable change in the surface area of the sample. The 5 wt% Nickel loaded system does not show any drastic variation in the activity. All the results of hydrogen absorption activity and the surface area are tabulated in Table 4.2.

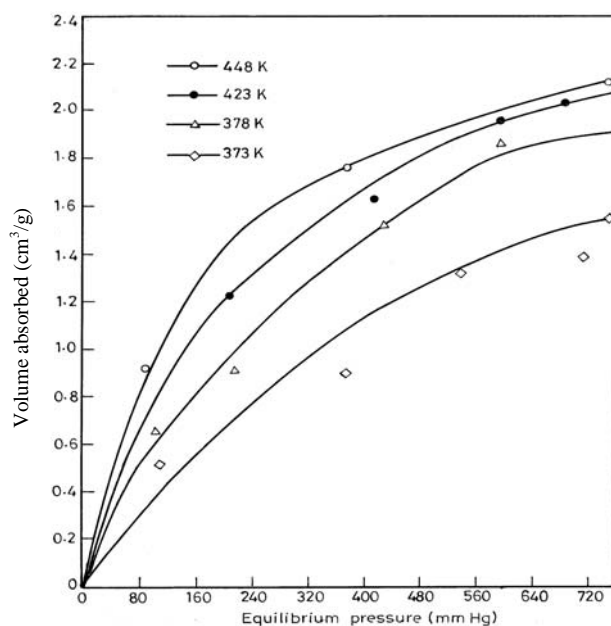


Fig. 4.5 Hydrogen absorption activity of 2 wt% Ni/C at various temperatures

Table 4.2 Hydrogen absorption activity at 1 atm and at various temperatures for the Calgon carbon and its modification by various percentage of nickel loading

Sorbent composition and surface area (m ² /g)	Calgon	Nickel/Carbon (Calgon)		
		20 wt%	5 wt%	2 wt%
	931	616	750	1066
Hydrogen storage capacity cm³/g				
77K	137.7	54.4	44.5	120.8
298K	0.70	0.5	-	-
373K	0.43	3.14	1.4	1.53
423K	-	1.95	1.7	2.05

The results obtained in this study show that nickel supported on active carbon could not show significant increase in the hydrogen absorption activity.

4.3.2 CDX-975 and its chemical modification

Chemical modification has been carried out on the commercial activated carbon CDX -975, in order to introduce functional groups of the carbon surface and make these sites to act as the activation centers for hydrogen storage. CDX-975 has been chemically treated with acid (TCDX) and amine (ACDX). The modified sample and the pure CDX-975 carbon have been studied for hydrogen absorption activity.

XRD studies of CDX-975 and the chemically modified carbon samples (Fig. 4.6) showed the predominant graphitic peak (002) plane at $2\theta = 24.3$ degree and the (001) plane at $2\theta = 42.3$ degree. The peak intensity increased for the amine treated samples and showed a maximum intensity and decreased with acid treatment and further decreased for acid and amine treated sample. From XRD studies, it was found that the graphitic nature of the carbon was increased by the chemical treatment compared to pure CDX-975.

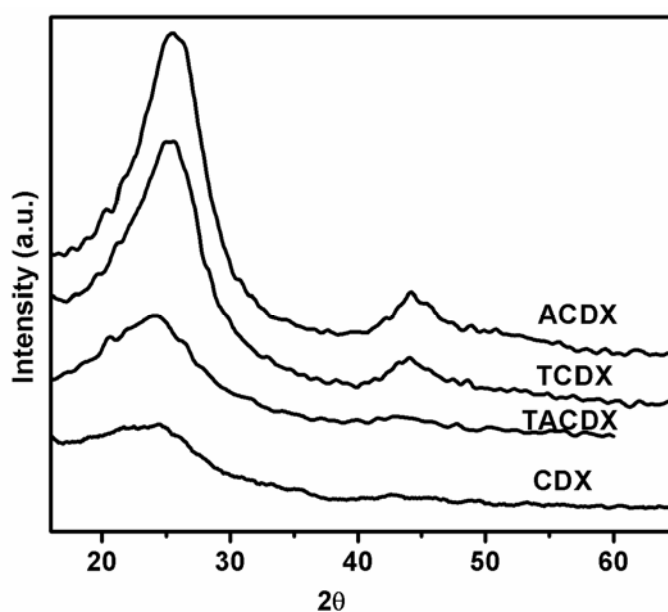


Fig. 4.6 XRD patterns of CDX carbon and its modification by the chemical treatment

FT-IR studies (Fig 4.7) showed predominant peak at 3400 cm^{-1} corresponding to N-H and O-H stretching frequency. This is observed for all the treated samples. Peak at 1026 cm^{-1} is observed for acid treated (TCDX) both acid and amine treated (TACDX) carbon samples, corresponding to CO stretching frequency. The carbonyl groups are introduced by the acid treatment of the sample. The C-H stretching frequency at 2950 and 2860 cm^{-1} are present for all the carbon samples. This shows that the basis property is not changed. But only additional functional groups are introduced onto CDX-975 carbon.

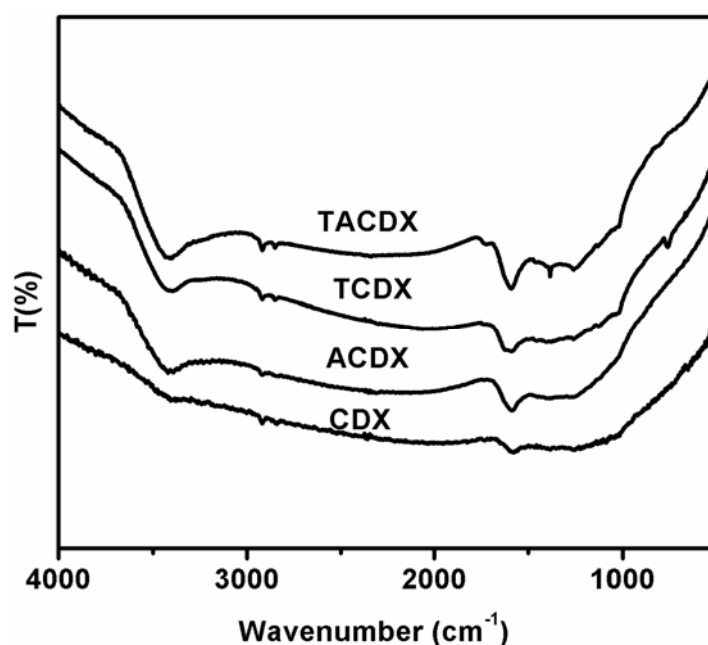


Fig. 4.7 FT-IR spectra of CDX-975 and treated CDX-975 samples

Hydrogen absorption activity of pure CDX-975 and chemically modified samples has been studied from 0 - 760 mm Hg pressure of hydrogen. The surface areas values of the samples were calculated using nitrogen absorption data (Table 4.3). The hydrogen absorption activity of pure CDX-975 is shown in Fig. 4.8. A maximum absorption capacity of $28\text{ cm}^3/\text{g}$ at 77K is obtained. From 298 K to higher temperature the

absorption increases with temperature. This corresponds to the absorption in the activated state.

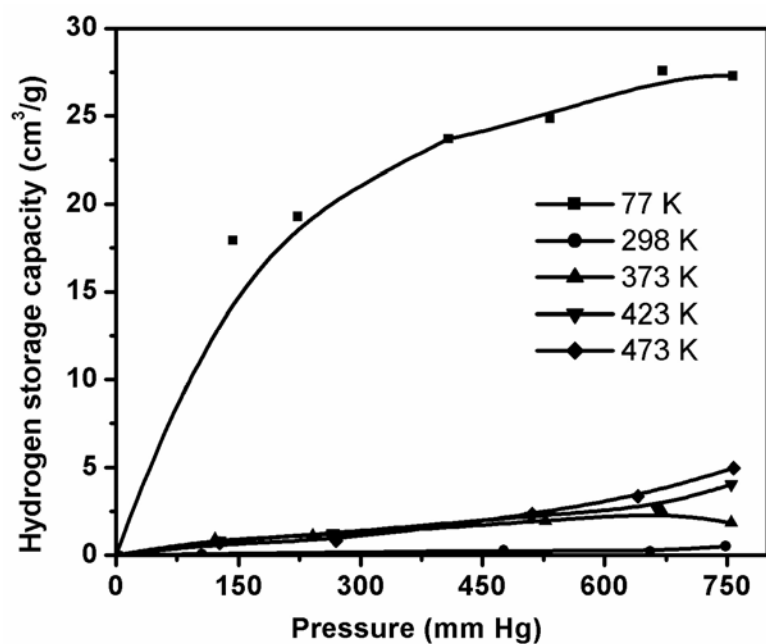


Fig. 4.8 Hydrogen absorption isotherms of CDX-975 at various temperatures

Table 4.3 Comparison of SSA and hydrogen absorption activity of CDX and chemically modified CDX samples

Sample	CDX- 975	T-CDX	A-CDX	TA-CDX
Specific surface area (m ² /g)	325	224	129	124
Hydrogen storage capacity (cm³/g) at 1 atm				
77 K	28.1	27.3	8.2	10.4
298 K	0.53	-	-	0.7
373 K	2.83	3.17	3.03	2.97
423 K	4.18	4.25	4.30	-
473 K	5.0	4.60	-	-
523 K	4.80	6.36	-	-

All the absorption data and their SSA for pure CDX-975 and the modified CDX-975 are given in Table 4.3. From the values given in table, it is clear that the surface area decreases due to chemical modification of the sample. The hydrogen absorption activity of CDX-975 is not enhanced by chemical modification.

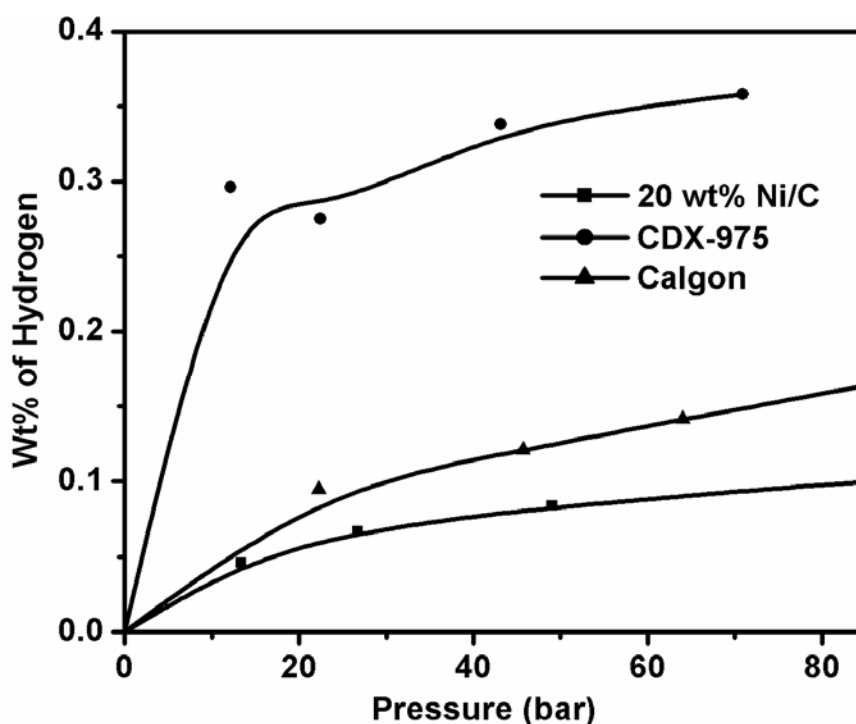


Fig. 4.9 Hydrogen storage capacity of CDX-975, Calgon carbon and 20 wt % Nickel loaded on Calgon carbon

High pressure hydrogen absorption studies have been carried out at 300 K to find the storage capacity of carbon materials. CDX-975 carbon showed a maximum of 0.35 wt % of hydrogen storage at 75 bar pressure of hydrogen, where as Calgon carbon showed 0.2 wt % (Fig 4.8) and 20 wt % nickel loaded Calgon carbon showed only 0.15 wt % of hydrogen storage capacity under these experimental conditions.

4.4 CONCLUSIONS

Pure carbon material does not interact with hydrogen. It is necessary to introduce some active centers to increase the interaction and hence attain higher hydrogen sorption capacity. In order to activate hydrogen molecule, modification in the carbon surface has been carried out by loading with various percentages of nickel metal and chemical treatment to introduce modifications of functional groups. These act as active centers for hydrogen activation. However, the observed results from this study showed that there is no appreciable enhancement in the hydrogen storage capacity either by metal loading or by chemical treatment.

CHAPTER 5

NITROGEN CONTAINING CARBON NANOTUBES – SYNTHESIS, CHARACTERIZATION AND HYDROGEN ABSORPTION ACTIVITY

5.1 INTRODUCTION

In the search for hydrogen storage media solid matrices remain better option. Among all, storage by carbon materials seems to be one good option. However, the reports of high storage capacity (up to 67 weight %) are not reproducible (Hynek *et al.*, 1997; Chambers *et al.*, 1998; Dillon *et al.*, 1997; Hirscher *et al.*, 2002). It has been shown that pure carbon surface cannot activate hydrogen molecule which is clear from the inelastic neutron scattering experiments (Ren *et al.*, 2001; Schimmel *et al.*, 2003). The binding strength of hydrogen molecule is almost the same for all kinds of carbon materials and the magnitude of interaction is nearly 5 kJ/mol. Modification of carbon surface has been advocated as one of the methods for higher hydrogen storage capacity. This has been a potential field of research in recent times. However, the addition of metal or metal oxides as catalysts and also the preparation of carbon in different forms (fibers and tubular forms) have not resulted in the enhancement of storage capacity (Liu *et al.*, 1999; Chen *et al.*, 1999; Yang, 2000). This is possibly due to the different storage mechanisms operative under experimental conditions. As the metals react to form hydrides and as the metal hydride could not store greater than its atomic combinations, the storage capacity is usually less than 3 wt % (Züttel, 2003; Grochala and Edwards, 2004). The choice of heteroatoms has been made on the basis of various parameters like the redox behaviour of the hetero atom and the feasibility of incorporation of the hetero atom in the carbon nanotube framework. Even among various heteroatoms, N, P, S and B differ in their behaviour. These

aspects have been studied by employing Density Functional Theory (DFT) and the results are discussed in the earlier chapter 3.

After the discovery of carbon nanotubes by Iijima (Iijima, 1991), carbon nanotubes have been used for variety of applications. The remarkable electronic properties of carbon nanotubes (Wong *et al.*, 1998; Fan *et al.*, 1999) (CNTs) combined with their excellent mechanical and thermal characteristics have stimulated enormous amount of research work on CNT growth methods and applications. The electronic properties of a CNT are completely governed by the tube chirality (the way the nanotube is rolled up from the graphite sheet). Unfortunately, the grown CNTs present a mixture of tubes with different structural morphologies (Stephan *et al.*, 1994; Glerup *et al.*, 2003). At the moment, there is no method to reliably separate CNTs depending on their metallicity. To have more control over the electronic properties, it has been suggested to dope CNTs with B and/or N atoms (Czerw *et al.*, 2001; Terrones *et al.*, 2002). This is a natural choice of the dopant, as B/N has roughly the same atomic radius as C, while it possesses one electron less/more respectively. Nitrogen doping has received particular attention, as N-impurities can also give rise to CNT functionalization (Burghard *et al.*, 1998; Chen *et al.*, 2005; Khare *et al.*, 2002; Okapalugo *et al.*, 2005) and transformations of the atomic network to bamboo-like structures (Lee *et al.*, 2002; Jang *et al.*, 2002; Zhao *et al.*, 2007). The template synthesis method has been widely used for preparing micro and nanostructured materials (Martin, 1994), which involves the synthesis of the desired material within the pores of a membrane to generate nanotubes of cylindrical nature with uniform diameter. Combination of CVD and template synthesis methods have been reported for the synthesis of highly aligned, uniform, hollow and open ended (suitable for filling with other materials) CNTs with diameters ranging from 20 to 200 nm (Che *et*

al., 1998; Kyotani *et al.*, 1996). Among all the preparation methods, the template synthesis method has several advantages like controlling composition, morphology and the size of the nanotubes (Che *et al.*, 2003). Nitrogen containing carbon nanotubes have been prepared by template synthesis method using nitrogen containing polymer precursors such as polyacrylonitrile and polypyrrole (Parthasarathy *et al.*, 1995; Jang and Oh, 2004). However, no specific methodology has been formulated to have control over the amount of nitrogen content in the carbon nanotubes.

In the application of carbon nanotubes, ruthenium supported on multi-wall carbon nanotubes have been shown to be potential systems for the production of ammonia compared to conventional systems at atmospheric pressure and 673 K. It is also observed that promotion of such systems with potassium enhances the activity (Chen *et al.*, 2001). Similarly hydrogen-absorbing intermetallics containing rare earth and Fe, Co or Ru have been examined as catalytic systems for the synthesis of ammonia. However, it has been shown that these catalytic systems underwent decomposition to give rise to Fe supported rare earth nitride systems. Hence essentially these catalytic systems were similar to conventional supported catalysts employed in ammonia synthesis (Takeshita *et al.*, 1976). The confinement in carbon nanotubes has been shown to reduce the activation energy and reaction endothermicity for the Menshutkin SN^2 reaction compared to those in the gas phase (Halls and Schlegel, 2002).

Against this background, heteroatom containing carbon nanomaterials are considered as another alternative material for hydrogen storage. In the present study hydrogen absorption activity of nitrogen containing carbon nanomaterials was compared with

that of pure carbon nanomaterials. Nitrogen containing carbon nanomaterials have been prepared by using various templates such as zeolite, clay and alumina membrane. The prepared nitrogen containing carbon nanotubes have been characterized by XRD, Raman, SEM, TEM, low pressure and high pressure hydrogen absorption measurements. The variation of template and the carbon precursor causes differences in the morphology, amount of nitrogen and the behavior of the materials towards hydrogen storage application.

5.2 RESULTS AND DISCUSSION

5.2.1 Nitrogen containing carbon nanomaterials

X-ray diffraction study of nitrogen containing carbon (PDC) has been carried out and the diffractograms are shown in Fig 5.1a. A predominant peak at 2θ approximately equal to 24.6° corresponding (002) indicates the graphitic nature of the carbon (JCPDS =23-0064). The peak at 43.2° corresponds to (100) plane of graphite.

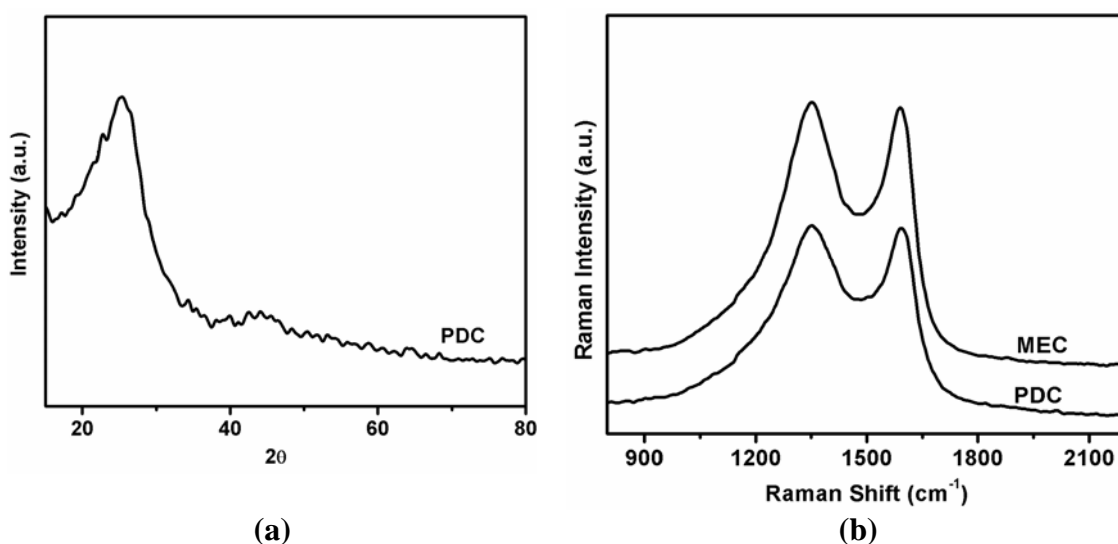


Fig. 5.1 (a-b) X-ray diffraction pattern of PDC and Raman spectrum of PDC and MEC carbon respectively

The Raman spectra of nitrogen containing carbon prepared from polymer precursor PDC and micro-emulsion mediated synthesis of nitrogen containing carbon MEC are shown in Fig 5.1b. The graphitic nature of carbon materials are determined by the D-band and G-band and both the carbon materials show predominant two sharp peaks located approximately at 1345 cm^{-1} and 1586 cm^{-1} respectively. The G-band corresponds to the high-frequency E_{2g} first-order mode and 1345 cm^{-1} (roughly corresponds to the D line associated with disorder-allowed zone-edge modes of graphite). The 1345 cm^{-1} band is normally explained by the relaxation of the wave vector selection rule due to the effect of the finite size of the crystal in the material. The D-band increases with increase in the disorder which is normally represented by the I_D/I_G ratio. Usually the I_D/I_G ratio increases with (i) increasing the amount of amorphous carbon in the material and (ii) decreasing the graphite crystal size. From the studies it is found that I_D/I_G ratio increased. This indicates the substitution of nitrogen in the carbon frame work and decrease of the graphitization process.

Microscopic characterization of the nitrogen containing carbon materials prepared from the silica matrix has been carried out. The Scanning Electron Micrographs (SEM) of PDC and MEC are shown in Fig. 5.2 (a and b). SEM analysis showed that the carbon materials prepared have the particle size in micron range for both PDC and MEC.

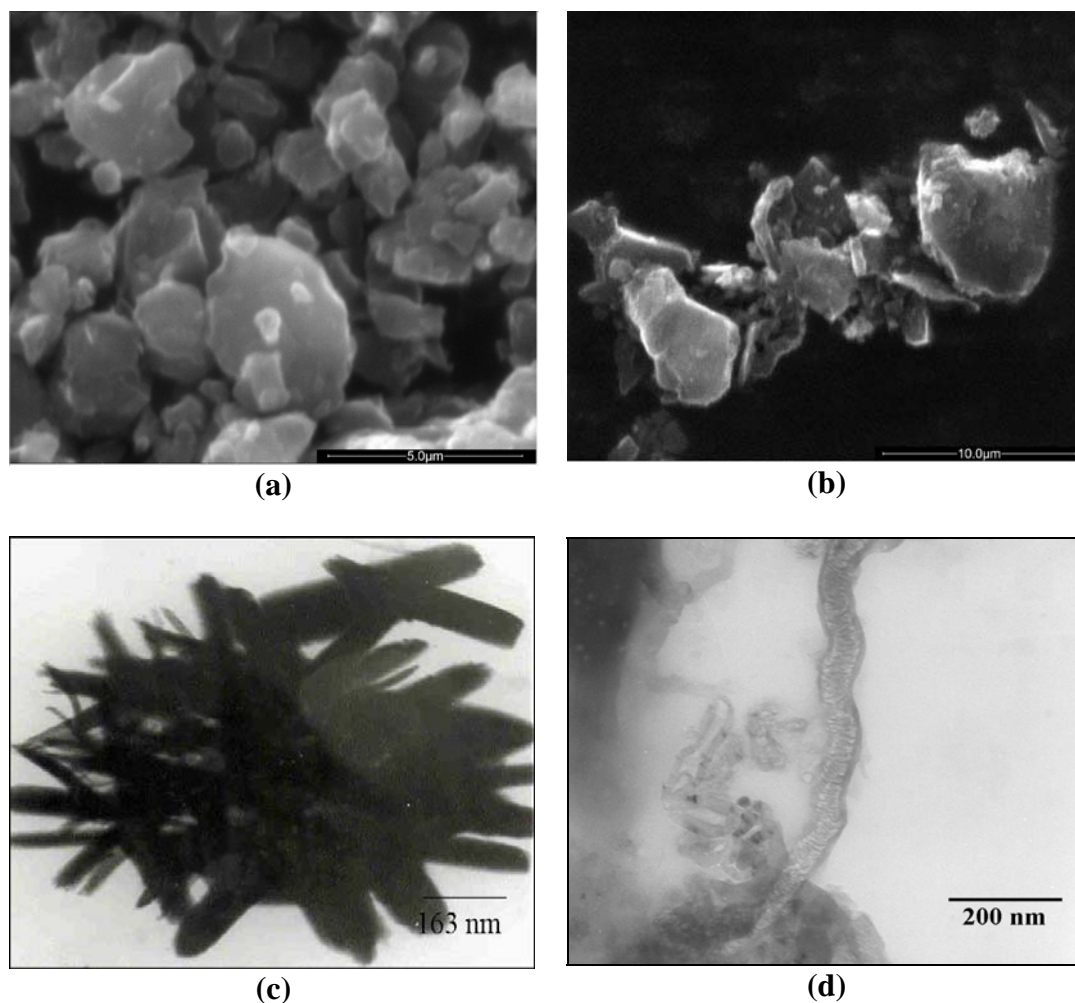


Fig. 5.2 (a-b) SEM pictures of nitrogen containing carbon nanomaterials prepared by using silica source PDC and MEC respectively (c - d) the TEM images of PDC and MEC

From the TEM analysis, the PDC showed rod shaped morphology but MEC showed a different morphology of coiled structure with more fibrous carbon material.

5.2.2 Template assisted synthesis of carbon nanotubes and nitrogen containing carbon nanotubes

5.2.2.1 Alumina membrane as the template

The scanning electron micrographs of carbon nanotubes prepared by alumina membrane template assisted method are shown in Fig. 5.3 (a and b). The synthesized carbon nanotubes showed the tubular nature and bunch of tubes are well oriented of with length in the range of 50–60 μm and open tube end.

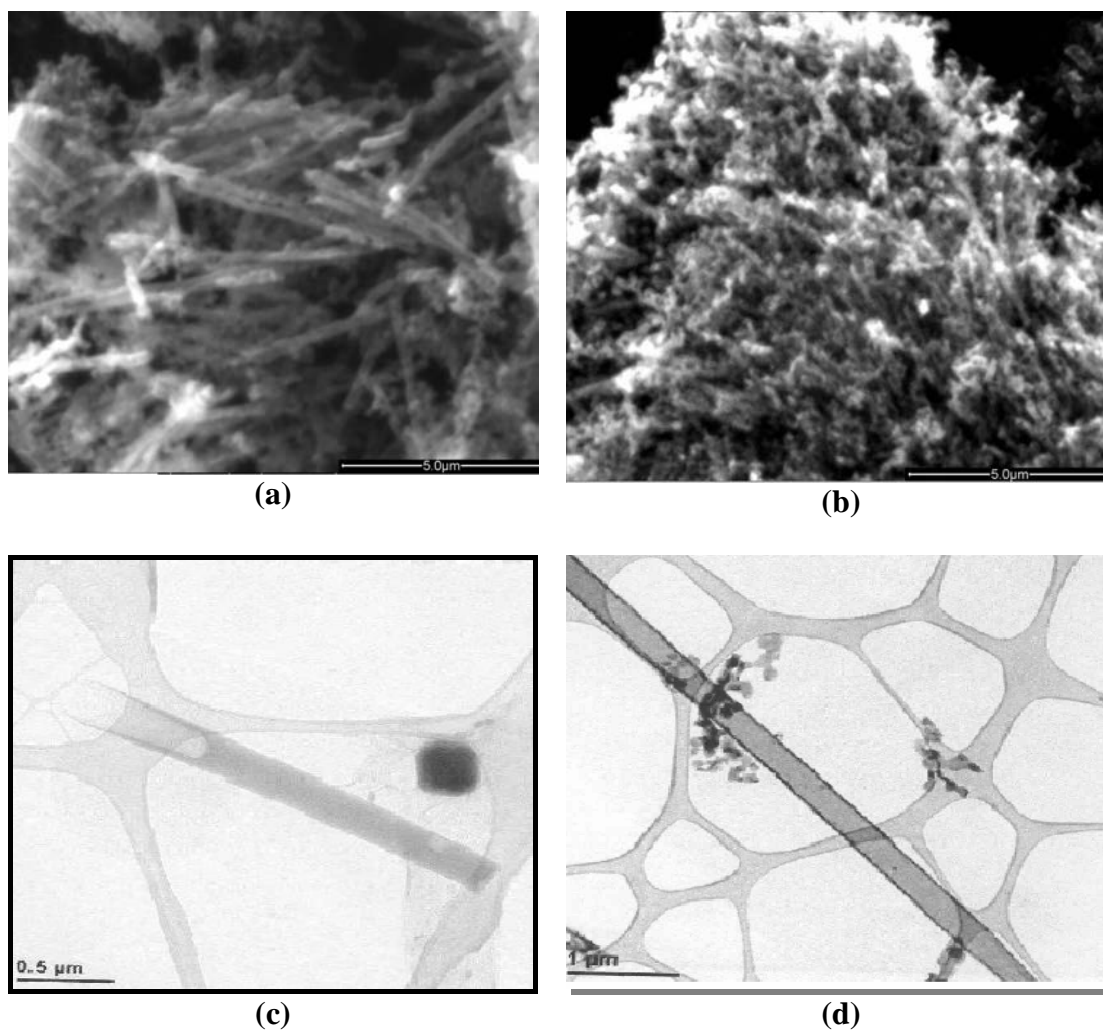


Fig 5.3 (a-b) SEM images of carbon nanotubes CNT1 and NCNT1. (c-d) TEM images of CNT1 and NCNT1 respectively

The TEM images (Fig 5.3.c and d) of CNT1 and NCNT1 after the carbonization at 1173 K for 6 h showed hollow tubes with slight deformation in the end of the tube probably caused by the ultrasonication and vigorous HF treatment. Micrograph also indicates the formation of cylindrical, hollow and transparent tubes. The outer diameter of the tube is less than 200 nm which is less than the channel diameter of the template used (also seen is a layer of amorphous carbon on the wall of the tube). Though the carbon tubes produced by this method are not completely graphitic in nature as those produced by arc-discharge process, their disordered structure is quite typical of fibers or nanotubes produced by decomposition of hydrocarbons, as is evident from the amorphous carbon on the wall of the carbon nanotube.

X-ray diffraction study of carbon nanotubes prepared from polymer precursor by using alumina membrane as templates are shown Fig 5.4a. A predominant peak at $2\theta = 25.6$ corresponds to (002) indicates the graphitic nature of the carbon is shown by NCNT1, whereas CNT1 showed a broad peak. The peak at $2\theta = 43.7$ corresponds to (100) plane of graphite is shown by both CNT1 and NCNT1. Usually the Raman spectra of sp^2 carbon materials are laser energy dependent and the frequency of the disorder – induced D- band are observed between 1250 and 1450 cm^{-1} . The D- band is activated in the first order scattering process by the presence of in-plane substitutional heteroatoms, vacancies, grain boundaries or other defects and by finite size effect, all of which lower the crystalline symmetry of the quasi-infinite lattice. The Raman spectra (Fig. 5.4b) showed that the carbon nanotubes prepared from the alumina membrane template with polymer as the carbon precursor shows a sharp D and G band at 1345 and 1595 cm^{-1} respectively with equal intensity. SEM and TEM analysis showed a well aligned tubular morphology. Due to the tubular morphology, the peaks are sharp and distorted. NCNT1 showed broad peak with high FWHM compared to pure carbon nanotubes (CNT1) due to the substitutional effect of nitrogen in the carbon nanotubes.

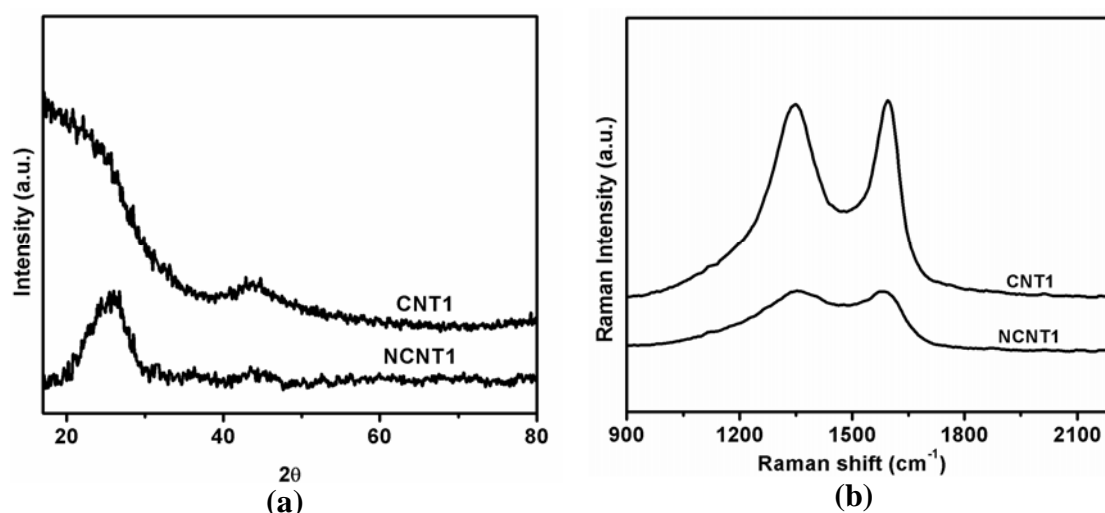


Fig 5.4 (a-b) XRD pattern and Raman spectra of CNT1 and nitrogen containing CNT (NCNT1) respectively

5.2.2.2 Zeolite as template

The carbon nanotubes prepared using zeolite as template showed the graphitic nature of the carbon as indicated by the XRD (Fig 5.5). The predominant (200) plane at $2\theta = 24.1^\circ$ and (100) plane of graphite at 44.7° are observed. Raman studies showed the graphitic D-band and G-band for the prepared carbon nanotubes using zeolite as template. The FWHM and the intensity of the D-band are higher than the G- band in NCNT2 compared to CNT2, which signify the greater disorderliness due to nitrogen substitution in the carbon nanotubes.

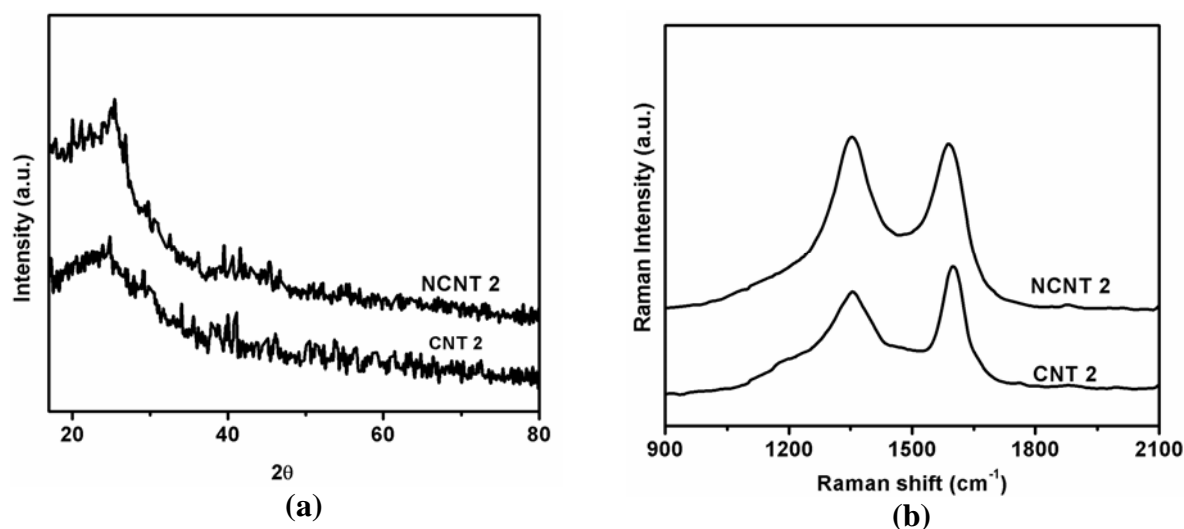


Fig. 5.5 XRD pattern and Raman spectra of CNT2 and NCNT2 prepared from zeolite as template by using chemical vapor deposition method

The SEM images of CNT2 and NCNT2 showed amorphous and fibrous nature of the carbon nanotubes produced. Usually carbon nanotubes produced by CVD method leads to the formation of nanotubes with disordered structure, amorphous carbon and fibers (Colomer *et al.*, 1999; Ci *et al.*, 2001), which as can be seen from the TEM images (Fig 5.6).

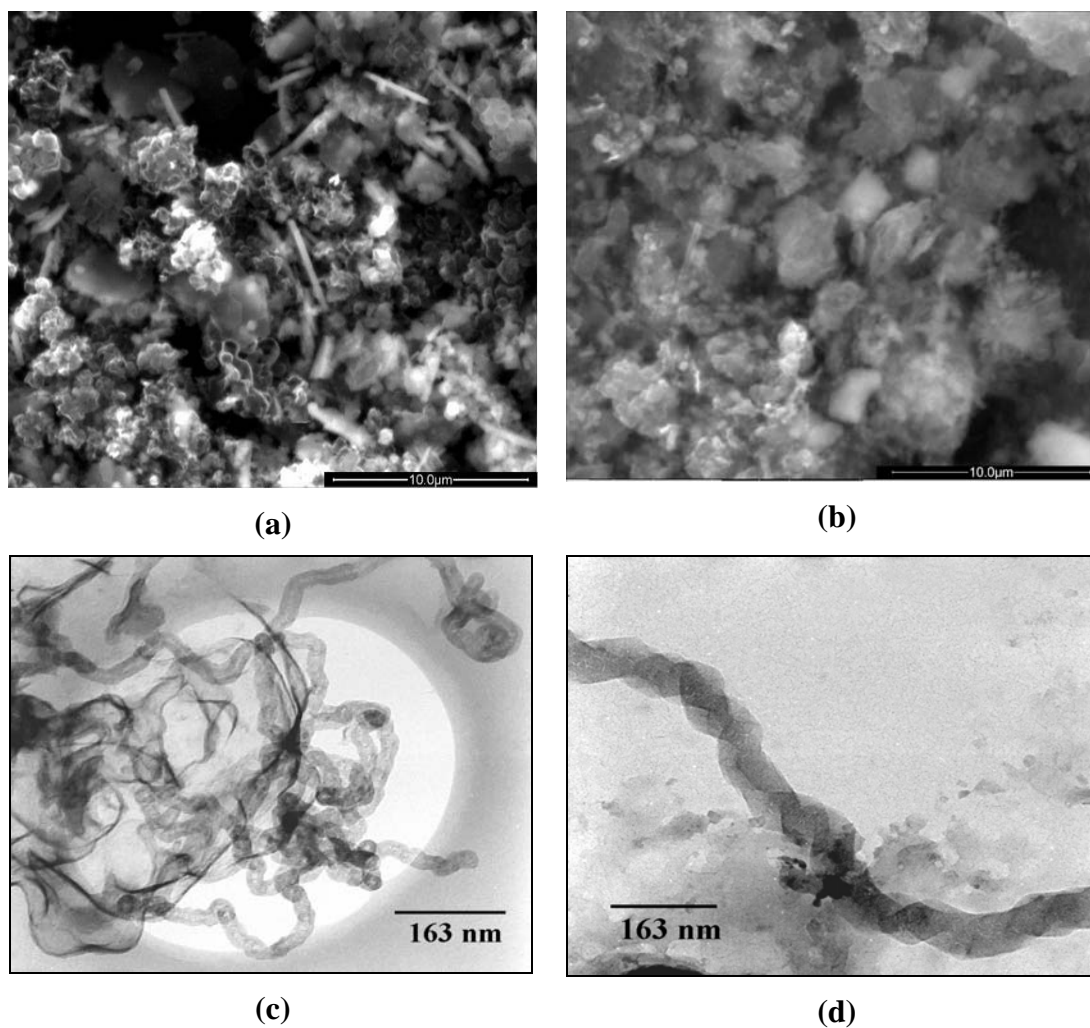


Fig. 5.6 (a-b) SEM images of CNT2 and NCNT2. (c-d) TEM images of CNT2 and NCNT2 respectively

5.2.2.3 Clay as template

The XRD pattern and Raman spectrum of CNT3 and NCNT3 are shown in Fig. 5.7. Graphitic nature of the carbon nanotubes produced is seen in Fig. 5.7. Predominant (002) plane of graphite at $2\theta = 23.8^\circ$ and (001) plane at 2θ equal to 45.1° are viewed. Well resolved D-band and G-bands are shown for both the carbon nanotubes, where NCNT3 showed broad peaks with high FWHM compared to pure CNT3. This can be attributed to the increased disorderliness by nitrogen substitution in the carbon nanotubes. The shift in the d-values is not significant by the substitution of heteroatom in to the carbon lattice. However Raman spectrum showed well resolved D-band characteristic peak for destabilization.

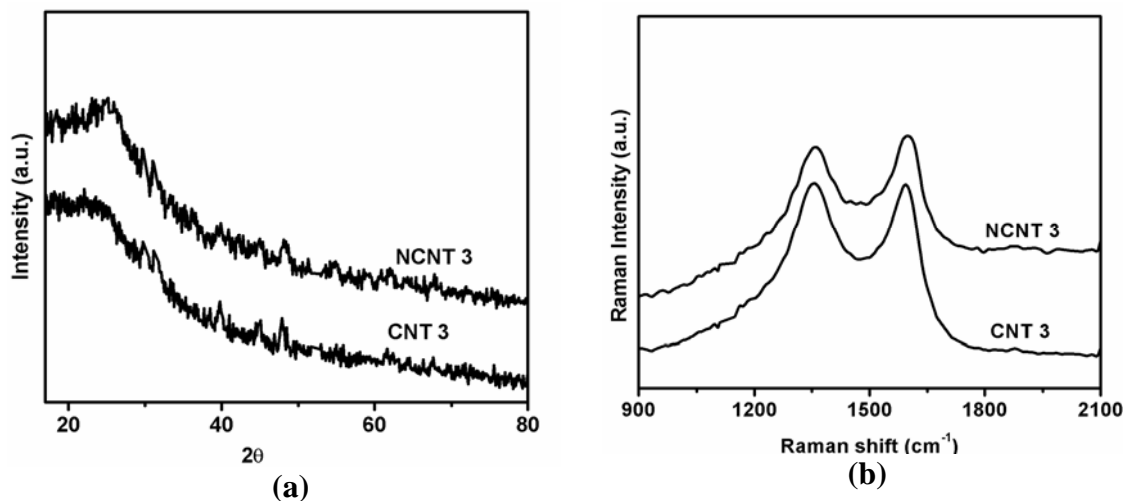


Fig 5.7 XRD pattern and Raman spectra of CNT3 and NCNT3

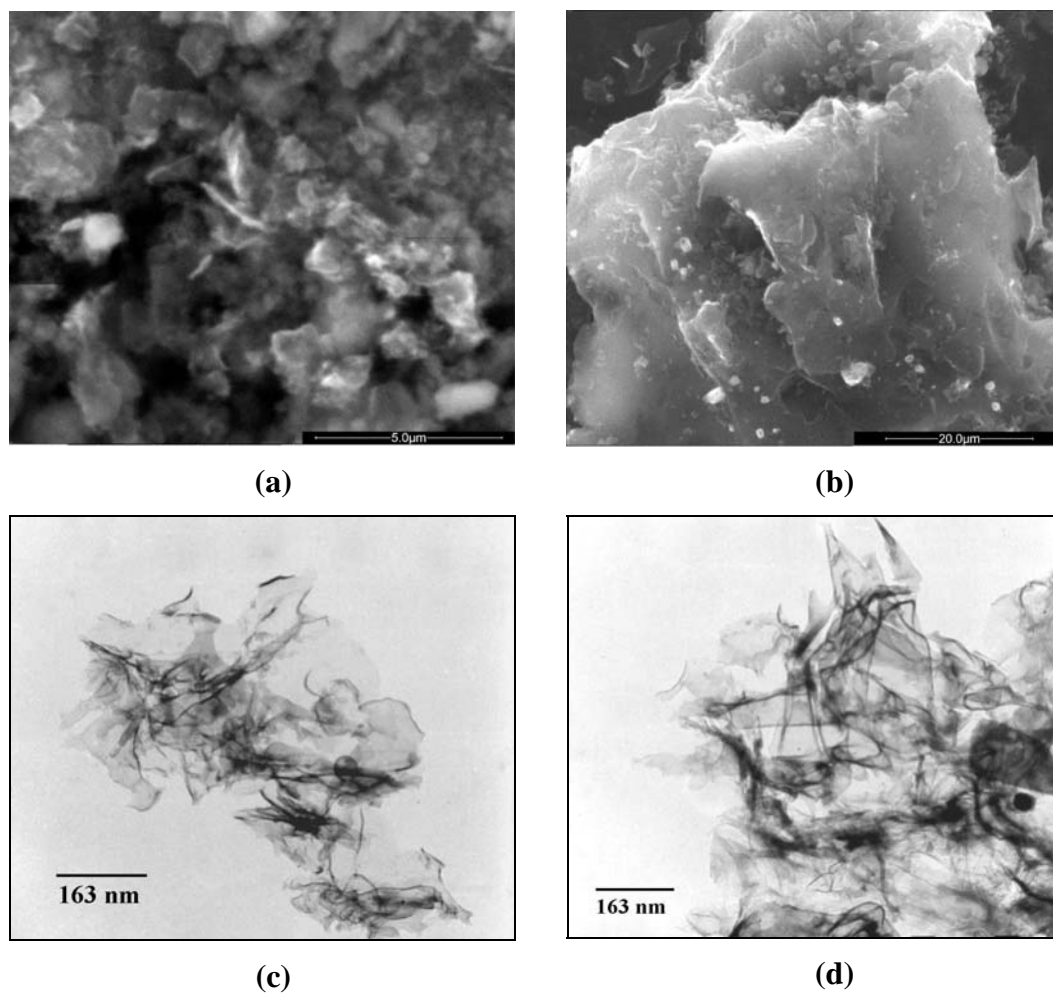


Fig. 5.8 SEM and TEM images of carbon nanotubes prepared by chemical vapor deposition (CVD) method using clay as template. (a-b) SEM images of CNT3 and NCNT3 and (c-d) TEM images of CNT3 and NCNT3 respectively

SEM and TEM images of carbon nanotubes prepared from clay as template are shown in Fig 5.8. SEM images showed layered type structure with amorphous nature. Peculiarly NCNT3 showed layered structure with open special arrangement. TEM images showed layered and disordered structure with amorphous and fibrous carbon. Since no catalyst has been used for the synthesis of carbon nanotubes, it is worth pointing out that the nanotubes produced by template synthesis under normal experimental conditions are almost free from impurities.

5.2.3 Elemental analysis

Elemental analysis was carried out to examine whether nitrogen has really entered the carbon nanotube framework or not. From the results given in Table 5.1, it is clear that nitrogen has been incorporated in the carbon frame work with various percentages for different source of carbon. It has been shown that a maximum of 7.6% of nitrogen has been incorporated when PVP was used as carbon source. In the template synthesis, it has been shown that carbon nanotubes prepared from polypyrrole showed a maximum of 6.4 % of nitrogen content in the sample.

Table 5.1 Total nitrogen content in the prepared nitrogen containing carbon nanomaterials

Carbon	Wt % nitrogen	Percentage of nitrogen content in the source used for synthesis
PDC	7.6	Polyvinylpyrrolidone 12.9%
MEC	4.3	Poly acrylonitrile 26.4%
NCNT1	6.4	poly pyrrole 21.2%
NCNT2	2.5	Pyridine 17.7%
NCNT3	1.8	Pyridine 17.7 %

5.2.4 Hydrogen activation studies

Evolved gas analysis (EGA) has been carried out to study the hydrogen activation on the pure carbon nanotube (CNT1) and nitrogen containing carbon nanotubes (NCNT1) prepared from alumina membrane template. The traces of evolved gas from the nitrogen containing carbon nanotubes (NCNT1) are shown in Fig. 5.9 a. It is seen from the trace that a species of trace corresponding to mass 17 was evolved which indicate the formation of ammonia. The evolution of ammonia was pronounced above 473 K showing that nitrogen present in the carbon network in CNT is capable of getting hydrided at room temperature. During recycling of the sample, it has been noticed that there is a decrease in ammonia formation (Fig. 5.9b), indicating the stiochiometric nature of the reaction. However the evolved gas traces from the pure carbon nanotube (CNT1) showed (Fig. 5.9c) the signal at back ground level. This confirms that nitrogen in the carbon nanotubes can play an important role in hydriding process. The nitrogen atomic sites may be the active sites where hydrogen atoms are generated from the activation of hydrogen molecule similar to the metallic sites (catalytic sites). If these activated hydrogen atoms were to spill over to the carbon surface then improvement in hydrogen storage capacity is achievable. The reason for activation of hydrogen at nitrogen sites may be due to favorable free energy of formation at these sites. The subsequent migration to carbon sites may be due to the favourable redox potential values of various species that can be formed. The redox potential of NH , NH_2 species may be suitable for producing hydrided carbon species like CH , CH_2 , and CH_3 . Formation of ammonia was also independently established by other chemical tests like spectrophotometry.

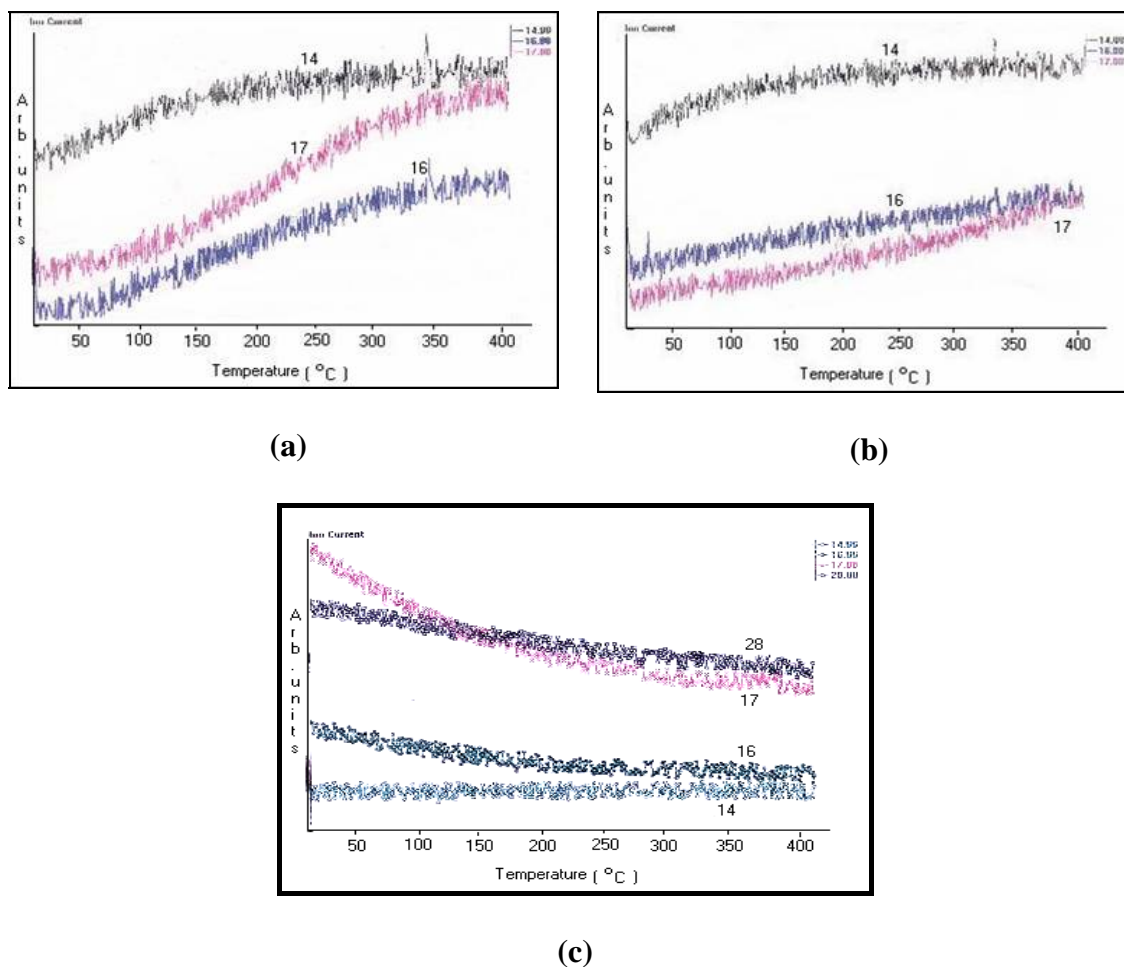


Fig 5.9 (a) EGA profile of Nitrogen containing CNT (b) The EGA profile of Nitrogen containing CNT after recycling (c) EGA profile of pure CNT prepared from polyphenyl acetylene

Electrochemical hydrogen storage experiments have been carried out in literature to measure the storage capacity (Nutzenadel *et al.*, 1999; Rajalakshmi *et al.*, 2000). However these results cannot be compared with other methods of determining storage capacity and each method has its own importance. The cyclic voltammetry experiments have been carried out to study the hydrogen interaction in the nitrogen containing carbon nanotubes compared to pure carbon nanotubes. The voltammograms were recorded in 6 N KOH using carbon nanotubes mounted on a glassy carbon as a working electrode, platinum as a counter electrode and Ag/AgCl as reference electrode with a scan rate of 25 mV/sec in the potential range of 0 to -1.3 V. It was observed (Fig. 5.10) that the glassy carbon electrode loaded with

NCNT1 alone showed a peak at -1.05 V corresponding to hydrogen desorption, thus showing CNT from polypyrrole source alone is capable of activating and absorbing hydrogen.

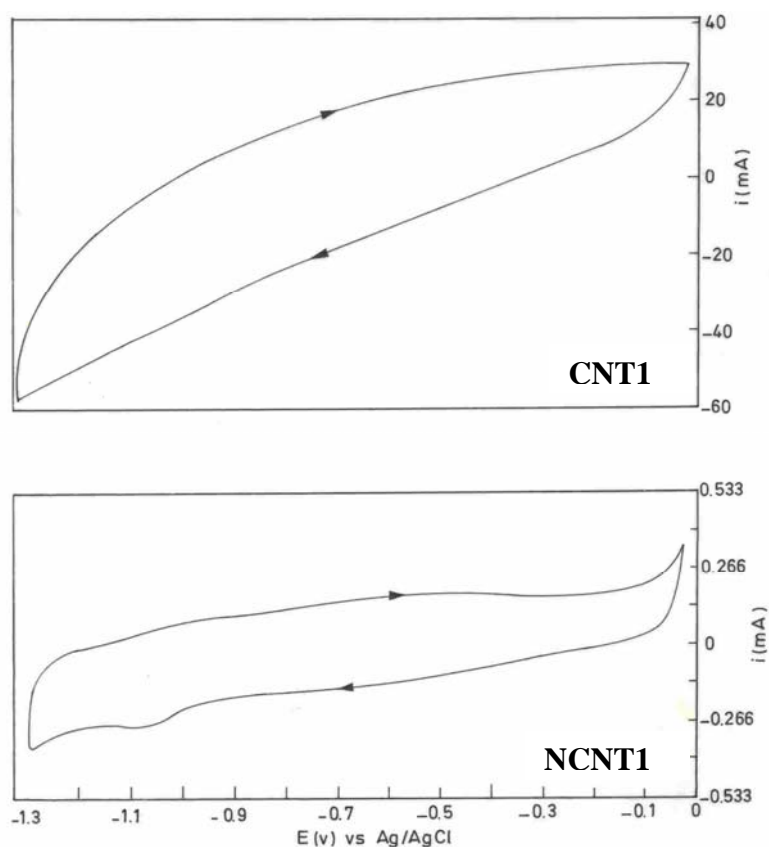


Fig. 5.10 Cyclic voltammograms of CNT1 and NCNT1

By independent method, the evolved gas analysis experiment has been carried out where the experimental conditions were similar to the evolved gas analyzer. The sample was initially evacuated and then heated to 393 K for 4 h then hydrogen gas was charged with atmospheric pressure and subsequently heated to 673 K followed by cooling to room temperature. After reaching room temperature the sample was heated slowly and the gas evolved was flushed to dilute H_2SO_4 solution by hydrogen as carrier gas. The acid solution has been tested for ammonia. The evolution of ammonia was ascertained by spectrophotometry using Nessler's reagent. Standard calibration

plot has been made with various concentrations of ammonium chloride which was used as ammonia source and from the calibration plot the amount of ammonia evolved from the NCNT sample has been determined. The amount of ammonia evolved from the sample was found to be 0.085 ml/mg of gas phase volume. After the reaction the samples were analyzed for nitrogen content by CHN analysis. The sample shows 4.3 % of nitrogen but the fresh sample had 6.6 % of nitrogen. From this result the total amount of ammonia evolved corresponds to 1/3 rd of the total nitrogen content in the sample. Theoretically one can predict the weight % of hydrogen from the amount of ammonia evolved, it is estimated that CNTs containing 20 % of nitrogen is capable of taking up about 1 wt % of hydrogen. If this hydrogen could be transported to the carbon skeleton, it may be possible to achieve DOE standards of hydrogen storage capacity in heteroatom containing CNTs.

5.2.6 Hydrogen storage capacity

The specific surface area (SSA) of the samples was evaluated by BET method and the results are given in Table 5.2. Hydrogen absorption activity of carbon nanomaterials has been evaluated at various temperatures namely 77 K, 298 K and 373 K at 0 – 760 mm Hg pressure. Hydrogen absorption values at 1 atm of hydrogen pressure are given in Table 5.2. The absorption at room temperature is negligible. However, absorption isotherm at 77 K showed that at this temperature the condensation of hydrogen is not possible and it requires either a low temperature of 20 K or higher pressure. At ambient temperatures NCNT1 showed higher absorption with respect to other carbons.

Table 5.2 Hydrogen absorption activity of carbon nanomaterials at 1 atm and at different temperatures (corresponding specific surface area (SSA) evaluated by BET method are indicated)

Sample	SSA (m ² /g)	Hydrogen absorption at 1 atm (cm ³ /g) at various temperatures (K)		
		77	298	373
PDC	93.0	20.2	0.34	0.90
MEC	182	64.4	-	2.78
CNT1	-	-	-	-
NCNT1	246	47.5	-	6.11
CNT2	633	28.0	-	3.42
NCNT2	646.5	-	-	-
CNT3	48.8	-	-	3.0
NCNT3	66.4	7.45	-	2.4

High pressure hydrogen absorption measurements showed that the hydrogen absorption increases with pressure. The hydrogen storage capacity of PDC and MEC shows a capacity of 0.25 and 0.53 wt% respectively. Differences in the synthetic procedures adopted leads to variation in the morphology of the prepared carbon materials. The morphology of the materials obtained plays an important role in hydrogen absorption activity. The PDC showed rod shape morphology (this information deduced from TEM analysis) stores hydrogen of 0.2 wt%. But the MEC showed the coiled structure with steps in the formation of tubular structure stores 0.53 wt% of hydrogen (Fig. 5.11).

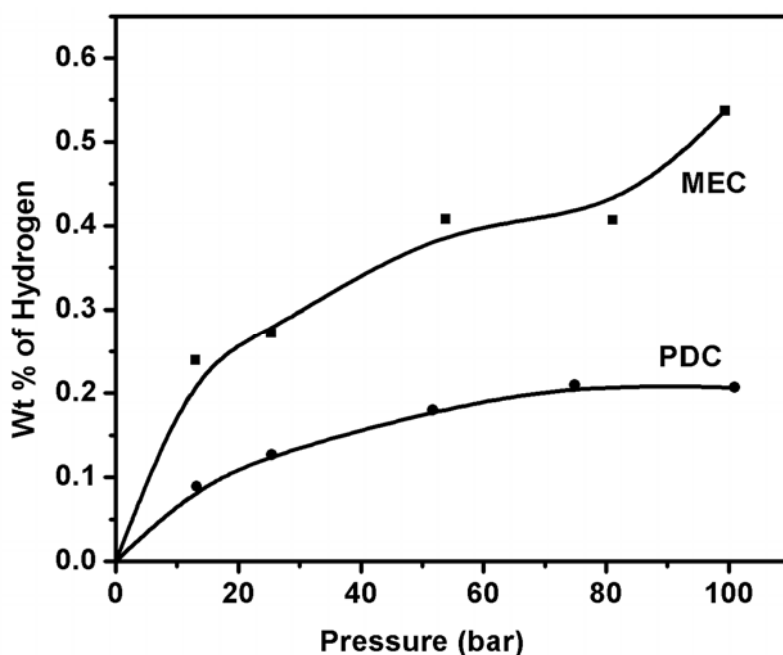


Fig 5.11 Hydrogen storage capacity of PDC and MEC as a function of hydrogen pressure

The hydrogen storage capacity of nitrogen containing carbon nanotubes prepared from alumina membrane (NCNT1) showed a maximum of 1.2 wt% at 100 bar hydrogen pressure (Fig. 5.12). However, in the second cycle, NCNT1 showed reduced hydrogen uptake of 0.6 wt%, which further confirms the role of nitrogen in hydrogen activation and its subsequent absorption. This is revealed from both the EGA and high pressure absorption experiments showing the role of nitrogen in hydrogen activation. The hydrogen storage capacity of the carbon nanotubes prepared from zeolite as template showed a maximum hydrogen absorption of 0.2 wt% for the pure carbon nanotubes (CNT2) and the nitrogen containing carbon nanotubes (NCNT2) show hydrogen storage capacity 0.72 wt %.

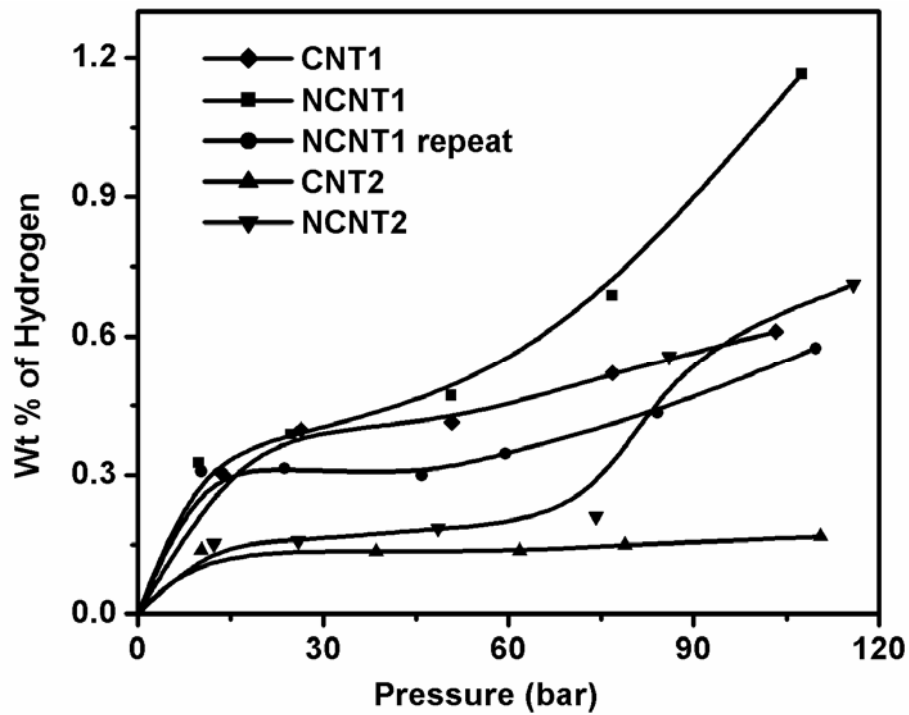


Fig. 5.12 High pressure hydrogen absorption activity of carbon nanotubes prepared from alumina membrane and zeolite templates

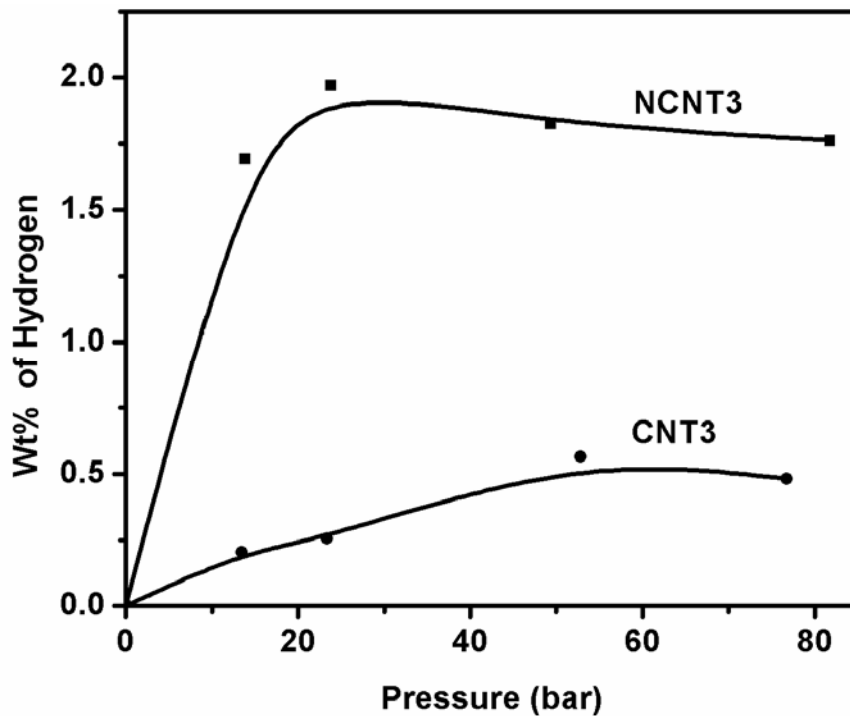


Fig. 5.13 High pressure hydrogen absorption activity of carbon nanotubes prepared from clay template (CNT3 and NCNT3)

The hydrogen storage capacity of carbon nanomaterials prepared from the pillared clay as the template (CNT3 and NCNT3) showed a maximum storage capacity of 0.35 wt % for pure CNT and a value of 1.75 wt % for the nitrogen containing carbon nanotubes (NCNT3) (Fig. 5.13). The structural features of the carbon prepared from clay as template facilitates efficient nitrogen incorporation. There is no reduction in hydrogen storage capacity in the second and third cycle which indicates strong interaction of nitrogen in carbon network.

5.3 CONCLUSIONS

Nitrogen containing carbon nanomaterials are amenable to hydrogen absorption compared to carbon materials. Nitrogen containing carbon nanomaterials have been synthesized by polymers as the carbon precursor. The template aided synthesis of carbon nanotubes using alumina membrane as the template yielded well-aligned carbon nanotubes and showed a maximum of 1.2 wt% hydrogen storage capacity where in polypyrrole is used as the carbon precursor. However, it decreases in the consecutive cycle to 0.6 wt% due to reduction of nitrogen concentration. Results from EGA studies also suggest the same decrease in the ammonia evolution from the nanotubes. This recommends that, nitrogen atoms in carbon nanotubes act as the active centre and these active sites should be made catalytic in nature by adopting and devising suitable preparation methods. Some sort of surface engineering should be necessary to achieve high hydrogen storage capacity. The nitrogen containing carbon nanomaterials produced by clay as the template showed a maximum of 1.75 wt %. The hydrogen storage capacity has not decreased with recycling up to three cycles. This may be attributed to the strong binding of nitrogen in the carbon nanotubes prepared from clay as the template using pyridine as the nitrogen containing carbon source. The heteroatom substitution in the carbon nanotubes opens up another avenue in the search for materials for hydrogen storage.

CHAPTER 6

BORON SUBSTITUTED CARBON NANOTUBES – SYNTHESIS, CHARACTERIZATION AND HYDROGEN ABSORPTION ACTIVITY

6.1 INTRODUCTION

Developing new nanostructured materials is of current interest. It is partly because of the potential applications they possess in various fields. It is more so in the field of electronics (Pool, 1990), optics (Foss *et al.*, 1994), catalysis (Che *et al.*, 1999) and energy systems (Che *et al.*, 1998). Since the discovery of carbon nanotubes (CNTs) by Iijima (Iijima, 1991), a number of studies on CNTs and related nanostructures have been carried out. The extraordinary mechanical and electronic properties of these structures have led to several applications, including nanoelectronic devices (Trans *et al.*, 1998), probe tips for scanning probe microscopy (Wong *et al.*, 1998) and field emitter arrays (Fan *et al.*, 1999). Substitution of heteroatoms like nitrogen or boron offers a way to tailor the structural and electronic properties of carbon nanotubes. Heteroatom substitution in carbon nanotubes not only provides the opportunity to study the level of perturbations in the physical properties but also gives an opportunity to exploit the unique properties generated there by in the sector of advanced technology (Stephan *et al.*, 1994; Carroll *et al.*, 1998).

Modifying the carbon surface has been advocated as one of the methods for achieving higher hydrogen storage capacity. This is a potential field of research in recent times. It has been proposed that hetero atoms may be the alternate centers for hydrogen activation and the activated hydrogen thus generated may migrate to the carbon surface. The choice of heteroatoms has been made on the basis of various parameters

like the redox behaviour of the hetero atom and the feasibility of incorporating the hetero atom in the carbon nanotube framework. It has been shown that heteroatoms like nitrogen, phosphorus, sulphur and boron in carbon nanotubes can activate hydrogen. The geometrical positions of these hetero atoms are important for hydrogen activation. These results are based on Density Functional Theory calculations discussed in chapter 3. Essentially substitution of boron at alternate position is geometrically favorable for the hydrogenation of carbon atoms, while the C-H bond formation is not that much favorable for the system where boron atoms are at adjacent positions.

Mainly boron containing carbon materials show promising applications in electronics (Wei *et al.*, 1999). In recent times boron has been used as an efficient dopant for improving the oxidation resistance of graphite, carbon fibers, carbon/carbon composites, and various other carbon materials (Radovic *et al.*, 1998). Though it has got wide applications, preparation of these materials seems to involve tedious procedure. The preparation of boron containing carbon materials is an art by itself. The same interest has also been followed in preparing the boron containing carbon nanotubes after the emergence of nanotechnology.

Various routes have been evolved for the synthesis of boron doped nanotubes, including arc discharge, laser ablation, substitution reactions and pyrolysis of precursors like acetylene–diborane mixtures in a flow of helium and hydrogen (Borowiak-Palen *et al.*, 2003; Han *et al.*, 1999; Golberg *et al.*, 1999). In the arc discharge and laser ablation techniques to produce CNTs, difficulties are encountered in the control of size and alignment of the nanotubes. Further, these techniques require purification processes to separate the CNTs from the catalyst particles used in the

synthesis. The general source of carbon used to produce the carbon nanotubes is hydrocarbons. But the complexity involved in the synthesis of carbon nanotubes using gaseous hydrocarbons is high. An alternate and easy method should be employed to synthesize these materials avoiding gaseous and toxic hydrocarbons. However, by using these methods it is difficult to synthesize heteroatom substituted carbon nanostructures. Alternately by choosing appropriate heteroatom containing polymers the substitution of heteroatom can be achieved in the carbon nanotube structure.

The template synthesis method has been widely used for preparing micro and nanostructured materials (Martin, 1994), involving the synthesis of desired material within the pores of a membrane to generate nanotubes of cylindrical nature with uniform diameter. The use of template (alumina membranes) for the synthesis of the carbon nanotubes was first perfected by Che *et al.* and Kyotani *et al.* used a combination of CVD and template synthesis methods to synthesize highly aligned, uniform, hollow and open ended (suitable for filling with other materials) CNTs with pore diameters ranging from 20 to 200 nm (Che *et al.*, 1998; Kyotani *et al.*, 1996). Among all the methods of preparation of CNTs, the template synthesis method has the advantage of controlling composition, morphology and the size of the nanotubes.

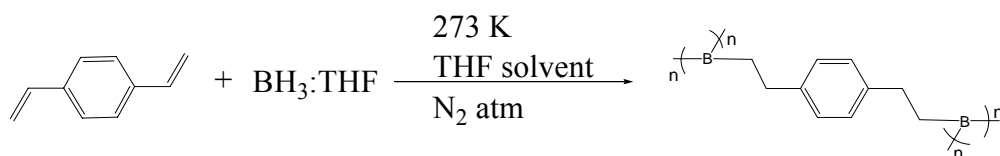
The synthesis of boron substituted carbon nanotubes has been carried out using hydroborane polymer as carbon source which is formed *in situ* during the polymerisation of divinyl benzene and borane in the pores of alumina membrane. The morphology and structural features of the nanotubes have been investigated using electron microscopy and Raman spectroscopy. The composition and bonding of the nanotubes were analyzed using FT-IR, XPS and MAS NMR. Hydrogen storage capacity of the as synthesized boron substituted carbon nanotubes has been reported.

6.2 EXPERIMENTAL SECTION

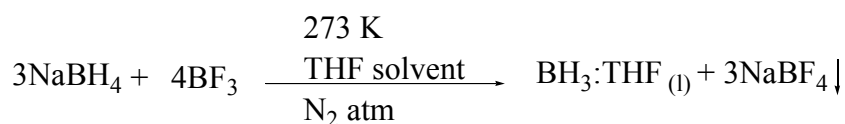
6.2.1 Synthesis of boron containing carbon from hydroborane polymers

Hydroborane polymers have the boron atom in the structure of skeleton which helps in the substitution of boron atoms in carbon network during the carbonization process. A stable crosslinked π -conjugated hydroborane polymer has been prepared by hydroboration polymerization. These polymers show interesting properties such as intense emission and excellent third order nonlinear optical susceptibilities. By introducing crosslinking structure in the polymer chains, more planer structure and more extended conjugation length would be expected. In addition, closely packed structure might improve the stability of the polymer.

The hydroborane polymer has been prepared by the crosslinking polymerization of 1,4-divinyl benzene with the borane in THF solution. $\text{BH}_3\cdot\text{THF}$ solution is prepared *insitu* by the reaction of sodium borohydride with $\text{BF}_3\cdot\text{etherate}$ solution at 273 K in nitrogen atmosphere as shown in the Scheme 6.1 and this has been added to the THF solution containing the 1,4-divinyl benzene. The resulting mixture was stirred for 2 h in 273 K and then for completion of reaction the system was stirred at room temperature for 6 h leading to solid viscous gel. Excess THF solvent was removed under reduced pressure.



Scheme 6.1 The preparation of hydroborane polymer



The polymer obtained was characterized by various methods. The obtained polymer was sparingly soluble in THF and CHCl_3 solvents, so it is difficult to identify the structure of the insoluble part. The measurements of ^1H NMR and ^{11}B NMR spectra of the soluble part were carried out. ^{11}B NMR spectrum of hydroborane polymer has been carried out in CDCl_3 solution locked with D_2O and BF_3 .etherate as the standard reference (Fig 6.1). ^{11}B NMR spectrum showed one peak at 31.3 ppm which is assignable to dialkenylborane unit (Matsumi et al., 1998; Matsumi et al., 2000) just as in the linear polymer. In the ^1H and ^{13}C NMR spectra, a peak owing to the ethylene proton disappeared (Fig 6.2 and Fig. 6.3).

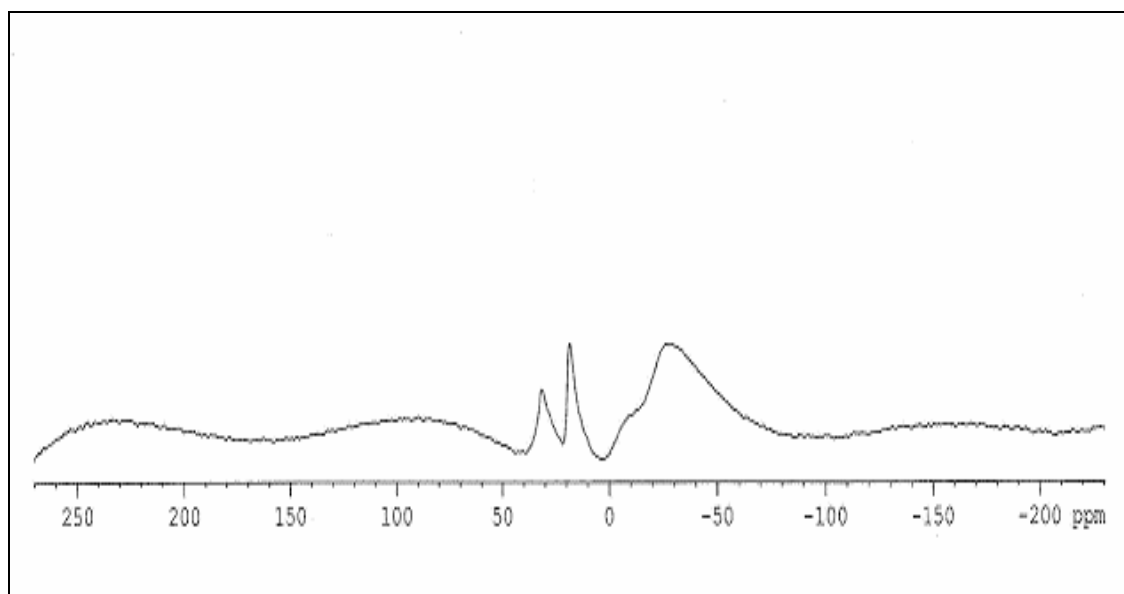


Fig. 6.1 ^{11}B NMR spectrum of hydroborane polymer in CDCl_3 solution locked with D_2O and BF_3 .etherate as the standard reference

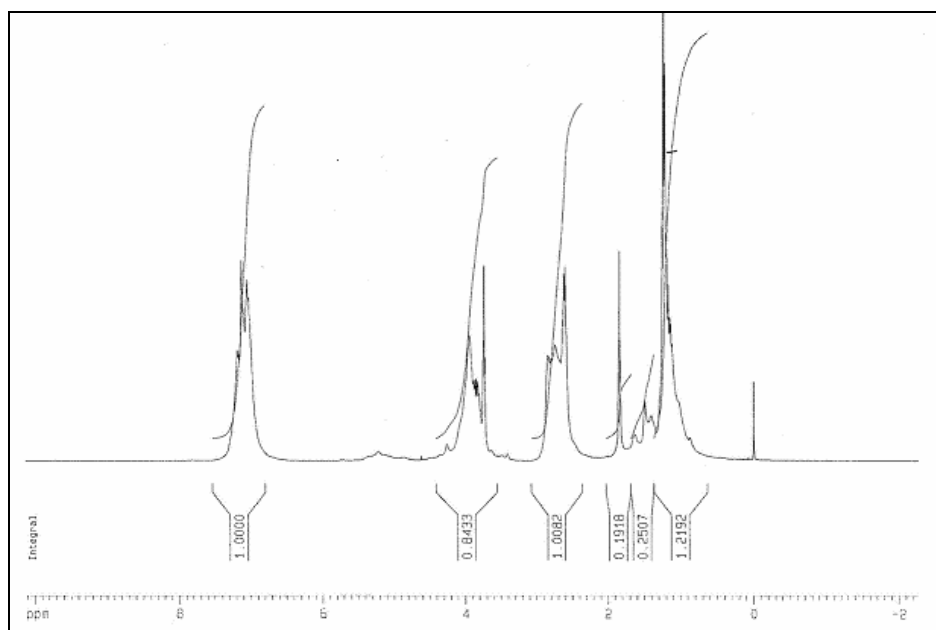


Fig. 6.2 ^1H NMR spectrum of hydroborane polymer taken in CDCl_3 solvent

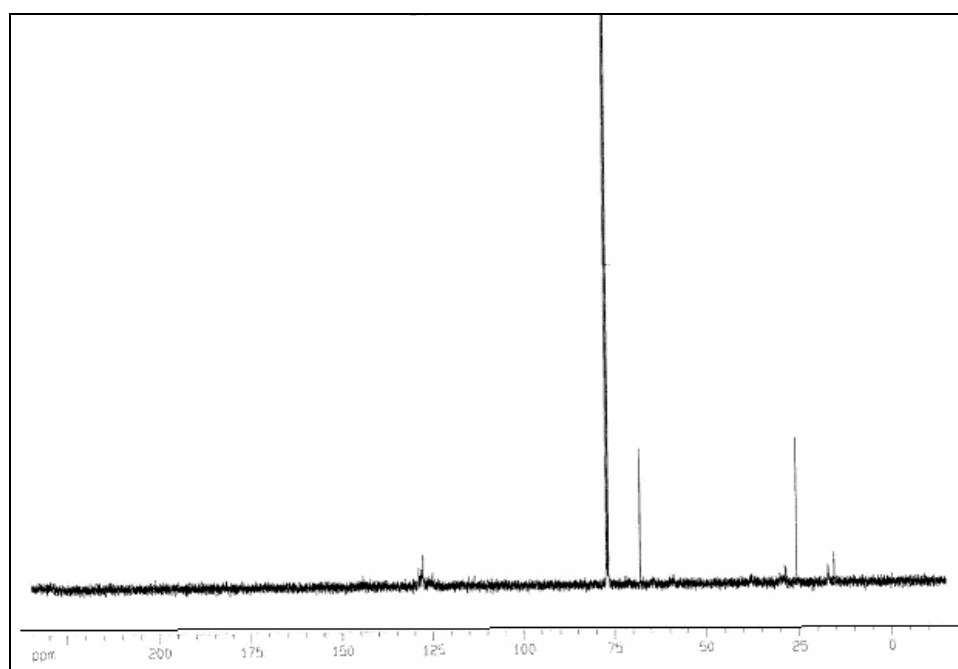
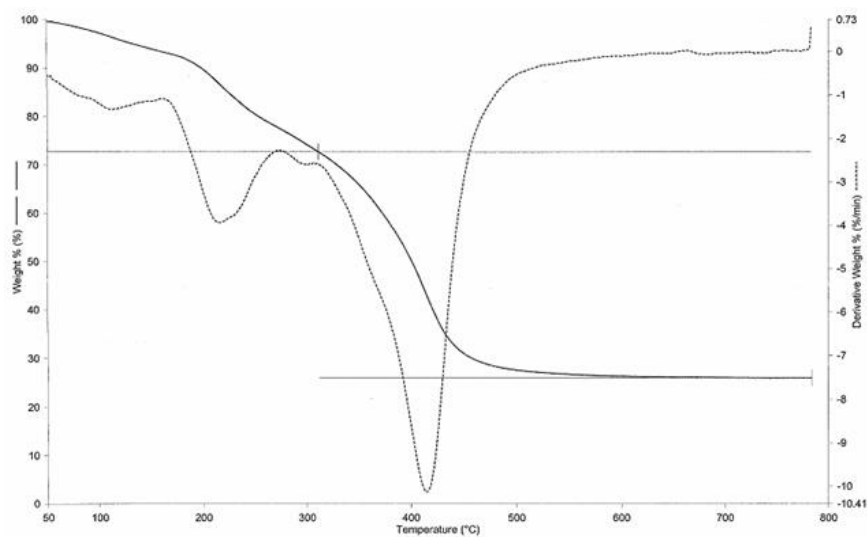
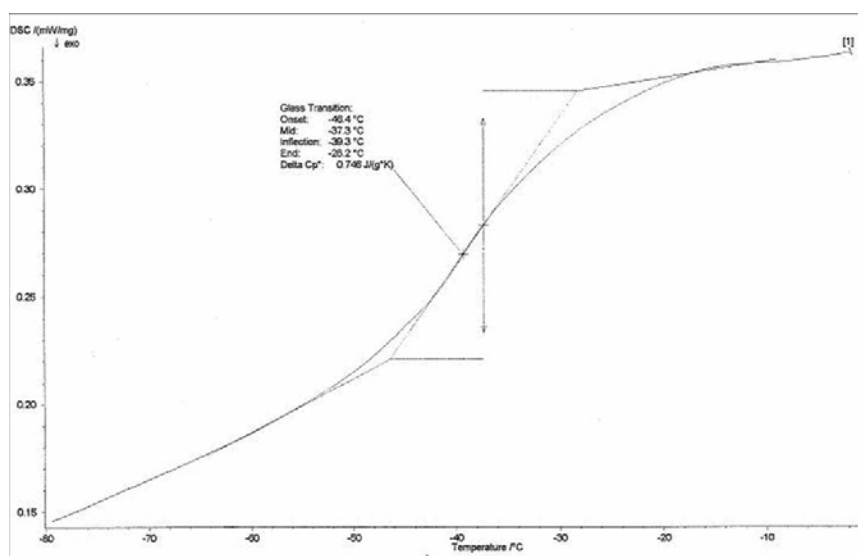


Fig. 6.3 ^{13}C NMR spectrum of hydroborane polymer

To investigate the thermal stability of the hydroborane polymer, thermogravimetric analysis (TGA) was carried out. As shown in Fig. 6.4 polymer showed complete decomposition around 773 K and the phase transition from the Differential Scanning Calorimetry (DSC) showed a glass transition temperature at 233 K.



(a)



(b)

Fig. 6.4 (a-b) TGA and DSC of hydroborane polymer respectively

Boron containing polymer was carbonized in inert atmosphere in the flow of Ar gas at 1173 K for 6 h. Boron containing carbon (BC) material obtained is characterized by physico-chemical techniques and the hydrogen absorption activity has been carried out at low and high pressure.

6.2.2 Synthesis of boron containing carbon from boron containing resin

Boron containing carbon material has been synthesized by the procedure adopted by Xiang *et al* via an esterification reaction of phenol hydroxyl groups by boric acid and pyrolysed at 900 °C in inert atmosphere (Xiang *et al.*, 2002). In detail, the procedure is 35.29 g of phenol and a 62.56 g of formaldehyde solution (>36 wt.%) were reacted through the catalysis of 2.22 g of 20 wt.% NaOH at 348 K for 1 h under nitrogen atmosphere. After adding 7.76 g of boric acid the mixture was heated to reflux temperature and further reacted at the reflux temperature for 0.5 h. Boron-containing phenolic resin was obtained after removal of water under reduced pressure. It was then heated in air atmosphere at 383 K for 2 h to get a cured resin. The resin sample was transferred into quartz boat and carbonized in a flow of argon gas at 1173 K. The characterization part of this material is not dealt in the present thesis. The carbon obtained (PBC) was used for hydrogen absorption study.

6.2.3 Template based synthesis of carbon nanotubes

6.2.3.1 Alumina membrane

Boron containing carbon nanotubes (BCNT 1) were prepared by using the boron containing polymer as the carbon precursor. Stable cross linked π - conjugated organoboron polymer was prepared by hydroboration polymerization of three equivalent 1, 4-divinylbenzene with diborane in THF medium as shown in Scheme 1.

In-situ polymerization has been carried out over the alumina membrane template (0.2 μm pore diameter, 60 μm thick – Whatman Anodisc) in THF under nitrogen atmosphere. After completion of polymerization, the membrane is removed, dried in vacuum and polished with alumina powder to remove the adhered polymers. The polymer / alumina composite membranes have been carbonized at 1173 K for 6 h in Ar atmosphere. The carbon/alumina composite was treated with 48% HF for 24 h to remove the template and washed with distilled water followed by drying at 373 K (BCNT).

6.2.3.2 Zeolite and clay as template

Other boron containing carbon nanotubes were prepared by chemical vapour deposition (CVD) method by using H- zeolite Y (BCNT2) and Al-pillared Clay (BCNT3) as template. Al-pillaring of clay has been carried out using aluminium polycationic species ($[Al_{13}O_4(OH)_{24}(H_2O)_{12}]^{7+}$) (Vaccari, 1998; Figueras, 1988). The polycations are prepared by the partial base hydrolysis of a dilute solution of aluminum chloride. Acetylene (5 ml / min) has been used as a carbon source and *in-situ* generation of borane gas by the addition of conc. H_2SO_4 to the $NaBH_4$ in THF medium, carbonized at 1173 K in Ar atmosphere as shown in Fig 6.5. The carbon/zeolite and carbon/clay composite have been treated with 48% HF for 24 h and the undissolved carbon has been washed with distilled water and dried at 373 K.

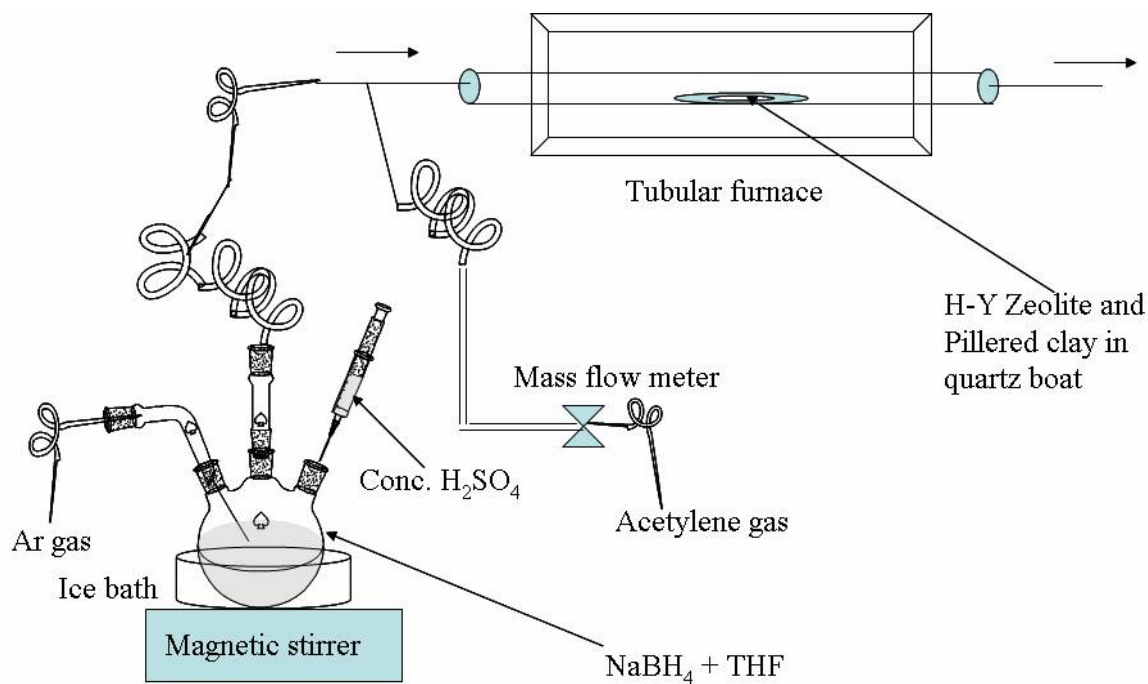


Fig. 6.5 Pictorial representation of chemical vapor deposition carried out for the production of boron containing carbon nanotubes

6.3 RESULTS AND DISCUSSION

6.3.1 XRD studies

The X-ray diffraction studies (XRD) of BC showed that the prepared carbon material is graphitic in nature and showed a sharp peak at $2\theta = 28.2$ which corresponds to (002) plane of graphite (Fig. 6.6). The calculated d value as 3.16 (\AA) calculated from 2θ value. From the XRD results shown in Fig. 6.7, the carbon nanotubes produced are found to be graphitic in nature. The diffraction (002) plane at $2\theta = 28.5$ corresponds to hexagonal planes of graphite (JCPDS car files, no. 41- 1487). This graphitic nature is mainly due to the carbonization of the carbon precursors at $900 \text{ }^\circ\text{C}$. A clear shift in the d value has been observed which is attributed to the substitution of boron in the carbon network. The 2θ value has been shifted from 26.0 to 28.5 for the (002) reflection (Fig. 6.7). Certainly, the intensities of in-plane reflections particularly for the 110 reflection are weaker in the case of BCNT. This may be due to the

presence of localised BC_3 domains slightly influencing the periodic atomic arrangement of the hexagonal carbon network (Shirasaki *et al.*, 2000).

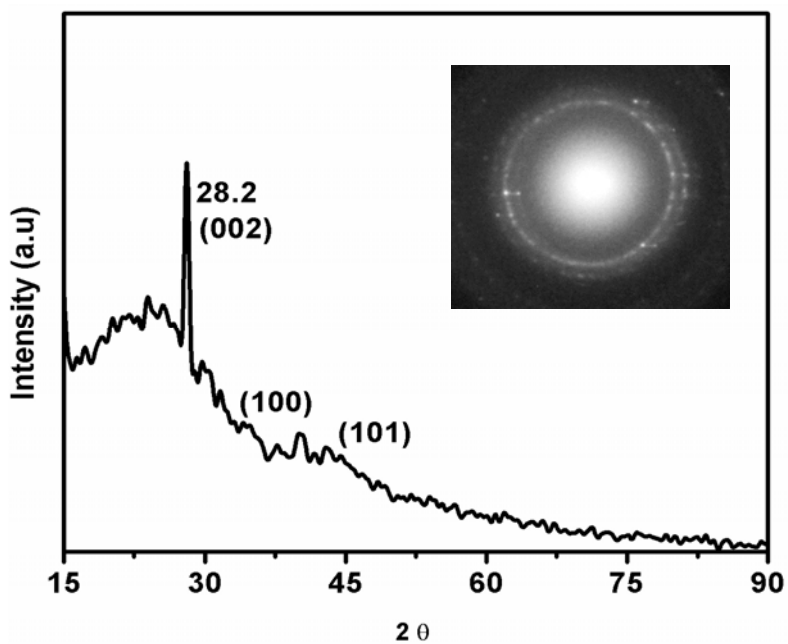


Fig. 6.6 X-ray diffraction pattern of boron containing carbon (BC) prepared by polymer carbonization and the inset diagram shows the selected area electron diffraction (SAED) of the sample from TEM analysis

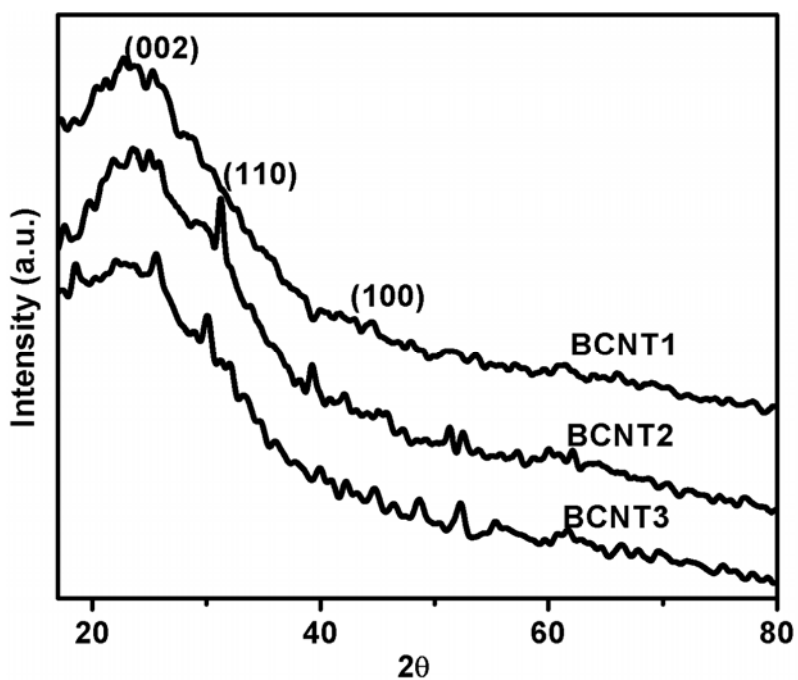


Fig. 6.7 X-ray diffraction patterns of boron containing carbon nanotubes (BCNTs)

6.3.2 FT-IR spectroscopy

Boron substitution in the carbon network displayed an effective downshift of the vibration stretching frequency. The downshift is attributed to the much lower force constant of B-C than that of C-C. A band at 1250 cm^{-1} corresponding to C-B bond is seen (Fig. 6.8). Usually C-B band occurs in the range 1050 cm^{-1} to 1200 cm^{-1} . Increase in the frequency of C-B stretching is correlated to higher carbon content (Shirai *et al.*, 1995). This showed that the prepared carbon nanotubes possess higher carbon content with the synthetic strategy currently adopted.

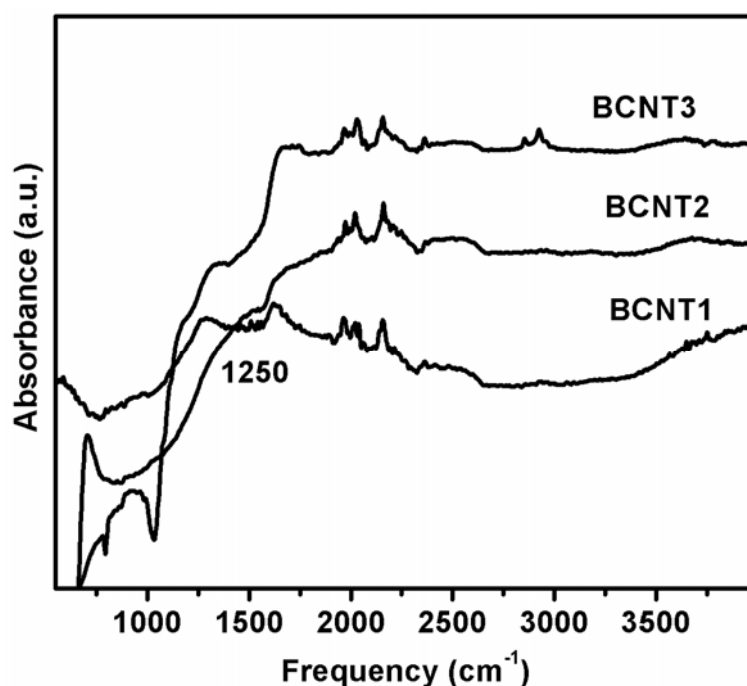


Fig. 6.8 FT-IR spectra of boron containing carbon nanotubes (BCNTs)

6.3.3 Raman studies

The D-peak at 1350 cm^{-1} due to the disorder-induced phonon mode (breathing mode, A_{1g} -band) and the G-peak at 1594 cm^{-1} assigned to the Raman-allowed phonon mode (E_{2g} -band) are shown in the Raman spectra (Fig. 6.9). All the carbon nanotubes

synthesized showed the same order of disorderness in the graphitic structure. Carbon nanotubes produced by the polymer precursor method using alumina membrane as template exhibited equal intensity of D and G band character due to systematic increase in intensity of the disorder-induced band (D-band) upon boron atom substitution (McGuire *et al.*, 2005).

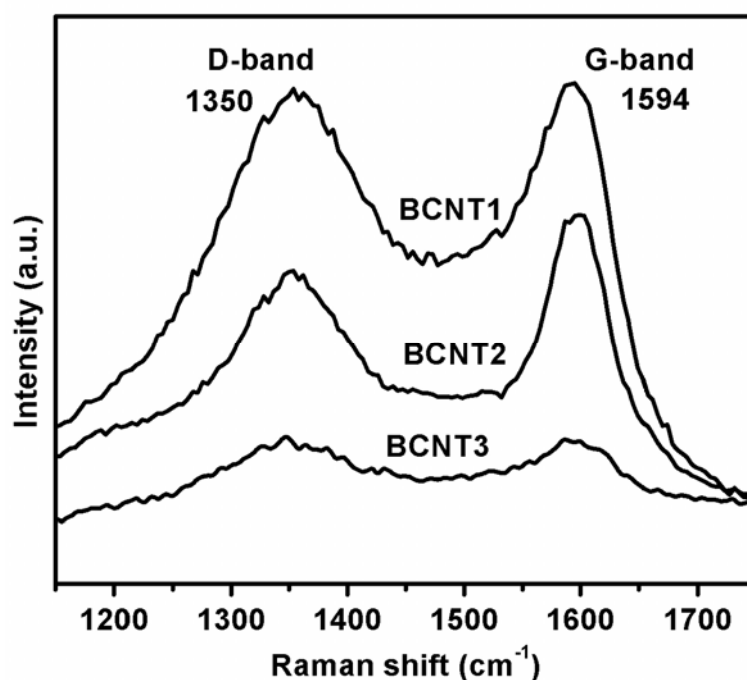


Fig. 6.9 Raman spectra of boron containing carbon nanotubes prepared by template assisted method

6.3.4 Electron microscopy study

Selected area electron diffraction (SAED) has been carried out using transmission electron microscopy (TEM) for the sample BC and presented in the inset of Fig. 6.6. From the diffraction a ring pattern has been obtained. By utilizing the diameter of the ring the d value ($d = 3.2$) has been calculated, which is comparable to the d value calculated from the X-ray diffraction measurements. This further confirms the shift in the 2θ value is due to the boron incorporation in the carbon. The Scanning electron microscopic (SEM) image (Fig. 6.10) of BC showed the crystalline nature of the

carbon material. The TEM picture showed the particle size of around 100 nm with uniform spherical morphology and the SEM images of boron substituted carbon nanotubes are shown in Fig. 6.11. Tubular morphology with well alignment nanotubes could be seen clearly. The HR-TEM image (Fig. 6.12) of BCNT1 after the carbonization at 1173 K for 6 h showed hollow and transparent tubes with slight deformation at the end of the tube probably caused by the ultrasonication and vigorous HF treatment. The outer diameter of the tube is approximately 200 nm which is equivalent to the channel diameter of the template used (also seen is a layer of amorphous carbon on the wall of the tube). Though the carbon tubes produced by this method are not completely graphitic in nature, as those produced by arc-discharge process their disordered structure is quite typical of fibers or nanotubes produced by decomposition of hydrocarbons, as is evident from the amorphous carbon on the wall of the carbon nanotube.

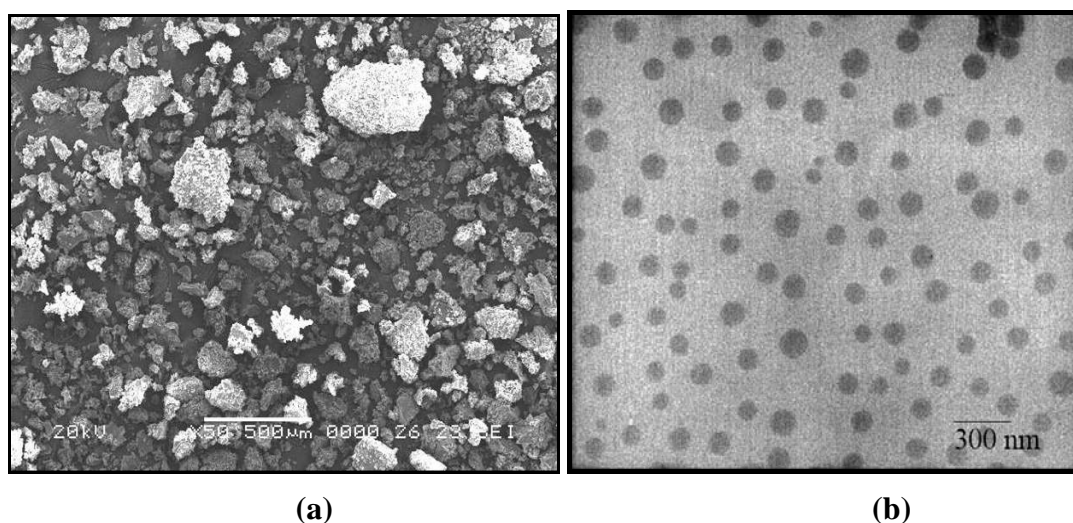
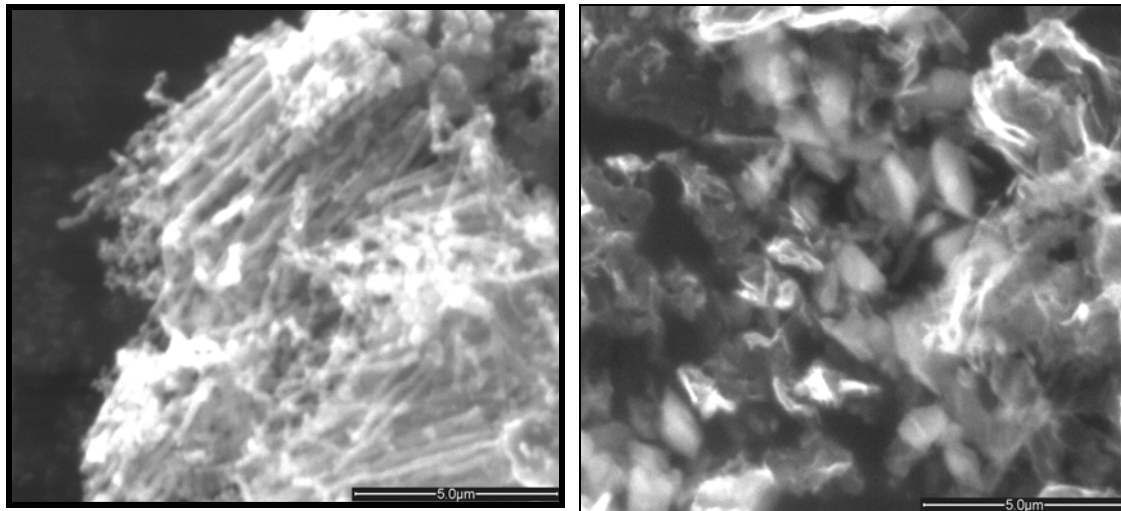
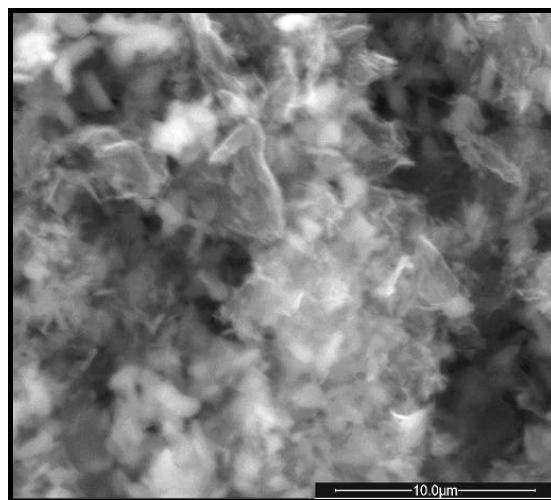


Fig. 6.10 (a-b) SEM and TEM images of boron containing carbon (BC) sample respectively



(a)

(b)



(c)

Fig. 6.11 SEM images of the boron containing carbon nanotube: (a) side view of the vertically aligned nanotubes of BCNT1 (b-c) top view of the carbon nanotubes (BCNTs 2 and 3) prepared by using zeolite and clay as template respectively

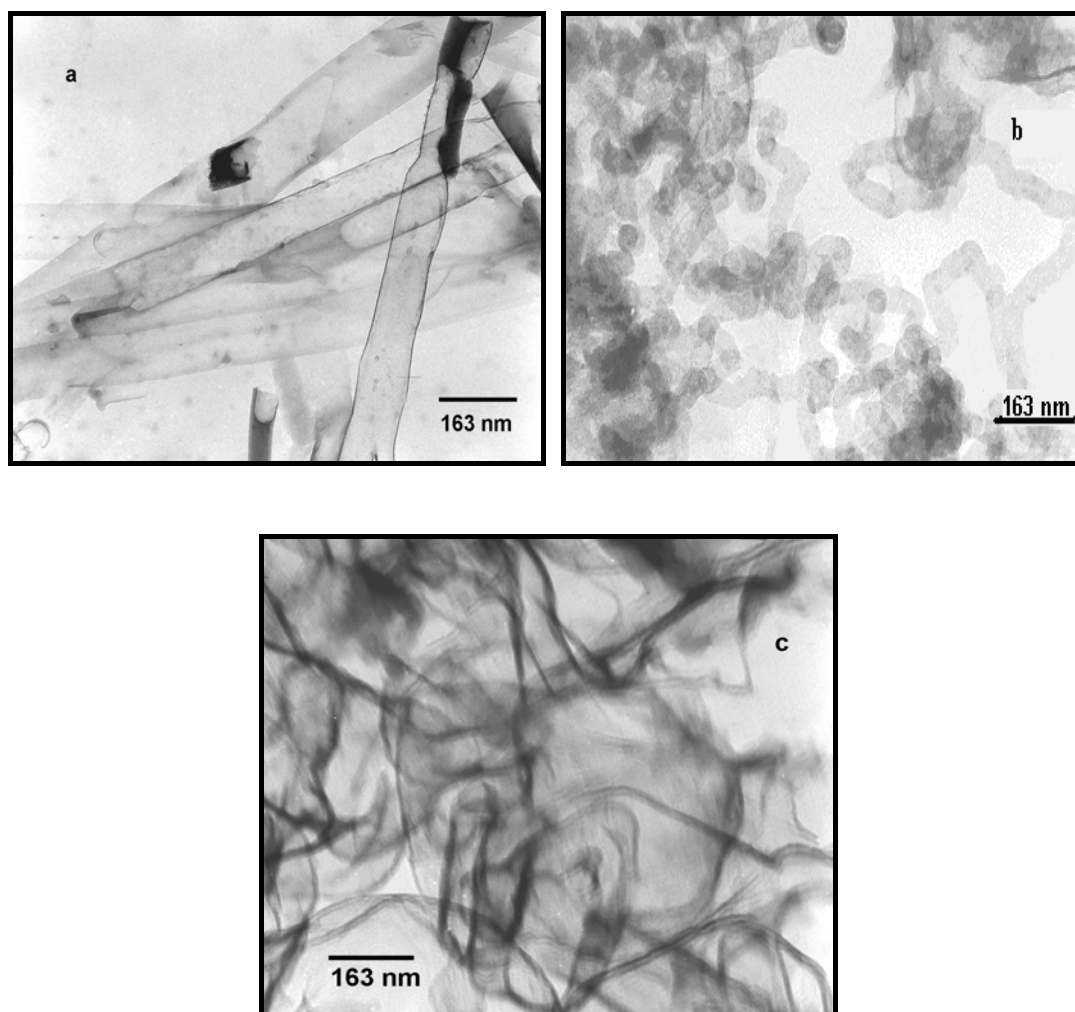
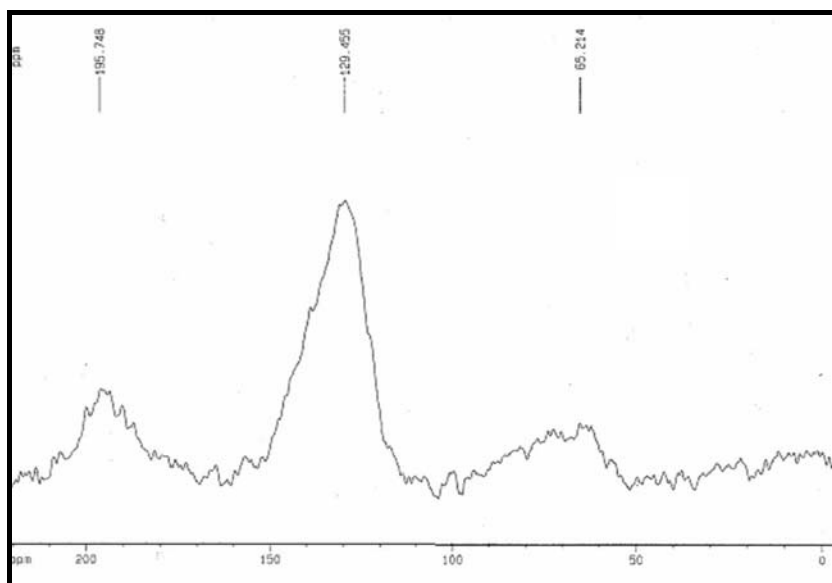


Fig. 6.12 (a) TEM picture of boron containing carbon nanotube (BCNT1) prepared from polymer precursor (b-c) TEM images of boron containing carbon nanotubes (BCNTs 2 and 3) prepared by chemical vapor deposition (CVD) method

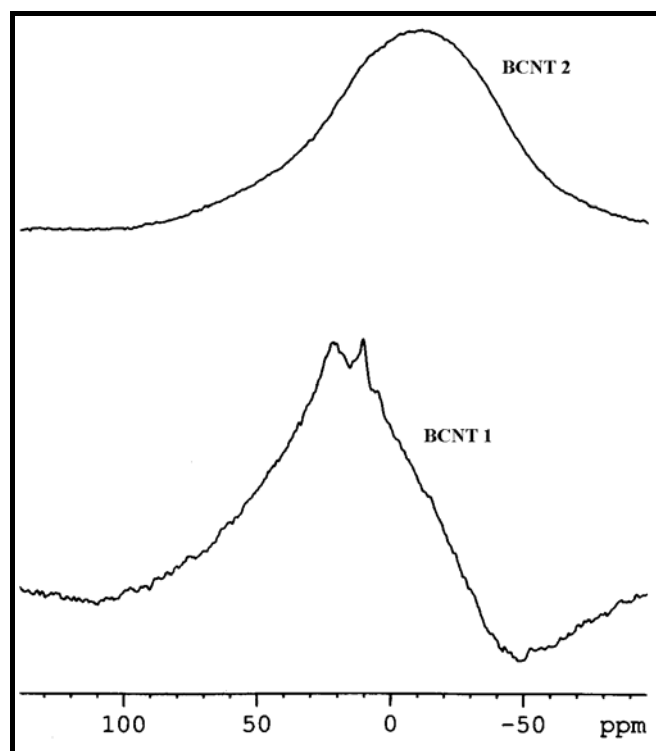
6.3.5 Solid state ^{13}C and ^{11}B MAS NMR Measurements

Chemical environment of boron in carbon nanotube was studied in great detail by MAS NMR spectroscopy. From ^{13}C CP MAS NMR spectrum the graphitic nature of the carbon nanotubes is evident as revealed by the characteristic peak at 129 ppm (Fig. 6.13) for the BCNT1. ^{11}B MAS NMR is one of the important tools to show the chemical environment of boron in carbon net work. In ^{11}B MAS NMR the dipolar interaction is only possible by the homonuclear B-B interaction whereas under MAS condition the heteroatom ^{13}C showed very low nuclear spin and the interaction is

negligible. Though there is a possibility for the second order quadrupole interaction due to ^{11}B ($I=3/2$), MAS (Magic Angle Spinning) does eliminate the secondary quadrupole interaction. It does not contribute to the line shape (Shirasaki *et al.*, 2000). In the experiments, two different chemical environments were observed for the BCNT 1 prepared by the polymer precursor route (Fig 6.13b). There is a clear indication that the boron atoms are bonded to carbon atom in two different environments and there is no possible quadrupole interaction due to B-B bond. Also the hetero nuclear interaction with ^{13}C is very weak. However, BCNT 2 showed a broad spectrum which has the possibility of multiple environment and also presence of B-B entity. These results suggest that boron atoms are present in two different chemical environments in BCNT1 prepared by polymer route.



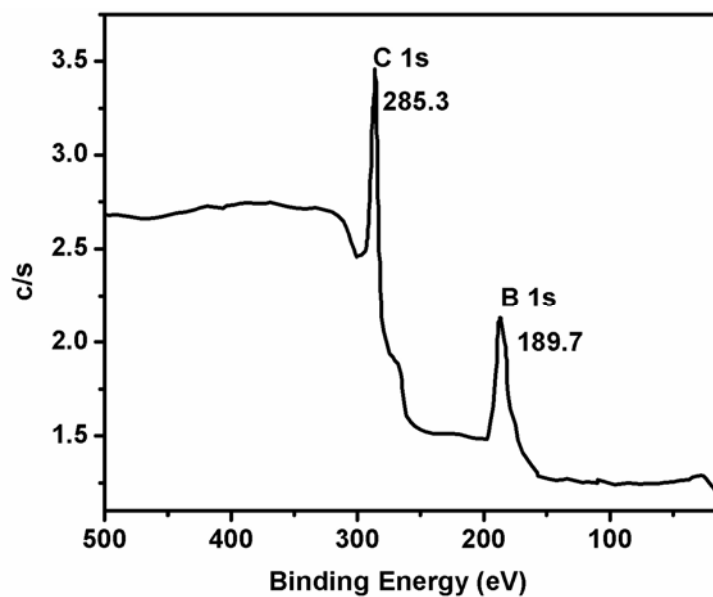
(a)



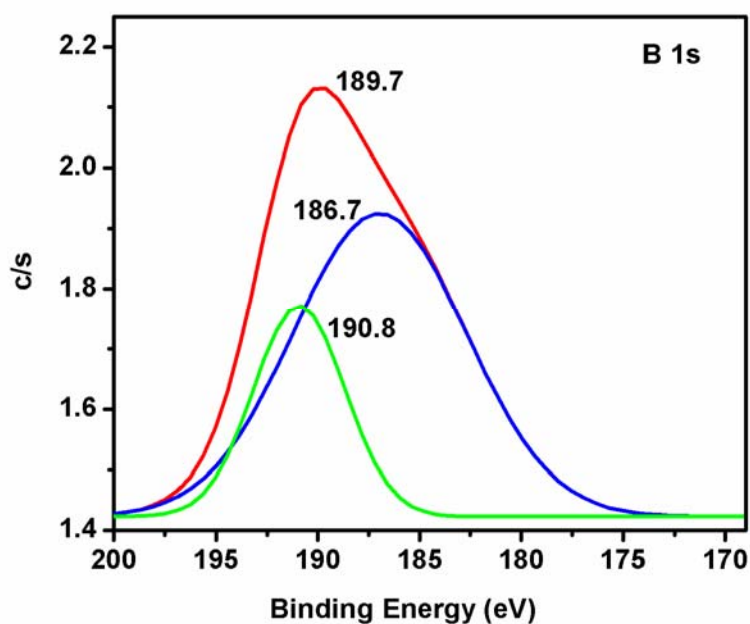
(b)

Fig. 6.13 (a) ^{13}C CP MAS NMR of BCNT and (b) ^{11}B MAS NMR spectrum of boron containing carbon nanotubes

The chemical state of the doped boron in the CNT was studied by X-ray photoelectron spectroscopy (XPS) and the spectra are shown in Fig. 6.14. As seen from the spectrum of BCNT (Fig. 6.14a) the presence of B in the carbon nanotubes established by the Binding Energy (BE) peak around 189.7 eV. There are no splitting or different peaks for the boron in carbon nanotubes to indicate explicitly the different chemical nature. However a clear peak broadening for boron has been observed at lower BE and this has been deconvoluted and shown in Fig. 6.14b.



(a)



(b)

Fig. 6.14 (a) X-ray photoelectron spectrum of boron substituted carbon nanotube (b) The deconvoluted XPS spectrum of B1s

X-ray photoelectron spectroscopy (XPS) of boron substituted carbon nanotubes showed the carbon 1s peak at 285.3 eV. Boron 1s peak was rather broad with a peak maximum at 189.7 eV which is greater than those reported for elemental boron (187.1eV), substitutional boron in HOPG (186.5 eV) and BC_4 (186.3 eV)

(Ottaviani *et al.*, 1998). The peak at $(188.8 \pm 0.1 \text{ eV})$ can be assigned to the boron atom substituted in the graphitic structure as proposed by Cermignani *et al* (Cermignani *et al.*, 1995). Jacques *et al* assigned the peak at 188.8 eV to boron atom substituted in the graphitic structure. The B 1s peak value of 190.4 - 191.4 eV has been assigned to boron atoms with the local environment of ideal BC_3 (Jacques *et al.*, 1996). From the deconvoluted B 1s spectrum it is clear that the boron atom exists in two different chemical environments which are attributable to the presence of different type of chemical environment of boron (Ottaviani *et al.*, 1998).

6.3.6 Hydrogen absorption activity

Hydrogen absorption capacity of BCNTs has been carried out at various temperatures namely 77 K, 298 K, 373 K and 423 K at 0 – 760 mm Hg pressure. Absorption at room temperature is negligible, however absorption isotherm at 77 K shows that at this temperature condensation of hydrogen is not possible and it requires either low temperature of 20 K or higher pressure.

The values of Specific Surface Area (SSA) evaluated by BET method using nitrogen gas absorption at 77 K and the maximum hydrogen absorption at 760 mm Hg of pressure for various temperatures are given in Table 6.1. The hydrogen absorption isotherms for BCNT1 are given in Fig 6.15. From the results, it is seen that hydrogen absorption at 77 K shows a maximum of 1.13 wt %.

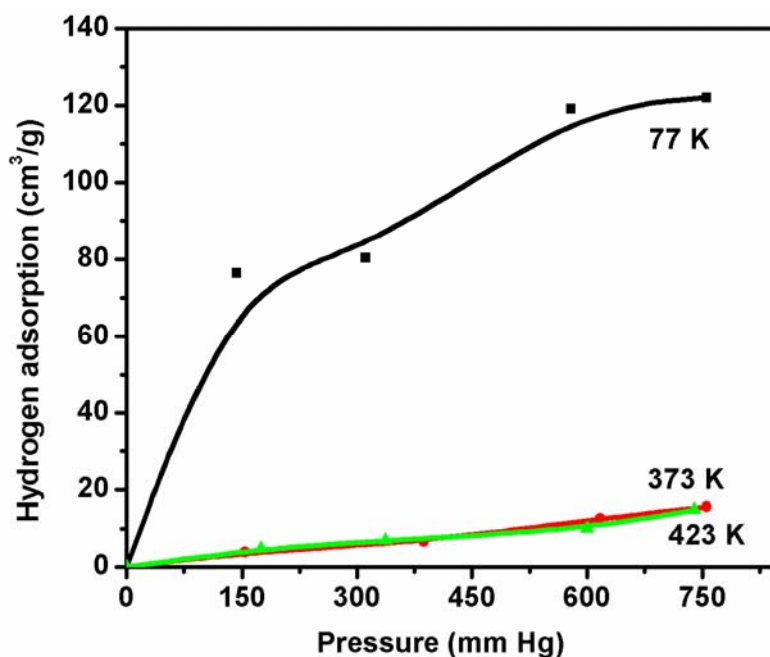


Fig. 6.15 Hydrogen adsorption isotherms of boron containing carbon nanotube (BCNT 1) at various temperatures (77 K, 373 K and 423 K)

Table 6.1 Specific surface area by BET method of various boron containing samples and their hydrogen absorption activity at 1 atm in different temperatures

Sample	SSA (m ² /g)	Hydrogen absorption at 1 atm (cm ³ /g) at various temperatures (K)			
		77	298	373	423
BC	12	3.63	0.6	3.63	4.68
PBC	430	73	-	2.90	3.02
BCNT1	523	127	-	16.5	14.8
BCNT2	62	3.22	-	2.38	4.73
BCNT3	33	1.09	-	1.7	-

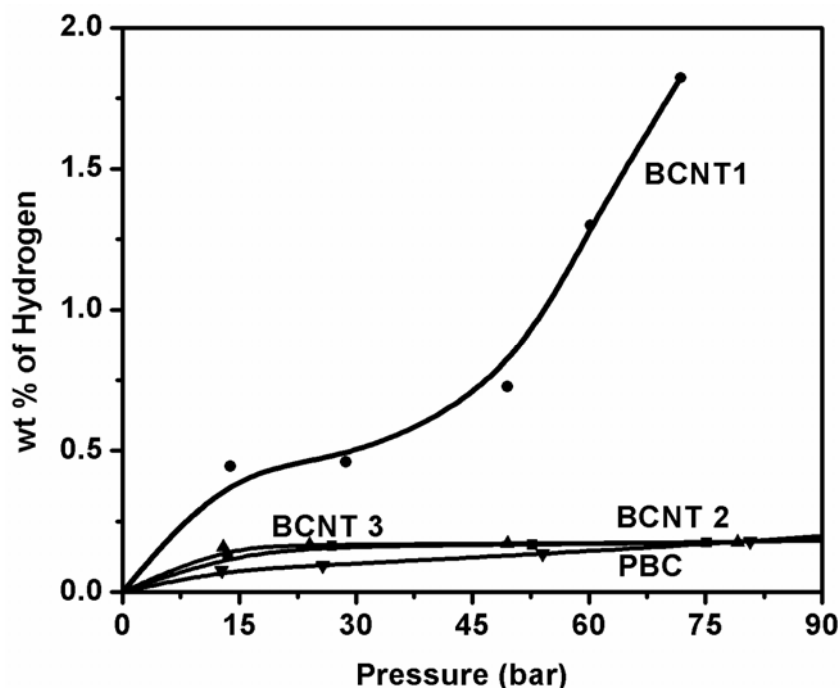


Fig. 6.16 High pressure hydrogen absorption activity of boron containing carbon nanotubes

High pressure hydrogen absorption measurements (Fig. 6.16) show that the hydrogen absorption increases with pressure and a maximum storage capacity of 2 wt % is attained at 80 bar and 300 K.

6.4 CONCLUSIONS

Boron containing carbon nanotubes have been prepared successfully by template synthesis method. An effective and reproducible method of preparing boron containing carbon nanotubes with uniform pore diameter has been demonstrated by using alumina membrane as template. BCNT produced by using polymer as the carbon precursor showed different chemical environments for boron. A maximum of 2 wt % of hydrogen storage capacity has been achieved by the BCNT at 80 bar and 300 K. These studies have a bearing in hydrogen sorption characteristics.

CHAPTER 7

SUMMARY AND CONCLUSIONS

The need for an activator for hydrogenation in carbon materials which should be easily hydridable than carbon and facilitate migration of the dissociated hydrogen to equipotential carbon surface has been realized. While considering these aspects, heteroatoms like N, P, S and B seem to be promising activators due to their properties like higher redox potential than that of carbon and the lower standard free energy of formation of hydrides. The heteroatom substitution results in tuning of the electronic property of the carbon materials. Therefore, the present study is to establish the role of heteroatom in the carbon materials for hydrogen storage by means of theoretical and experimental methodologies.

Theoretical studies have been carried out on the models of carbon nanotubes and fullerene using Density Functional Theory (DFT). The DFT cluster model calculations have been carried out with the geometrical parameters obtained from Force Field (UFF 1.02) optimized clusters. The energy values obtained were analyzed to find out the dissociation energy of hydrogen. From the results it is understood that the substitution of heteroatoms (N, P, S and B) in the carbon nanotubes and fullerene drastically decreases the dissociation energy of hydrogen. Simple cluster model has been constructed to study the reaction pathway of hydrogenation using Transition State Theory. From the transition state calculations, the process of activation and the path of hydrogenation process have been evaluated.

Results show that activation energy of hydrogen interaction which is the first step possess lower activation energy for the heteroatoms substituted carbon nanotubes

compared to pure carbon nanotubes and fullerene. The geometrical positions of boron substitution in carbon nanotubes and fullerene showed difference in the hydrogen activation. Single boron substitution does not activate hydrogen and substitution of two boron atoms is essential and the substitution should be in the alternate positions. The conclusion arising out of the studies is that the B-B bond distance plays a crucial role in the activation of hydrogen by bond stretching which destabilizes the hydrogen.

Theoretical studies have shown that hydrogenation of CNTs requires activation centers and the heteroatom containing CNTs are able to activate hydrogen in a facile manner compared to pure CNTs. For the effective hydrogenation and hydrogen storage these heteroatoms should be incorporated geometrically and chemically into the carbon network.

Experimentally to determine the storage capacity of the carbon materials volumetric low pressure (glass) and high pressure apparatus have been constructed. From the theoretical studies it was found that there should be optimum interaction between incoming hydrogen and the storage medium. Carbon materials should be modified to have appreciable interaction for good storage property. One of the ways of achieving this is to activate hydrogen by metal loading (transition metals). It is believed that supporting Ni on carbon hydrogen can activate. Another method is surface modification by introducing functional groups through chemical treatment.

Various weight percentages of nickel supported on commercial Calgon activated carbon and the chemical treatments like acid and amine treatments employed on commercial CDX-975 activated carbon have been prepared and investigated. But the modifications like metal loading and chemical treatment do not seem to enhance the hydrogen storage capacity. There should be some alternative like incorporation of

heteroatoms (N, P, S and B) in the carbon frame work. Such substitutions in the carbon lattice will act as active centres for hydrogen activation.

Against this background, heteroatom containing carbon nanomaterials were considered as another alternative material for hydrogen storage. Hydrogen absorption activity of nitrogen and boron containing carbon nanomaterials were compared with that of pure carbon nanomaterials. Carbon nanomaterials have been prepared by using various templates such as Zeolite, Clay and Alumina membranes. The prepared carbon nanomaterials have been characterized by XRD, Raman, SEM, TEM, low pressure and high pressure hydrogen absorption measurements.

The variation of template and the carbon precursor cause differences in the morphology and the behavior of the materials towards hydrogen storage application. From the studies, it is shown that heteroatom containing carbon nanomaterials are amenable to hydrogen absorption compared to pure carbon materials. Template aided synthesis of nitrogen containing carbon nanotubes using alumina membrane as the template yielded well-aligned carbon nanotubes and resulted a maximum of 1.2 wt% hydrogen storage capacity where in polypyrrole is used as the carbon precursor. However in the consecutive cycle the value decreased to 0.6 wt% due to reduction of nitrogen concentration. Result from EGA studies reveal the equal amount of ammonia evolution from the nanotubes. Thus the nitrogen atoms in carbon nanotubes act as the active centre and these active sites should be made catalytic in nature by adopting and devising suitable preparation methods. Some sort of surface engineering should be necessary to achieve high hydrogen storage capacity. Nitrogen containing carbon nanomaterials produced by clay as the template showed a maximum of 1.75 wt %. The maximum storage capacity retained even after three cycles. This may be

attributed to the strong binding of nitrogen in the carbon network in the carbon nanotubes prepared from clay as the template using pyridine as the nitrogen containing carbon source.

The synthesis of boron substituted carbon nanotubes has been carried out using hydroborane polymer as carbon source which is formed *in situ* during the polymerisation of divinyl benzene and borane in the pores of alumina membrane. This method seems to be an effective and reproducible method for preparing boron containing carbon nanotubes with uniform pore diameter and was demonstrated by using alumina membrane as template. BCNT produced by using polymer as the carbon precursor showed two different chemical environments for boron. A maximum of 2 wt % of hydrogen storage capacity has been achieved by the BCNT at 80 bar and 300 K, whereas BCNT produced by other method showed multiple environments for boron and exhibited a hydrogen storage capacity of 0.2 wt% only. These results correlate with the theoretical studies, that differences in the chemical environment alter the hydrogen absorption activity.

The significant conclusions arrived at from these studies are

- ❖ DFT studies have shown that there is a decrease in dissociation energy of hydrogen in heteroatom substituted carbon nanotubes and fullerene molecule.
- ❖ The geometrical position of the boron substitution plays a crucial role in hydrogen activation.
- ❖ Significant hydrogen sorption capacity could not be realized for commercial activated carbon and its modification.

- ❖ Nitrogen containing carbon nanotubes prepared by various templates showed increased hydrogen absorption activity compared to that of pure carbon nanotubes. A maximum of 1.75 wt% of hydrogen storage capacity obtained for the carbon nanotubes prepared from clay as the template.
- ❖ Boron containing carbon nanotubes prepared from alumina membrane template showed difference in chemical environment of boron with a maximum storage capacity of 2 wt% at 300 K and 100 bar pressure of hydrogen.
- ❖ Various templates used for preparation of carbon nanotubes and their structural morphology with hydrogen storage capacity are given in Fig. 7.1.

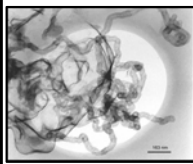
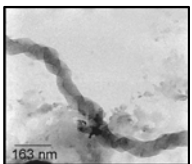
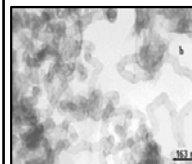
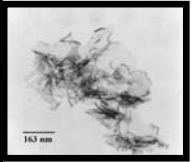
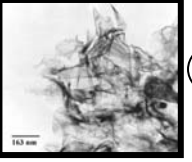
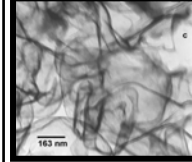
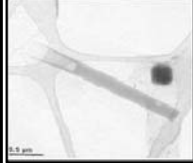
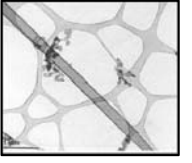
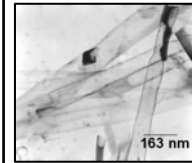
CNT/Zeolite  0.2 Wt %	NCNT/ Zeolite  0.17 (0.72) Wt%	BCNT/ Zeolite  0.18 Wt%
CNT/ Clay  0.48 Wt %	NCNT/ Clay  1.75 Wt %	BCNT/ Clay  0.2 Wt %
CNT/ Membrane  0.61 Wt%	NCNT/ Membrane  1.2 (0.6) Wt %	BCNT/ Membrane  2.03 Wt %

Fig. 7.1 Comparison of hydrogen storage capacity and their morphology variation due to templates used in preparation of carbon nanotubes

SUGGESTIONS FOR FUTURE STUDIES

The studies that can be pursued are:

1. Synthesis and hydrogen absorption activity of other heteroatoms and various combinations of heteroatoms substituted carbon nanotubes.
2. The change in structural features of carbon nanotubes during absorption and desorption process.
3. Heteroatom containing polymer precursor can be logically varied further and carbon structures with specific morphology and composition can be obtained and such materials can be evaluated for hydrogen sorption.

REFERENCES

1. **Aceves, S. M., J. Martinez-Frias and O. Garcia-Villazana** (2000) "Analytical and experimental evaluation of insulated pressure vessels for cryogenic hydrogen storage". *International Journal of Hydrogen Energy*, **25**, 1075-1085.
2. **Ahn, C.C., Y. Ye, B.V. Ratnakumar, C. Witham, R.C. Bowman and B. Fultz** (1998) "Hydrogen desorption and adsorption measurements on graphite nanofibers". *Applied Physics Letters*, **73**, 3378-3380.
3. **Andreoni W., F. Gygi and M. Parrinello** (1992) "Impurity states in doped fullerenes: C₅₉B and C₅₉N". *Chemical Physics Letter*, **190**, 159-162.
4. **Arellano, J.S., L.M. Molina, A. Rubio, M.J. Lopez and J.A. Alonso** (2002) "Interaction of molecular and atomic hydrogen with (5,5) and (6,6) single-wall carbon nanotubes". *Journal of Chemical Physics*, **117**, 2281- 2288.
5. **Attalla, I., M. Vassallo, N. Tattam and V. Hanna**, (1993) "Preparation of hydrofullerenes by hydrogen radical induced hydrogenation". *Journal of Physical Chemistry*, **97**, 6329 - 6331.
6. **Avent, A.G., A. D. Darwish, D.K. Heimbach, H.W. Kroto, M.F. Meidine, J.P. Parsons, C. Remars, R. Roers, O. Ohashi, R. Taylor and D.R.M. Walton** (1994) "Formation of hydrides of fullerene-C₆₀ and fullerene-C₇₀". *Journal of the Chemical Society, Perkin Transactions 2*, 15-22.
7. **Badzian, A., T. Badzian, E. Breval, and A. Piotrowski** (2001) "Nanostructured, nitrogen-doped carbon materials for hydrogen storage". *Thin Solid Films*, **398**, 170-174.
8. **Bai, X. D., D.Y. Zhong, G.Y. Zhang, X.C. Ma, S. Liu, E.G. Wang, Y. Chen and D.T. Shaw** (2001) "Hydrogen storage in carbon nitride nanobells". *Applied Physics Letters*, **79**, 1552-1554.
9. **Banks, R., J. Dale, I. Gosney, G. Hodgson, K. Jennings, C. Jones, J. Lecoultre, R. Langridge, P. Maier, H. Scrivens, C. Smith, J. Smyth, T. Taylor, P. Thorburn and S.Webster** (1993) "Birch reduction of C₆₀ - a new appraisal". *Chemical Communications*, 1149 - 1152.
10. **Bauschlicher C.W.Jr and R.So. Christopher Rso** (2002) "High coverage of hydrogen on (10,0) (9,0) and (5,5) carbon nanotubes". *Nano Letters*, **2**, 337-341.
11. **Becke A.D** (1993) "Density-functional thermochemistry. III. The role of exact exchange". *Journal of Chemical Physics*, **98**, 5648-5652.
12. **Becke, A.D** (1988) "A multicenter numerical integration scheme for polyatomic molecules. *The Journal of Chemical Physics*, **88**, 2547-2553.
13. **Benemann, J.R and N.M. Weare** (1974) "Hydrogen evolution by nitrogen-fixing *Anabaena cylindrica* cultures". *Science*, **184**, 174-175.

14. **Bentzen, J. J., A.S. Pedersen and J. Kjoller** (2001) "Screening of hydrogen storage media applying high pressure thermogravimetry". *Journal of Thermal Analysis and Calorimetry*, **64**, 859-866.
15. **Berry G.D and S.M. Aceves**, (1998) "Onboard storage alternatives for hydrogen vehicles". *Energy Fuels*, **12**, 49-55.
16. **Bluhm, M.E., M.G. Bradley, R. Butterick III, U. Kusari and L.G. Sneddon** (2006) "Amineborane based chemical hydrogen storage: enhanced ammonia borane dehydrogenation in ionic liquids". *Journal of American Chemical Society*, **128**, 7748-7749.
17. **Bogdanovic, B and M. Schwickardi** (1997) "Ti-doped alkali metal aluminium hydrides as potential novel reversible hydrogen storage materials". *Journal of Alloys and Compounds*, **253**, 1-9.
18. **Borowiak-Palen, E., T. Pichler, G.G. Fuentes, A. Graff, R.J. Kalenczuk, M. Knupfer and J. Fink** (2003) "Efficient production of B-substituted single-wall carbon nanotubes". *Chemical Physics Letters*, **378**, 516-520.
19. **Browning, D. J., M.I. Gerrard, J.B. Lakeman, I.M. Mellor, R. Mortimer and M.C. Turpin** (2002) "Studies into the storage of hydrogen in carbon nanofibers: Proposal of a possible reaction mechanism". *Nano Letters*, **2**, 201-205.
20. **Burghard, M., G. Duesberg, G. Philipp, J. Muster and S. Roth** (1998) "Controlled Adsorption of Carbon Nanotubes on Chemically Modified Electrode Arrays". *Advanced Materials*, **10**, 584-588.
21. **Cao, A. Y., H.W. Zhu, X.F. Zhang, X.S. Li, D.B. Ruan, C.L. Xu, B.Q. Wei, J. Liang and D.H. Wu** (2001) "Hydrogen storage of dense-aligned carbon nanotubes". *Chemical Physics Letters*, **342**, 510-514.
22. **Carl-Jochen, W** (2005) "Into the hydrogen energy economy—milestones". *International Journal of Hydrogen Energy*, **30**, 681-685.
23. **Carroll, D.L., Ph. Redlich, X. Blase, J-C. Chalker, S. Curran, P.M. Ajayan, S. Roth and M. Rühle** (1998) "Effects of nanodomain formation on the electronic structure of doped carbon nanotubes". *Physical Review Letters*, **81**, 2332 - 2335.
24. **Cermignani, W., T.E. Paulson, C. Onneby and C.G. Pantano** (1995) "Synthesis and characterization of boron-doped carbons". *Carbon*, **33**, 367-374.
25. **Chahine, R and T.K. Bose** (1994) "Low-pressure adsorption storage of hydrogen". *International Journal of Hydrogen Energy*, **19**, 161-164.
26. **Chakrabarti, S and B.K. Dutta** (2004) "Photocatalytic degradation of model textile dyes in wastewater using ZnO as semiconductor catalyst". *Journal of Hazardous Materials*, **112**, 269-278.

27. **Challet, S., P. Azais, R.J.M. Pellenq, O. Isnard, J.L. Soubeyroux and L. Duclaux** (2004) "Hydrogen adsorption in microporous alkali-doped carbons (activated carbon and single wall nanotubes)". *Journal of Physics and Chemistry of Solids*, **65**, 541-544.
28. **Chambers, A., C. Park, R.T.K. Baker and N.M. Rodriguez** (1998) "Hydrogen storage in graphite nanofibers". *Journal of Physical Chemistry B*, **102**, 4253-4256.
29. **Chan, S.P., G. Chen, X.G. Gong and F.L. Liu** (2001) "Chemisorption of hydrogen molecules on carbon nanotubes under high pressure". *Physical Review Letters*, **87**, 205502-1-4.
30. **Che, G. L., B.B. Lakshmi, C.R. Martin and E.R. Fisher** (1999) "Metal-Nanocluster-Filled Carbon Nanotubes: Catalytic Properties and Possible Applications in Electrochemical Energy Storage and Production". *Langmuir*, **15**, 750-758.
31. **Che, G. L., B.B. Lakshmi, E.R. Fisher and C.R. Martin** (1998) "Carbon nanotubule membranes for electrochemical energy storage and production". *Nature*, **393**, 346-349.
32. **Che, G. L., B.B. Lakshmi, E.R. Fisher C.R. Martin, and R.A. Ruoff** (1998) "Chemical Vapor Deposition Based Synthesis of Carbon Nanotubes and Nanofibers Using a Template Method". *Chemistry of Materials*, **10**, 260-267.
33. **Chen, P., X. Wu, J. Lin and K.L. Tan** (1999) "High hydrogen uptake by alkali-doped carbon nanotubes under ambient pressure and moderate temperatures". *Science*, **285**, 91-93.
34. **Chen, S.,W. Shen, G. Wu, D. Chen and M. Jiang,** (2005) "A new approach to the functionalization of single-walled carbon nanotubes with both alkyl and carboxyl groups". *Chemical Physics Letters*, **402**, 312-317.
35. **Chen, Y., D.T. Shaw, X.D. Bai, E.G. Wang, C. Lund, W.M. Lu and D.D.L. Chung** (2001) "Hydrogen storage in aligned carbon nanotubes". *Applied Physics Letters*, **78**, 2128-2130.
36. **Cheng, H.M., C. Liu, Y.Y. Fan, F. Li, G. Su and H.T. Cong, L.L. He and M. Liu** (2000) "Synthesis and hydrogen storage of carbon nanofibers and single-walled carbon nanotubes". *Zeitschrift fur Metallkunde*, **91**, 306-310.
37. **Cheng, H.M., F. Li, G. Su, H.Y. Pan, L.L. He, X. Sun and M.S. Dresselhaus** (1998) "Large-scale and low-cost synthesis of singlewalled carbon nanotubes by catalytic pyrolysis of hydrocarbons". *Applied Physics Letters*, **72**, 3282-3284.
38. **Christmann, K** (1981) "Hydrogen Adsorption on Metal Surfaces". In: *Atomistics of Fracture Conference Proceedings*, Eds. Latanision and Pickensr, Plenum, NY, USA.

39. **Chuang, K., N. Cui and J. Luo** (2001) "Study of Hydrogen Diffusion in α - and β -phase Hydrides of Mg_2Ni Alloy by Microelectrode Technique". *Journal of Electroanalytical Chemistry*, **503**, 92-98.
40. **Ci, L., S. Xie, D. Tang, X. Yan, Y. Li, Z. Liu, X. Zou, W. Zhou and G. Wang** (2001) "Controllable growth of single wall carbon nanotubes by pyrolyzing acetylene on the floating iron catalysts". *Chemical Physics Letters*, **349**, 191-195.
41. **Ci, L.J., H.W. Zhu, B.Q. Wei, C.L. Xu and D.H. Wu** (2003) "Annealing amorphous carbon nanotubes for their application in hydrogen storage". *Applied Surface Science*, **205**, 39-43.
42. **Colomer, J.F., G. Bister, I. Willems, Z. Konya, A. Fonseca, G. Van Tendeloo and J.B. Nagy** (1999) "Synthesis of single-walled carbon nanotubes by catalytic decomposition of hydrocarbons". *Chemical Communications*, 1343-1344.
43. **Czerw, R., M. Terrones, J.C. Charlier, X. Blase, B. Foley, R. Kamalakaran, N. Grobert, H. Terrones, D. Tekleab, P.M. Ajayan, W. Blau, M. Ruhle and D.L. Carroll** (2001) "Identification of Electron Donor States in N-Doped Carbon Nanotubes". *Nano Letters*, **1**, 457-460.
44. **Darkrim, F.L., P. Malbrunot and G.P. Tartaglia** (2002) "Review of hydrogen storage by adsorption in carbon nanotubes". *International Journal of Hydrogen Energy*, **27**, 193-202.
45. **Das, D and T.N. Veziroglu** (2001) "Hydrogen Production by Biological Processes: A Survey of Literature". *International Journal of Hydrogen Energy*, **26**, 13-28.
46. **de la Casa-Lillo, M.A., F. Lamari-Darkrim, D. Cazorla-Amoros and A. Linares-Solano** (2002) "Hydrogen storage in activated carbons and activated carbon fibers". *Journal of Physical Chemistry B*, **106**, 10930-10934.
47. **Dennington II, R., T. Keith, J. Millam, K. Eppinnett, W.L. Hovell, and R. Gilliland** GaussView, Version 3.09, *Semichem, Inc.*, Shawnee Mission, KS, 2003.
48. **Dillon, A.C and M.J. Heben** (2001) "Hydrogen storage using carbon adsorbents: past, present and future". *Applied Physics A-Materials Science & Processing*, **72**, 133-142.
49. **Dillon, A.C., K.M. Jones, T.A. Bekkedahl, C.H. Kiang, D.S. Bethune and M.J. Heben** (1997) "Storage of hydrogen in single-walled carbon nanotubes". *Nature*, **386**, 377-379.
50. **Dodziuk, H and G. Dolgonos** (2002) "Molecular modeling study of hydrogen storage in carbon nanotubes". *Chemical Physics Letters*, **356**, 79-83.

51. **Dunn, S** (2002) "Hydrogen futures: toward a sustainable energy system". *International Journal of Hydrogen Energy*, **27**, 235-264.
52. **Dutta, S** (1990) "Technology Assessment of Advanced Electrolytic Hydrogen Production". *International Journal of Hydrogen Energy*, **15**, 379–386.
53. **Ernst S., M. Fritz and J. Weitkamp** (1995) "Zeolites as Media for Hydrogen Storage". *International Journal of Hydrogen Energy*, **20**, 967-970.
54. **Fan, S.S., M.G. Chapline, N.R. Franklin, T.W. Tomblor, A.M. Cassell and H.J. Dai** (1999) "Self-oriented regular arrays of carbon nanotubes and their field emission properties". *Science*, **283**, 512-514.
55. **Fan, Y.Y., B. Liao, M. Liu, Y.L. Wei, M.Q. Lu and H.M. Cheng** (1999) "Hydrogen uptake in vapor-grown carbon nanofibers". *Carbon*, **37**, 1649-1652.
56. **Ferey, G., M. Latroche, C. Serre, F. Millange, T. Loiseau and A. Percheron-Guegan** (2003) "Hydrogen adsorption in the nanoporous metal-benzenedicarboxylate $M(OH)(O_2C-C_6H_4-CO_2)$ ($M = Al^{3+}, Cr^{3+}$), MIL-53". *Chemical Communications*, 2976-2977.
57. **Figueras, F** (1988) "Pillared clays as catalysts". *Catalysis Reviews: Science and Engineering*, **30**, 457–99.
58. **Foresman, J.B and Frish, A** (1996) "Exploring Chemistry with Electronic Structure Methods". 2nd Edition, Gaussian Inc., Pittsburgh, USA.
59. **Foss, C.A., Jr. Gabor, I. Hornyak, J.A. Stockert and C.R. Martin** (1994) "Template-Synthesized Nanoscopic Gold Particles: Optical Spectra and the Effects of Particle Size and Shape". *Journal of Physical Chemistry B* , **98**, 2963- 2971.
60. **Fraenkel, D and J. Shabtai** (1977) "Encapsulation of hydrogen in molecular sieve zeolites". *Journal of American Chemical Society*, **99**, 7074 – 7076.
61. **Frisch M. J., G.W.Trucks, H.B. Schlegel, G.E. Scuseria, M.A. Robb, J.R. Cheeseman, V.G. Zakrzewski, J.A. Montgomery, R.E. Stratmann, J.C. Burant, S. Dapprich, J.M. Millam, A.D. Daniels, K.N. Kudin, M.C. Strain, O. Frakas, J. Tomasi, V. Barone, M. Cossi, R. Cammi, B. Mennucci, C. Pomelli, C. Adamo, S. Clifford, J. Ochterski, G.A. Petersson, P.Y. Ayala, Q. Cui, K. Morokuma, D.K. Malick, A.D. Rabuck, K. Raghavachari, J.B. Foresman, J. Cioslowski, J.V. Ortiz, B.B. Stefanov, G. Liu, A. Liashenko, P. Piskorz, L. Komaromi, R. Gomperts, R.L. Martin, D.J. Fox, T. Keith, M.A. Al-laham, C.Y. Peng, A. Nanayakkara, C. Gonzalez, M. Challacombe, P.M.W. Gill, B.G. Johnson, W. Chen, M.W. Wong, J.L. Andres, M. Head-Gordon, E.S. Replogle and J.A. Pople.** (1998) *Gaussian98*, revision A.9: Gaussian Inc.: Pittsburgh, PA.
62. **Frisch, M.J., G.W. Trucks, H.B. Schlegel, G.E. Scuseria, M.A. Robb, J.R. Cheeseman, J.A. Montgomery, Jr., T. Vreven, K.N. Kudin, J.C. Burant, J.M. Millam, S.S. Iyengar, J. Tomasi, V. Barone, B. Mennucci, M. Cossi, G.**

- Scalmani, N. Rega, G. A. Petersson, H. Nakatsuji, M. Hada, M. Ehara, K. Toyota, R. Fukuda, J. Hasegawa, M. Ishida, T. Nakajima, Y. Honda, O. Kitao, H. Nakai, M. Klene, X. Li, J.E. Knox, H.P. Hratchian, J.B. Cross, V. Bakken, C. Adamo, J. Jaramillo, R. Gomperts, R.E. Stratmann, O. Yazyev, A.J. Austin, R. Cammi, C. Pomelli, J.W. Ochterski, P.Y. Ayala, K. Morokuma, G.A. Voth, P. Salvador, J.J. Dannenberg, V.G. Zakrzewski, S. Dapprich, A.D. Daniels, M.C. Strain, O. Farkas, D.K. Malick, A.D. Rabuck, K. Raghavachari, J.B. Foresman, J.V. Ortiz, Q. Cui, A.G. Baboul, S. Clifford, J. Cioslowski, B.B. Stefanov, G. Liu, A. Liashenko, P. Piskorz, I. Komaromi, R.L. Martin, D.J. Fox, T. Keith, M.A. Al-Laham, C.Y. Peng, A. Nanayakkara, M. Challacombe, P.M. W. Gill, B. Johnson, W. Chen, M.W. Wong, C. Gonzalez and J.A. Pople (2004) *Gaussian 03*, Revision C.02, Gaussian, Inc., Wallingford CT.
63. **Froudakis, G.E** (2001) “Hydrogen interaction with single walled carbon nanotubes: A combined quantum mechanical / molecular mechanics study”. *Nano Letters*, **1**, 179-182.
 64. **Froudakis, G.E** (2002) “Hydrogen interaction with carbon nanotubes: a review of ab initio studies”. *Journal of Physics-Condensed Matter*, **14**, R453-R465.
 65. **Fumiaki, T., J.D. Chang, N. Mizukami, S.T. Tatsuo and H. Katsushige** (1993) “Isolation of a hydrogen-producing bacterium *Clostridium beijerinckii* strain AM21B from termites”. *Canadian Journal of Microbiology*, **39**, 726–730.
 66. **Fumiaki, T., J.D. Chang, N. Mizukami, S.T. Tatsuo and H. Katsushige** (1996) “Continuous hydrogen production by *Clostridium* sp. Strain No. 2 from cellulose hydrolysate in an aqueous two-phase system”. *Journal of Fermentation and Bioengineering*, **82**, 80–83.
 67. **Gadd, G.E., M. Blackford, S. Moricca, N. Webb, P.J. Evans, A.N. Smith, G. Jacobsen, S. Leung, A. Day and Q. Hua** (1997) “The world's smallest gas cylinders?”. *Science*, **277**, 933-936.
 68. **Gaffron, H and J. Rubin** (1942) “Fermentative and photochemical production of hydrogen in algae”. *Journal of General Physiology*, **26**, 219-240.
 69. **Glerup, M., J. Steinmetz, D. Samaille, O. Stéphan, S. Enouz, A. Loiseau, S. Roth and P. Bernier** (2004) “Synthesis of N-doped SWNT using the arc-discharge procedure”. *Chemical Physics Letters*, **387**, 193-197.
 70. **Golberg, D., Y. Bando, W. Han, K. Kurashima and T. Sato** (1999) “Single-walled B-doped carbon, B/N-doped carbon and BN nanotubes synthesized from single-walled carbon nanotubes through a substitution reaction”. *Chemical Physics Letters*, **308**, 337–342.
 71. **Gordon, P.A and P.B Saeger** (1999) “Molecular modeling of adsorptive energy storage: Hydrogen storage in single-walled carbon nanotubes”. *Industrial & Engineering Chemistry Research*, **38**, 4647-4655.

72. **Greenwood, N.N** and **A. Earnshaw** (1997) "Chemistry of the Elements". Oxford; Boston, Butterworth-Heinemann.
73. **Grochala, W** and **P.P. Edwards** (2004) "Thermal Decomposition of the Non-Interstitial Hydrides for the Storage and Production of Hydrogen". *Chemical Reviews*, **104**, 1283- 316.
74. **Gross, K.J., G.J. Thomas** and **C.M. Jensen** (2002) "Catalyzed alanates for hydrogen storage". *Journal of Alloys and Compounds*, **330**, 683-690.
75. **Gururnathan, K** (2004) "Photocatalytic hydrogen production using transition metal ions-doped γ -Bi₂O₃ semiconductor particles". *International Journal of Hydrogen Energy*, **29**, 933 – 940.
76. **Hall, L.E., D.R. McKenzie, M.I. Attalla, A.M. Vassallo, R.L. Davis, J.B. Dunlop** and **D.J.H. Cockayne** (1993) "The structure of hydrogenated fullerene (C₆₀H₃₆)". *Journal of Physical Chemistry*, **97**, 5741 – 5744.
77. **Halls, M.D** and **H.B. Schlegel** (2002) "Chemistry Inside Carbon Nanotubes: the Menshutkin S_N2 Reaction". *Journal of Physical Chemistry B*, **106**, 1921 -1925.
78. **Hamada, N., S. Sawada,** and **A. Oshiyama** (1992) "New one-dimensional conductors: Graphitic microtubules". *Physics Review Letters*, **68**, 1579-1581.
79. **Han, M.G** and **S.S. Im** (1998) "Processable conductive blends of polyaniline/polyimide". *Journal of Applied Polymer Science*, **67**, 1863 – 1870.
80. **Han, W., Y. Bando, K. Kurashima** and **T. Sato** (1998) "Synthesis of boron nitride nanotubes from carbon nanotubes by a substitution reaction". *Applied Physics Letters*, **73**, 3085-3087.
81. **Han, W., Y. Bando, K. Kurashima** and **T. Sato** (1999) "Boron-doped carbon nanotubes prepared through a substitution reaction". *Chemical Physics Letters*, **299**, 368–373.
82. **Hancock, Jr.O.G** (1984) "A Photovoltaic-Powered Water Electrolyzer: Its Performance and Economics". *HYDROGEN ENERGY PROGRESS V (New York: Pergamon Press, 1984)*, 335–344.
83. **Haufler, R.E., J. Conceicao, L.P.F. Chibante, Y. Chai, N.E. Byrne, S. Flanagan, M.M. Haley, S.C. O'Brien, C. Pan, and. C. Pan, Z. Xiao, W.E. Billups, M.A. Ciufolini, R.H. Hauge, J.L. Margrave, L.J. Wilson, R.F. Curl** and **R.E. Smalley** (1990) "Efficient production of C₆₀ (buckminsterfullerene), C₆₀H₃₆, and the solvated buckide ion". *Journal of Physical Chemistry*, **94**, 8634 - 8636
84. **Henderson, C.C** and **P.A. Cahill** (1992) "Semi-empirical calculations of the isomeric C₆₀ dihydrides". *Chemical Physics Letters*, **198**, 570-576.
85. **Henderson, C** and **P.Cahill** (1992) "Semi-empirical calculations of the isomeric C₆₀ dihydrides". *Chemical Physics Letters*, **198**, 570-576.

86. **Hirscher, M., M. Becher, M. Haluska, A. Quintel, V. Skakalova, Y.M. Choi, U. Dettlaff-Weglikowska, S. Roth, I. Stepanek, P. Bernier, A. Leonhardt and J. Fink** (2002) "Hydrogen storage in carbon nanostructures". *Journal of Alloys and Compounds*, **330**, 654-658.
87. **Hirscher, M., M. Becher, M. Haluska, U. Dettlaff-Weglikowska, A. Quintel, G. S. Duesberg, Y. M. Choi, P. Downes, M. Hulman, S. Roth, I. Stepanek and P. Bernier** (2001) "Hydrogen storage in sonicated carbon materials". *Applied Physics A-Materials Science & Processing*, **72**, 129-132.
88. **Hodoshima, S., H. Arai and Y. Saito** (2003) "Liquid-film-type catalytic decalin dehydrogenation-aromatization for long-term storage and long-distance transportation of hydrogen". *International Journal of Hydrogen Energy*, **28**, 197 - 204.
89. **Hohenberg, P and W. Kohn** (1964) "Inhomogeneous electron gas". *Physical Review B*, **136**, B864-B871.
90. **Hwang, J.Y., S.H. Lee, K.S. Sim, and J.W. Kim** (2002) "Synthesis and hydrogen storage of carbon nanofibers". *Synthetic Metals*, **126**, 81-85.
91. **Hynek, S., W.J. Fuller and J. Bentley** (1997) "Hydrogen storage by carbon sorption". *International Journal of Hydrogen Energy*, **22**, 601-610.
92. **Iijima, S** (1991) "Helical microtubules of graphitic carbon". *Nature*, **354**, 56-58.
93. **Jacques, S., A. Guette, X. Bourrat, F. Langlais, C. Guimon and C. Labrugère** (1996) "LPCVD and characterization of boron-containing pyrocarbon materials". *Carbon*, **34**, 1135-44.
94. **Jang, J and J.H. Oh**, (2004) "A facile synthesis of polypyrrole nanotubes using a template-mediated vapor deposition polymerization and the conversion to carbon nanotubes". *Chemical Communications*, 882-883.
95. **Jang, J W., C.E. Lee, S.C. Lyu, T.J. Lee and C.J. Lee** (2004) "Structural study of nitrogen -doping effects in bamboo-shaped multiwalled carbon nanotubes". *Applied Physics Letters*, **84**, 2877-2879.
96. **Jang, J. W., D. K. Lee, C. E. Lee, T. J. Lee, C. J. Lee and S. J. Noh** (2002) "Metallic conductivity in bamboo-shaped multiwalled carbon nanotubes". *Solid State Communications*, **122**, 619-622
97. **Jin, C., R. Hettich, R. Compton, D. Joyce, J. Blencoe, and T. Burch** (1994) "Direct Solid-Phase Hydrogenation of Fullerenes". *Journal of Physical Chemistry*, **98**, 4215 - 4217.
98. **Kamat, P.V** (1993) "Photochemistry on Nonreactive and Reactive (Semiconductor) Surfaces". *Chemical Reviews*, **93**, 207-300.
99. **Kato, H and A. Kudo** (1998) "New tantalate photocatalysts for water decomposition into H₂ and O₂". *Chemical Physics Letters*, **295**, 487-492.

100. **Khare, B.N., M. Meyyappan, Alan M. Cassell, Cattien V. Nguyen and J. Han** (2002) "Functionalization of Carbon Nanotubes Using Atomic Hydrogen from a Glow Discharge". *Nano Letters*, **2**, 73 – 77.
101. **Kim, K., H. Lee, K. Han, J. Kim, M. Song, M. Park, J. Lee and J. Kang** (2005) "Hydrogen Storage in Ni Nanoparticle-Dispersed Multiwalled Carbon Nanotubes". *Journal of Physical Chemistry B*, **109**, 8983 -8986.
102. **Kiyobayashi, T., H.T. Takeshita, H. Tanaka, N. Takeichi, A. Zuttel, L. Schlappbach and N. Kuriyama**, (2002) "Hydrogen adsorption in carbonaceous materials – how to determine the storage capacity accurately". *Journal of Alloys and Compounds*, **330**, 666–669.
103. **Kroto, H. W., J.R. Heath, S.C. O'Brien, R. F. Curl and R.E. Smalley** (1985) "C₆₀: Buckminsterfullerene". *Nature*, **318**, 162-163.
104. **Kumar, N and D. Das** (2000) "Enhancement of hydrogen production by *Enterobacter cloacae* IIT-BT08". *Process Biochemistry*, **35**, 589–593.
105. **Kurita N., K. Kobayashi, H. Kumahora, K. Tago and K. Ozawa** (1992) "Molecular structures, binding energies and electronic properties of dopyballs C₅₉X (X=B, N and S)". *Chemical physics Letter*, **198**, 95-99.
106. **Kyotani, T., L.F. Tsai and A. Tomita** (1996) "Preparation of Ultrafine Carbon Tubes in Nanochannels of an Anodic Aluminum Oxide Film". *Chemistry of Materials*, **8**, 2109-2113.
107. **Langmi, H.W., A. Walton, M.M. Al-Mamouri, S.R. Johnson, D. Book, J.D. Speight, P.P. Edwards, I. Gameson, P.A. Anderson and I.R. Harris** (2003) "Hydrogen adsorption in zeolites A, X, Y and RHO". *Journal of Alloys and Compounds*, **356**, 710-715.
108. **Langreth, D.C and S.H. Vosko** (1987) "Exact electron-gas response functions at high density". *Physical Review Letters*, **59**, 497-500.
109. **Lee, C., W. Yang and R.G. Parr** (1998) "Development of the Colle-Salvetti correlation-energy formula into a functional of the electron density". *Physical Review B*, **37**, 785-789.
110. **Lee, C., W. Yang and W.G. Parr** (1988) "Development of the Colle-Salvetti correlation –energy formula into a functional of the electron density". *Physical review B*, **37**, 785-789.
111. **Lee, S. M., K.H. An, W.S. Kim, Y.H. Lee, Y.S. Park, G. Seifert and T. Frauenheim** (2001) "Hydrogen storage in carbon nanotubes". *Synthetic Metals*, **121**, 1189-1190.
112. **Lee, S. M., K.H. An, Y.H. Lee, G. Seifert and T. Frauenheim** (2001) "A hydrogen storage mechanism in single-walled carbon nanotubes". *Journal of American Chemical Society*, **123**, 5059-5063.

113. **Lee, S.M** and **Y.H. Lee** (2000) “Hydrogen storage in single-walled carbon nanotubes”. *Applied Physics Letters*, **76**, 2877-2879.
114. **Levesque, D., A. Gicquel, F.L. Darkrim** and **S.B. Kayiran** (2002) “Monte Carlo simulations of hydrogen storage in carbon nanotubes”. *Journal of Physics-Condensed Matter*, **14**, 9285-9293.
115. **Li, X.S., H.W. Zhu, L.J. Ci, C.L. Xu, Z.Q. Mao, B.Q. Wei, J. Liang** and **D.H. Wu** (2001) “Hydrogen uptake by graphitized multi-walled carbon nanotubes under moderate pressure and at room temperature”. *Carbon*, **39**, 2077-2079.
116. **Licht, S., B. Wang, S. Mukerji, T. Soga, M. Umeno** and **H. Tributsch** (2001) “Over 18% solar energy conversion to generation of hydrogen fuel; theory and experiment for efficient solar water splitting”. *International Journal of Hydrogen Energy*, **26**, 653-659.
117. **Litter, M.I** (1999) “Heterogeneous photocatalysis transition metal ions in photocatalytic systems”. *Applied Catalysis B: Environmental*, **23**, 89–114.
118. **Liu, C., Y.Y. Fan, M. Liu, H.T. Cong, H.M. Cheng** and **M.S. Dresselhaus** (1999) “Hydrogen storage in single-walled carbon nanotubes at room temperature”. *Science*, **286**, 1127-1129.
119. **Liu, H., S. Grot** and **B.E. Logan** (2005) “Electrochemically assisted microbial production of hydrogen from acetate”. *Environmental Science and Technology*, **39**, 4317–4320.
120. **Liu, J., S. Webster,** and **D.L. Carroll** (2006) “Highly aligned helical nitrogen doped carbon nanotubes synthesized by injection assisted chemical vapor deposition”. *Applied Physics Letters*, **88**, 213119 - 2132121
121. **Loutfy, R.O.** and **E.M. Wexler** (2001) “Investigation of Hydrogen Storage in Fullerene Hydrides”. In *Metal Hydrides and Carbon for Hydrogen Storage* (Final Report for IEA Task 12) <http://www.eren.doe.gov/hydrogen/iea>.
122. **Lueking, A** and **R.T. Yang** (2002) “Hydrogen spillover from a metal oxide catalyst onto carbon nanotubes - Implications for hydrogen storage”. *Journal of Catalysis*, **206**, 165-168.
123. **Lueking, A** and **R.T. Yang** (2003) “Hydrogen storage in carbon nanotubes: residual metal content and pretreatment temperature”. *AIChE* **49**, 1556–1568.
124. **Lueking, A.D., R.T. Yang, N.M. Rodriguez** and **R.T.K. Baker** (2004) “Hydrogen storage in graphite nanofibers: Effect of synthesis catalyst and pretreatment conditions”. *Langmuir*, **20**, 714-721.
125. **Lyu, S.C., B.C. Liu, T.J. Lee, Z.Y. Liu, C.W. Yang, C.Y. Park** and **C.J. Lee** (2003) “Synthesis of high-quality single-walled carbon nanotubes by catalytic decomposition of C₂H₂”. *Chemical Communications*, 734-735.

126. **Ma, Y. C., Xia, Y. Y., Zhao, M. W., Ying, M. J.** (2002) Hydrogen storage capacity in single-walled carbon nanotubes. *Physical Review B*, 65, art. no.-155430.
127. **Maria, G., A. Marin, C. Wyss, S. Muller and E. Newson** (1996) “Modeling and scaleup of the kinetics with deactivation of methylcyclohexane dehydrogenation for hydrogen energy storage”. *Chemical Engineering Science*, **51**, 2891–2896.
128. **Martin, C.R** (1994) “Nanomaterials: A membrane-based synthetic approach”. *Science*, **266**, 1961-1966.
129. **Matsumi, N., K. Naka and Y. Chujo** (1998) “Extension of Π -Conjugation Length via the Vacant p-Orbital of the Boron Atom. Synthesis of Novel Electron Deficient Π -Conjugated Systems by Hydroboration Polymerization and Their Blue Light Emission”. *Journal of American Chemical Society*, **120**, 5112 – 5113.
130. **Matsumi, N., T. Umeyama and Y. Chujo** (2000) “Novel Π -conjugated organoboron polymers: Poly (ethynylene-phenylene-ethynylene-borane)s”. *Polymer Bulletin*, **44**, 431–436.
131. **McEnaney, B.** (2002) Properties of activated carbons. In Schüth, F., Sing, K. S. W., Weitkamp, J. (Eds.) *Handbook of porous solids*. Weinheim, Wiley-VCH.
132. **McGuire, K., N. Gothard, P.L. Gai, M.S. Dresselhaus, G. Sumanasekera and A.M. Rao** (2005) “Synthesis and Raman characterization of boron-doped single-walled carbon nanotubes”. *Carbon*, **43**, 219-227.
133. **Meier, S., S. Corbin, K. Vance, M. Clayton, and M. Mollman** (1994) “Synthesis of hydrogenated fullerenes by zinc/acid reduction”. *Tetrahedron Letters*, **35**, 5789-5792.
134. **Meregalli, V and M. Parrinello** (2001) “Review of theoretical calculations of hydrogen storage in carbon-based materials”. *Applied Physics A-Materials Science & Processing*, **72**, 143-146.
135. **Nath, M., B.C. Satishkumar, A. Govindaraj, C.P. Vinod and C.N.R. Rao** (2000) “Production of bundles of aligned carbon and carbon nitrogen nanotubes by the pyrolysis of precursors on silicasurported iron and cobalt catalyst”. *Chemical Physics Letters*, **322**, 333 -340.
136. **Nijkamp, M.G., J.E.M.J. Raaymakers, A.J. van Dillen and K.P. de Jong** (2001) “Hydrogen storage using physisorption – materials demands”. *Applied Physics A-Materials Science & Processing*, **72**, 619–623.
137. **Nutzenadel, C., A. Zuttel, D. Chartouni and L. Schlapbach** (1999) “Electrochemical Storage of Hydrogen in Nanotube Materials”. *Electrochemical Solid-State Letters*, **2**, 30-32.

138. **Okpalugo, T.I.T., P. Papakonstantinou, H. Murphy, J. McLaughlin and N.M.D. Brown** (2005) “High resolution XPS characterization of chemical functionalized MWCNTs and SWCNTs”. *Carbon*, **43**, 153–161.
139. **Orimo, S., Matsushima, T., Fujii, H., Fukunaga, T., Majer, G.** (2001) “Hydrogen desorption property of mechanically prepared nanostructured graphite”. *Journal of Applied Physics*, **90**, 1545-1549.
140. **Ottaviani, B., A. Derre, E. Grivei, Q.A.M. Mahmoud, M. Guimon, S. Flandrois and P. Delhaes** (1998) “Boronated carbons: structural characterization and low temperature physical properties of disordered solids”. *Journal of Materials Chemistry*, **8**, 197–203.
141. **Panella, B., M. Hirscher and S. Roth** (2005) “Hydrogen adsorption in different carbon nanostructures”. *Carbon*, **43**, 2209–2214.
142. **Park, C and M.A. Keane** (2001) “Controlled growth of highly ordered carbon nanofibers from Y zeolite supported nickel catalysts”. *Langmuir*, **17**, 8386-8396.
143. **Park, C., P.E. Anderson, A. Chambers, C.D. Tan, R. Hidalgo and N.M. Rodriguez** (1999) “Further studies of the interaction of hydrogen with graphite nanofibers”. *Journal of Physical Chemistry B*, **103**, 10572-10581.
144. **Parthasarathy, R.V., K.L.N. Phani and C.R. Martin** (1995) “Template synthesis of graphitic nanotubules”. *Advanced. Materials*, **7**, 896 – 897.
145. **Perdew, J.P** (1986) “Density –functional approximation for the correlation energy of the inhomogenous electron gas”. *Physical Review B*, **33**, 8822-8824.
146. **Perdew, J.P. and Y. Wang** (1986) “Accurate and simple density functional for the electronic exchange: Generalized gradient approximation”. *Physical ReviewB*, **33**, 8800-8802.
147. **Pinkerton, F. E., B.G. Wicke, C.H. Olk, G.G. Tibbetts, G.P. Meisner, M.S. Meyer and J.F. Herbst** (2000) “Thermogravimetric measurement of hydrogen absorption in alkali- modified carbon materials”. *Journal of Physical Chemistry B*, **104**, 9460-9467.
148. **Pool, R** (1990) “Uses for Tiny Tubules”. *Science*, **247**, 1410- 1411.
149. **Quantum** (2003) *www.qtw.com*.
150. **Rachman, M.A., Y. Furutani, Y. Nakashimada, T. Kakizono and N. Nishio** (1997) “Enhanced hydrogen production in altered mixed acid fermentation of glucose by *Enterobacter aerogenes*”. *Journal of Fermentation and Bioengineering*, **83**, 358–363.
151. **Radovic, L.R., M. Karra, K. Skokova and P. Thrower** (1998) “The role of substitutional boron in carbon oxidation”. *Carbon*, **36**, 1841-1854.

152. **Rajalakshmi, N., K.S. Dhathathreyan, A. Govindaraj and B.C. Satishkumar** (2000) “Electrochemical investigation of single-walled carbon nanotubes for hydrogen storage”. *Electrochimica Acta*, **45**, 4511-4515.
153. **Rapp, D.B and J.E. Shelby** (2004) “Photo-induced hydrogen outgassing of glass”. *Journal of Non-Crystalline Solids*, **349**, 254-259.
154. **Rappe A.K., C.J Casewit, K.S Colwell, W.A Goddard and W.M Skiff** (1992) “UFF, a full periodic table force field for molecular mechanics and molecular dynamics simulations”. *Journal of American Chemical Society*, **114**, 10024-10035.
155. **Rathna, A and J. Chandrasekhar** (1993) “Theoretical study of hydrogenated buckminsterfullerene derivatives with benzenoid rings, $C_{60}H_{60-66n}$ (n= 1–8)”. *Chemical Physics Letters*, **206**, 217-224.
156. **Raymundo-Pinero, E., P. Azais, T. Cacciaguerra, D. Cazorla-Amoros, A. Linares-Solano and F. Beguin** (2005) “KOH and NaOH activation mechanisms of multiwalled carbon nanotubes with different structural organization”. *Carbon*, **43**, 786–795.
157. **Ren, Y and D.L. Price** (2001) “Neutron scattering study of H₂ adsorption in single-walled carbon nanotubes”. *Applied Physics Letters*, **79**, 3684-3686.
158. **Rosi, N. L., J. Eckert, M. Eddaoudi, D.T. Vodak, J. Kim, M. O’Keeffe and O.M. Yaghi** (2003) “Hydrogen storage in microporous metal-organic frameworks”. *Science*, **300**, 1127-1129.
159. **Rowsell, J.L., A.R. Millward, K.S. Park, and O.M. Yaghi** (2004) “Hydrogen sorption in functionalized metal-organic frameworks” *Journal of American Chemical Society*, **126**, 5666-5667.
160. **Rozendal, R.A., H.V.M. Hamelers, G.J.W. Euverink, S.J. Metz and C.J.N. Buisman** (2006) “Principle and perspectives of hydrogen production through biocatalyzed electrolysis”. *International Journal of Hydrogen Energy*, **31**, 1632-1640.
161. **Rzepka, M., P. Lamp and M.A. de la Casa-Lillo** (1998) “Physisorption of hydrogen on microporous carbon and carbon nanotubes”. *Journal of Physical Chemistry B*, **102**, 10894-10898.
162. **Sandrock, G., K. Gross and G. Thomas** (2002) “Effect of Ti-catalyst content on the reversible hydrogen storage properties of the sodium alanates”. *Journal of Alloys and Compounds*, **339**, 299-308.
163. **Satishkumar, B.C., A. Govindaraj, R. Sen and C.N.R. Rao** (1998) “Singlewalled nanotubes by the pyrolysis of acetylene-organometallic mixtures”. *Chemical Physics Letters*, **293**, 47-52.
164. **Satyapal, S., J. Petrovic, C. Read, G. Thomas and G. Ordaz** (2007) “The U.S. Department of Energy's National Hydrogen Storage Project: Progress

- towards meeting hydrogen-powered vehicle requirements". *Catalysis Today*, **120**, 246 - 256.
165. **Schimmel, H.G., G.J. Kearley, M.G. Nijkamp, C.T. Visser, K.P. de Jong and F.M. Mulder** (2003) "Hydrogen adsorption in carbon nanostructures: Comparison of nanotubes, fibres, and coals". *Chemistry - A European Journal*, **9**, 4764 - 4770.
 166. **Schlapbach, L** (1998) "Introduction. In: Hydrogen in Intermetallic Compounds I". Ed. Schlapbach, Springer-Verlag, Germany.
 167. **Schlapbach, L and A. Zuttel** (2001) "Hydrogen-storage materials for mobile applications". *Nature*, **414**, 353–358.
 168. **Schmitt, M.L., J.E. Shelby and M.M. Hall** (2006) "Preparation of hollow glass microspheres from sol-gel derived glass for application in hydrogen gas storage". *Journal of Non-Crystalline Solids*. **352**, 626-631.
 169. **Schur, V., P. Tarasov, M. Shul'ga, Yu. Zaginaichenko, A. Matysina and P. Pomytkin** (2003) "Hydrogen in fullerites". *Carbon*, **41**, 1331-1342.
 170. **Selampinar, F., U. Akbulut, T. Yalçın, S. Süzer and L. Toppare** (1994) "A conducting composite of polypyrrole I. Synthesis and characterization". *Synthetic Metals*, **62**, 201-206.
 171. **Sen, R., B.C. Satishkumar, S. Govindaraj, K.R. Harikumar, M.K. Renganathan and C.N.R. Rao** (1997) "Nitrogen-containing carbon nanotubes". *Journal of Material Chemistry*, **12**, 2335 – 2337.
 172. **Sherif, S. A., N. Zeytinoglu and T.N. Veziroglu** (1997) "Liquid hydrogen: Potential, problems, and a proposed research program". *International Journal of Hydrogen Energy*, **22**, 683-688.
 173. **Shirai, K., S. Emura, S. Gonda and Y. Kumashiro** (1995) "Infrared study of amorphous B_{1-x}C_x films". *Journal of Applied Physics*, **78**, 3392-3400.
 174. **Shirasaki, T., A. Derré, M. Ménétrier, A. Tressaud, and S. Flandrois** (2000) "Synthesis and characterization of boron-substituted carbons". *Carbon*, **38**, 1461-1467.
 175. **Stal, L.J and R. Moezelaar** (1979) "Fermentation in cyanobacteria FEMS". *Microbiological Research*, **21**, 179–211.
 176. **Stan, G and M.W. Cole** (1998) "Hydrogen Adsorption in Nanotubes". *Journal of Low Temperature Physics*, **110**, 539-544.
 177. **Stephan, O., P.M. Ajayan, C. Colliex, Ph. Redlich, J.M. Lambert, P. Bernier and P. Lefin** (1994) "Doping graphitic and carbon nanotube structures with boron and nitrogen". *Science*, **266**, 1683-1685.

178. **Strobel, R., L. Jorissen, T. Schliermann, V. Trapp, W. Schutz and K. Bohmhammel, G. Wolf and J. Garche** (1999) “Hydrogen adsorption on carbon materials”. *Journal of Power Sources*, **84**, 221-224.
179. **Ström-Olsen J., A. Zaluska and L. Zaluski** (2001) “Structure, Catalysis and Atomic Reactions on the Nano-Scale: a Systematic Approach to Metal Hydrides for Hydrogen Storage”. *Applied Physics A: Materials Science and Processing*, **72**, 157-165.
180. **Takagi, H., H. Hatori, Y. Soneda, N. Yoshizawa and Y. Yamada** (2004) “Adsorptive hydrogen storage in carbon and porous materials”. *Materials Science and Engineering: B*, **108**, 143–147.
181. **Takeshita, T., W.E. Wallace and R.S. Craig** (1976) “Rare earth intermetallics as synthetic ammonia catalysts”. *Journal of Catalysis*, **44**, 236-243.
182. **Terres, E., B. Panella, T. Hayashi, Y.A. Kim, M. Endo and J.M. Dominguez, M. Hirscher, H. Terrones and M. Terrones** (2005) “Hydrogen storage in spherical nanoporous carbons”. *Chemical Physics Letters*, **403**, 363-366.
183. **Terrones, M., P. Redlich, N. Grobert, S. Trasobares, W-K. Hsu, H. Terrones, Y.Q. Zhu, J.P. Hare, C.L. Reeves, A.K. Cheetham, M. Rühle, H.W. Kroto and D.R.M. Walton** (1999) “Carbon nitride nanocomposites formation of aligned CxNy nanofibers”. *Advanced Materials*, **11**, 655 - 658.
184. **Texier-Mandoki, N., J. Dentzer, T. Piquero, S. Saadallah, P. David and C. Vix-Guterl** (2004) “Hydrogen storage in activated carbon materials: role of the nanoporous texture”. *Carbon*, **42**, 2744–2747.
185. **Trans, S.T., A.R.M. Verscheren and C. Dekker** (1998) “Room-temperature transistor based on a single carbon nanotube”. *Nature*, **393**, 49 - 51.
186. **Vaccari, A.** (1998) “Preparation and catalytic properties of cationic and anionic clays”. *Catalysis Today*, **41**, 53 - 71.
187. **von Barth, U** (1979) “Local-density theory of multiplet structure”. *Physics Review A*, **20**, 1693 - 1703
188. **Vosko, S.H and L. Wilk** (1980) “Influence of an improved local-spin-density correlation-energy functional on the cohesive energy of alkali metals”. *Physics Review B*, **22**, 3812 – 3815.
189. **Wang, Q. K., C.C. Zhu, W.H. Liu and T. Wu** (2002) “Hydrogen storage by carbon nanotube and their films under ambient pressure”. *International Journal of Hydrogen Energy*, **27**, 497 - 500.
190. **Wang, Q. Y. and J.K. Johnson** (1999a) “Optimization of carbon nanotube arrays for hydrogen adsorption”. *Journal of Physical Chemistry B*, **103**, 4809 - 4813.

191. **Wang, Q. Y. and J.K. Johnson** (1999b) “Molecular simulation of hydrogen adsorption in single-walled carbon nanotubes and idealized carbon slit pores”. *Journal of Chemical Physics*, **110**, 577 - 586.
192. **Weast RC.** Handbook of Chemistry and Physics. CRC Press. 1978:59th ed.; F217.
193. **Wei, B., R. Spolenak, P. Kohler-Redlich, M. Rühle and E. Arzt** (1999) “Electrical transport in pure and boron-doped carbon nanotubes”. *Applied Physics Letters*, **74**, 3149 - 3151.
194. **Weitkamp, J., M. Fritz and S. Ernst** (1995) “Zeolites as media for hydrogen storage”. *International Journal of Hydrogen Energy*, **20**, 967-970.
195. **Wendt, H** (1987) “Thermochemical Hydrogen Production”. *International Journal of Hydrogen Energy*, **12**, 291 - 295.
196. **Wolf, J** (2002) “Liquid-hydrogen technology for vehicles”. *MRS Bulletin*, **27**, 684 -687.
197. **Wong, S.S., E. Joselevich, A.T. Woolley, C.I. Cheung and C.M. Lieber** (1998) “Covalently functionalized nanotubes as nanometresized probes in chemistry and biology”. *Nature*, **394**, 52 - 55.
198. **Wu, X.B., P. Chen, J. Lin and K.L. Tan** (2000) “Hydrogen uptake by carbon nanotubes”. *International Journal of Hydrogen Energy*, **25**, 261–265.
199. **Yamamoto, K., S. Orimo, H. Fujii and Y. Kitano** (1999) “Hydriding properties of the heat-treated MgNi alloys with nanostructural designed multiphase”. *Journal of Alloys and Compounds*, **295**, 546 - 551.
200. **Yang F. H. and R.T. Yang** (2002) “Ab initio molecular orbital study of adsorption of atomic hydrogen on graphite: Insight into hydrogen storage in carbon nanotubes”. *Carbon*, **40**, 437 - 444.
201. **Yang, R.T.** (2000) “Hydrogen storage by alkali-doped carbon nanotubes-revisited”. *Carbon*, **38**, 623 - 626.
202. **Ye, Y., C.C. Ahn, C. Witham, B. Fultz, J. Liu and A.G. Rinzler** (1999) “Hydrogen adsorption and cohesive energy of single-walled carbon nanotubes”. *Applied Physics Letters*, **74**, 2307 - 2309.
203. **Yin, Y.F., T. Mays and B. McEnaney** (2000) “Molecular simulations of hydrogen storage in carbon nanotube arrays”. *Langmuir*, **16**, 10521-10527.
204. **Zaginaichenko, S.Yu., Z.A. Matysina, D.V. Schur and V.A. Chumak** (2002) “Theoretical study of structural transformations at fullerite hydrogenation”. *Hydrogen solubility. NATO Science Series, II: Mathematics, Physics and Chemistry*, **71**(Hydrogen Materials Science and Chemistry of Metal Hydrides), 429-440.

205. **Zaluska, A., L. Zaluski and J.O. Strom-Olsen** (1999a) “Nanocrystalline magnesium for hydrogen storage”. *Journal of Alloys and Compounds*, **288**, 217 - 225.
206. **Zaluska, A., L. Zaluski and J.O. Strom-Olsen** (1999b) “Synergy of hydrogen sorption in ball-milled hydrides of Mg and Mg₂Ni”. *Journal of Alloys and Compounds*, **289**, 197 - 206.
207. **Zaluska, A., L. Zaluski and J.O. Strom-Olsen** (2000) “Sodium alanates for reversible hydrogen storage”. *Journal of Alloys and Compounds*, **298**, 125 - 134.
208. **Zhang, C., X.S. Lu and A.Z. Gu** (2004) “How to accurately determine the uptake of hydrogen in carbonaceous materials”. *International Journal of Hydrogen Energy*, **29**, 1271 - 1276.
209. **Zhao, N.Q., C.N. He, J. Ding, T.C. Zou, Z.J. Qiao, C.S. Shi, X.W. Du, J.J. Li and Y.D. Li** (2007) “Bamboo-shaped carbon nanotubes produced by catalytic decomposition of methane over nickel nanoparticles supported on aluminum”. *Journal of Alloys and Compounds*, **428**, 79 – 83.
210. **Zhao, X.B., B. Xiao, A.J. Fletcher and K.M. Thomas** (2005) “Hydrogen adsorption on functionalized nanoporous activated carbons”. *Journal of Physical Chemistry B*, **109**, 8880 - 8888.
211. **Zhou, L., Y. Zhou and Y. Sun** (2004) “A comparative study of hydrogen adsorption on superactivated carbon versus carbon nanotubes”. *International Journal of Hydrogen Energy*, **29**, 475 - 479.
212. **Zhu, H. W., A.Y. Cao, X.S. Li, C.L. Xu, Z.Q. Mao, D.B. Ruan, J. Liang and D.H. Wu** (2001) “Hydrogen adsorption in bundles of well-aligned carbon nanotubes at room temperature”. *Applied Surface Science*, **178**, 50 - 55.
213. **Zhu, H. W., X.S. Li, L.J. Ci, C.L. Xu, D.H. Wu and Z.Q. Mao** (2003) “Hydrogen storage in heat-treated carbon nanofibers prepared by the vertical floating catalyst method”. *Materials Chemistry and Physics*, **78**, 670 - 675.
214. **Zhu, Z.H., H. Hatori, S.B. Wang and G.Q. Lu** (2005) “Insights into hydrogen atom adsorption on and the electrochemical properties of nitrogen substituted carbon materials”. *Journal of Physical Chemistry B*, **109**, 16744 - 16749.
215. **Züttel, A and S.I. Orimo** (2002) “Hydrogen in Nanostructured, Carbon-Related, and Metallic Materials”. *MRS Bulletin*, **27**, 705-711.
216. **Züttel, A** (2004) “Hydrogen storage methods”. *Naturwissenschaften*, **91**, 157–172.
217. **Züttel, A.** (2003) “Materials for hydrogen storage”. *Materials Today*, **6**, 24 - 33.

LIST OF PUBLICATIONS BASED ON RESEARCH WORK

REFERRED JOURNALS

1. **Sankaran, M., A. Kalaiselvan, R. Ganesan, P. Venuvanalingam and B. Viswanathan**, (2002) "Heteroatom substituted carbon nanotubes: can they be the activating centers for hydrogen absorption". *Bulletin of Catalysis Society of India*, **1**, 167-17.
2. **Sankaran, M. and B. Viswanathan** (2003) "Hydriding of nitrogen containing carbon nanotubes". *Bulletin of Catalysis Society of India*, **2**, 9-11.
3. **Viswanathan, B., M. Sankaran and M. Aulice Scibioh**, (2003) "Carbon nanomaterials -are they appropriate candidates for hydrogen storage?". *Bulletin of Catalysis Society of India*, **2**, 13-26.
4. **Viswanathan, B., M. Sankaran and R. Ganesan** (2003) "Can heteroatoms be the activators for hydrogen storage in carbon nanotubes", *Preprints - American Chemical Society, Division of Fuel Chemistry*. **48**, 943-944.
5. **Muthukumar, K., M. Sankaran and B. Viswanathan** (2004) "Hydrogenation of substituted Fullerenes – A DFT study". *Eurasian Chemical Technology Journal*, **6**, 139-143.
6. **Sankaran, M., K. Muthukumar and B. Viswanathan** (2005) "Boron Substituted Fullerene – Can they be one of the Option for Hydrogen Storage?". *Fullerene, Nanotubes and Carbon Nanostructures*, **13**, 43-52.
7. **Sankaran, M. and B. Viswanathan** (2006) "The role of heteroatoms in carbon nanotubes for hydrogen storage". *Carbon*, **44**, 2816-2821.
8. **Sankaran, M. and B. Viswanathan** (2006) "Heteroatom substituted carbon nanotubes as candidate for hydrogen storage". *Preprints - American Chemical Society, Division of Fuel Chemistry*. **51**, 803-804.
9. **Sankaran, M., B. Viswanathan and S. Srinivasa Murthy**, (2006) "Possibility of Hydrogen Storage by Boron Substituted Carbon nanotubes". *Bulletin of Catalysis Society of India*, **5**, 56-61.
10. **Sankaran, M. and B. Viswanathan** (2007) Hydrogen storage in boron substituted carbon nanotubes, *Carbon*. (In Press).
11. **Sankaran, M., B. Viswanathan and S. Srinivasa Murthy**, (2007) "Boron substituted carbon nanotubes-How appropriate are they for hydrogen storage?". *International Journal of Hydrogen Energy*, (Under Revision).

NATIONAL/INTERNATIONAL CONFERENCES

1. **Viswanathan, B., M. Sankaran and R. Ganesan** (2003) “Can hetroatoms be the activators for hydrogen in carbon nanotubes?”. (Oral presentation) Presented in Fuel Cell Systems and Fuel Processing for Fuel Cell Applications- 226th American Chemical Society (ACS) National Meeting Co-sponsored by the ACS Fuel & Petroleum Chemistry Divisions held at New York City, NY, September 7-11.
2. **Viswanathan, B., M. Sankaran and S. Srinivasa Murthy** (2004) “Carbon Nanomaterials for Hydrogen Storage”. Indo-Belarus workshop on ‘Advances in sorption based thermal devices’ held at Minsk, Belarus, November 2-3.
3. **Sankaran, M. and B. Viswanathan** (2005) “Hydrogen storage by carbon materials – Heteroatoms as activating centers”. (Oral presentation) presented in International Conference on SOLID STATE HYDROGEN STORAGE – Materials and Applications held at Hyderabad, India, January 31 – February 1.
4. **Sankaran, M. and B. Viswanathan** (2006) “Heteroatom substituted carbon nanotubes as candidate for hydrogen storage”. (Oral presentation) accepted for presentation in Chemistry and Applications of carbon nanotubes and nanoparticles in Fuel Chemistry division – 232nd American Chemical Society (ACS) National Meeting held at San Francisco, CA, USA, September 10 – 14.
5. **Sankaran, M., B. Viswanathan and S. Srinivasa Murthy** (2006) “Hydrogen storage in boron substituted carbon nanotubes”. (Oral presentation) presented in International Workshop on Hydrogen Energy (Production, Storage and Application) held at Jaipur, India, November 5-9, 2006,
6. **Viswanathan, B. and M. Sankaran** (2007) “Options for hydrogen storage – the current status”. (Invited lecture) presented in Indo – German Workshop on “Fuel cells and Hydrogen Energy” held at Kolkata, India, January 29-31.